

STUDIES ON THE REACTIVITY OF THIOPHOSPHATE/THIOPHOSPHINATE
AND ETHYL XANTHATE WITH PRECIOUS METALS

by

DongSu Kim

Dissertation submitted to the Faculty of the
Virginia Polytechnic Institute and State University
in partial fulfillment of the requirements for the degree of
Doctor of Philosophy
in
Materials Engineering Science

APPROVED:



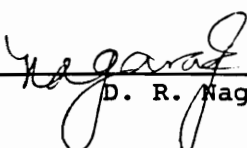
Roe-Hoan Yoon, Chairman



Gregory T. Adel



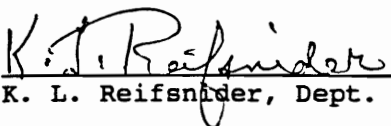
Gerald H. Luttrell



D. R. Nagaraj



P. E. Richardson



K. L. Reifsnider, Dept. Head

December, 1992

Blacksburg, Virginia

**STUDIES ON THE REACTIVITY OF THIOPHOSPHATE/THIOPHOSPHINATE
AND ETHYL XANTHATE WITH PRECIOUS METALS**

by

DongSu Kim

Roe-Hoan Yoon, Chairman

Materials Engineering Science

(ABSTRACT)

Adsorption mechanisms of modified thiol collectors on gold, silver, and gold-silver alloys have been studied and compared with those of ethyl xanthate (EX). The modified thiol collectors include dicresyl monothiophosphate (DCMTP), dialkyl dithiophosphinate (DTPI) and monothiophosphinate (MTPI).

In general, the adsorption mechanisms on silver and gold-silver alloys can be explained by the EC-mechanism involving an electron transfer step and a chemical reaction step. Thus, the adsorption should be controlled by the E_a of the electrochemical oxidation of the electrode involved and the pK of the metal collector complex. According to this mechanism, DCMTP should adsorb on silver and gold-silver alloys at a lower potential than DTPI and MTPI since the pK of silver-DCMTP complex is larger than those of silver-DTPI and silver-MTPI. This has been verified to be the case by voltammetry, FTIR and contact angle studies. Likewise, EX adsorbs on silver at a lower potential than the modified thiol collectors because the pK of silver-EX is larger than those of the silver-modified thiol collectors.

Both EX and the modified thiol collectors adsorb on silver at lower potentials than on the gold-silver alloys, which can be attributed to the lower activity of silver on the alloy surface. For the same reason, the potential for the onset of collector adsorption on alloys decreases with increasing silver content.

There are no significant differences between the reactivities of DTPI

and MTPI with precious metals except that the dithio-compound can be oxidized to dimers on gold at high potentials, while the monothio-homologue cannot. In this regard, DTPI may be a better collector for pure gold than MTPI. It has been found that EX is also oxidized to dixanthogen on gold.

Unlike the modified thiol collectors, EX can chemisorb on silver and gold-silver alloys at potentials significantly below the reversible potentials for the silver-EX formation. The potential for the onset of EX adsorption decreases with increasing silver content in the gold-silver alloys. Based on the rest potential measurements involving the chemisorbed xanthates, E_h -pH diagrams for the gold-silver-EX systems have been constructed.

Acknowledgements

The author wishes to express his sincere appreciation to Professor Roe-Hoan Yoon for his guidance and support throughout the course of this study. The author is also thankful to his committee members, Drs. G. T. Adel, G. H. Luttrell, D. R. Nagaraj, P. E. Richardson, and K. L. Reifsnider for their helpful suggestions and advice. The author is also grateful to Drs. R. Woods and C. I. Basilio for their constructive criticisms and guidance.

The financial support from the American Cyanamid Company is greatly appreciated. Special thanks are also extended to the fellow graduate students at the Virginia Center for Coal and Minerals Processing.

Finally, the author wishes to express his deepest appreciation to his family and Professor Y. S. Kim of Seoul National University for their encouragement and endless love.

Table of Contents

Chapter 1. Introduction.....	1
1.1. General.....	1
1.2. Gold Recovery Processes.....	2
1.3. Flotation of Precious Metals.....	4
1.3.1. Gold Flotation.....	5
1.3.2. Silver Flotation.....	5
1.4. Reagents.....	6
1.5. Objectives of the Study.....	8
 Chapter 2. Monothiophosphate System.....	 10
2.1. Introduction.....	10
2.2. Experiments.....	12
2.2.1. Materials.....	12
2.2.2. Voltammetry.....	13
2.2.3. FTIR Spectroscopy.....	13
2.2.4. Contact Angle Measurements.....	13
2.2.5. E_h -pH Diagram.....	16
2.3. Results and Discussion.....	17
2.3.1. Voltammetry.....	17
2.3.2. FTIR Spectroscopy.....	24
2.3.2.1. Standard Spectra.....	24
2.3.2.2. Effect of Potential.....	27
2.3.2.3. Effect of pH.....	34
2.3.2.4. Effect of Conditioning Time.....	37
2.3.3. Contact Angle Measurements.....	44

2.3.3.1. Effect of Potential.....	44
2.3.3.2. Effect of pH.....	48
2.3.4. E_h -pH Diagram.....	48
2.4. Summary.....	51
Chapter 3. Thiophosphinate System.....	53
3.1. Introduction.....	53
3.2. Experiments.....	55
3.2.1. Materials.....	55
3.3. Results and Discussion.....	56
3.3.1. Voltammetry.....	56
3.3.1.1. Diethyl Dithiophosphinate.....	56
3.3.1.2. Diisobutyl Dithiophosphinate.....	64
3.3.1.3. Diisobutyl Monothiophosphinate.....	67
3.3.2. FTIR Spectroscopy.....	70
3.3.2.1. Diethyl Dithiophosphinate.....	70
3.3.2.1.1. FTIR Spectra.....	70
3.3.2.1.2. Effect of Potential.....	73
3.3.2.2. Diisobutyl Dithiophosphinate.....	79
3.3.2.2.1. FTIR Spectra.....	79
3.3.2.2.2. Effect of Potential.....	81
3.3.2.3. Diisobutyl Monothiophosphinate.....	86
3.3.2.3.1. FTIR Spectra.....	86
3.3.2.3.2. Effect of Potential.....	86
3.3.3. Contact Angle Measurements.....	89
3.3.3.1. Diethyl Dithiophosphinate.....	89
3.3.3.2. Diisobutyl Dithiophosphinate.....	98
3.3.3.3. Diisobutyl Monothiophosphinate.....	102
3.3.4. E_h -pH Diagrams.....	105

3.4. Summary.....	108
Chapter 4. Ethyl Xanthate System.....	109
Part I. Silver/Ethyl Xanthate System.....	109
4.1. Introduction.....	109
4.2. Experiments.....	111
4.2.1. Voltammetry.....	111
4.2.2. Adsorption Isotherm for Ag^0	112
4.2.3. FTIR Spectroscopy.....	115
4.2.4. UV/Vis Spectroscopy.....	116
4.2.5. Contact Angle Measurements.....	116
4.2.6. E_h -pH Diagram.....	118
4.3. Results and Discussion.....	119
4.3.1. Voltammetry.....	119
4.3.2. Adsorption Isotherm for Ag^0	121
4.3.3. FTIR Spectroscopy.....	124
4.3.4. UV/Vis Spectroscopy.....	126
4.3.4.1. UV/Vis Spectra of the Chemisorbed Xanthate and Bulk Silver Xanthate.....	126
4.3.4.2. Stability of the Chemisorbed Ethyl Xanthate.....	132
4.3.5. Contact Angle Measurements.....	134
4.3.6. E_h -pH Diagram.....	136
4.3.6.1. Rest Potential Measurements.....	136
4.3.6.2. E_h -pH Diagram.....	138
4.4. Summary.....	140
Part II. Gold-Silver Alloy/Ethyl Xanthate System.....	142
4.5. Introduction.....	142
4.6. Experimental Materials.....	143
4.7. Results and Discussion.....	143
4.7.1. Voltammetry.....	143

4.7.2. Adsorption Isotherm for Au-Ag Alloy.....	145
4.7.2.1. Calculation of Adsorption Isotherm.....	145
4.7.2.2. Adsorption Isotherm.....	146
4.7.3. Contact Angle Measurements.....	148
4.7.4. E_h -pH Diagram.....	150
4.8. Summary.....	154
 Chapter 5. Summary and Conclusions.....	 156
5.1. Monothiophosphate.....	156
5.2. Di- and Monothiophosphinates.....	158
5.3. Ethyl Xanthate.....	160
 Chapter 6. Recommendations for Future Study.....	 164
 Appendix.....	 167
 Bibliography.....	 178
 Vita.....	 184

List of Illustrations

Figure 2.1.	Schematic diagram showing the experimental set-up used for the linear sweep voltammetry.....	14
Figure 2.2.	Schematic diagram of the modified electrochemical cell for the contact angle measurements.....	15
Figure 2.3.	Voltammograms of Ag° at (a) pH 4.6 and (b) pH 9.2 in the absence and presence of 1×10^{-4} M DCMTF.....	18
Figure 2.4.	Voltammograms of Au° at (a) pH 4.6 and (b) pH 9.2 in the absence and presence of 1×10^{-4} M DCMTF.....	21
Figure 2.5.	Voltammograms of AuAg alloy (80:20) at (a) pH 4.6 and (b) pH 9.2 in the absence and presence of 1×10^{-4} M DCMTF.....	23
Figure 2.6.	Voltammograms of AuAg alloy (50:50) at (a) pH 4.6 and (b) pH 9.2 in the absence and presence of 1×10^{-4} M DCMTF.....	25
Figure 2.7.	FTIR spectra of DCMTF and AgDCMTF.....	26
Figure 2.8.	FTIR reflection spectra of Ag° conditioned in 1×10^{-4} M DCMTF at pH 4.6 and different potentials.....	28
Figure 2.9.	Effect of potential on the IR relative signal intensities of DCMTF adsorbed on Ag° at pH 4.6.....	29
Figure 2.10.	FTIR reflection spectra of AuAg alloy (80:20) conditioned in 1×10^{-4} M DCMTF at pH 4.6 and different potentials.....	31
Figure 2.11.	Effect of potential on the IR relative signal intensities of DCMTF adsorbed on AuAg alloy (80:20) at pH 4.6.....	32
Figure 2.12.	FTIR reflection spectra of AuAg alloy (50:50) conditioned in 1×10^{-4} M DCMTF at pH 4.6 and different potentials.....	33
Figure 2.13.	Effect of potential on the IR relative signal intensities of DCMTF adsorbed on AuAg alloy (50:50) at pH 4.6.....	35
Figure 2.14.	FTIR reflection spectra of Ag° conditioned in 1×10^{-4} M DCMTF at different pH's.....	36
Figure 2.15.	Effect of pH on the IR relative signal intensities of DCMTF adsorbed on Ag°	38
Figure 2.16.	FTIR reflection spectra of Ag° conditioned in 1×10^{-4} M DCMTF for different periods (722; P-S, 870 & 1100; 1:4 substitution in aromatic ring, 922; acetate buffer, 1210; aromatic ring or P-O, 1507; aromatic ring).....	39

Figure 2.17. Schematic representation of molecular structure of DCMTTP adsorbed on silver. Plane (a) shows the initial stage of adsorption and, plane (b) shows the stage for the formation of close-packed monolayer.....	40
Figure 2.18. Adsorption model of collector (DCMTTP) on the substrate depending on time.....	43
Figure 2.19. Effect of potential on the contact angle of DCMTTP adsorbed on Ag° at pH 4.6.....	45
Figure 2.20. Effect of potential on the contact angle of DCMTTP adsorbed on AuAg alloy (80:20) at pH 4.6.....	46
Figure 2.21. Effect of potential on the contact angle of DCMTTP adsorbed on AuAg alloy (50:50) at pH 4.6.....	47
Figure 2.22. Effect of pH on the contact angle of DCMTTP adsorbed on Ag°.	49
Figure 2.23. E _p -pH diagram for silver/water/MTP system for an initial DCMTTP concentration of 1x10 ⁻⁴ M.....	50
Figure 3.1. Voltammograms for Au° in the absence and presence of 2 x 10 ⁻⁴ M DEDTPI at pH 9.2.....	57
Figure 3.2. Voltammograms for Ag° in the absence and presence of 2 x 10 ⁻⁴ M DEDTPI at pH 9.2.....	59
Figure 3.3. Voltammograms for 80:20 Au-Ag alloy in the absence and presence of 2 x 10 ⁻⁴ M DEDTPI at pH 9.2.....	61
Figure 3.4. Voltammograms for 50:50 Au-Ag alloy in the absence and presence of 2 x 10 ⁻⁴ M DEDTPI at pH 9.2.....	63
Figure 3.5. Voltammograms for Au° in the absence and presence of 2 x 10 ⁻⁴ M DIBDTPI at pH 9.2.....	65
Figure 3.6. Voltammograms for Ag° in the absence and presence of 2 x 10 ⁻⁴ M DIBDTPI at pH 9.2.....	66
Figure 3.7. Voltammograms for Au° in the absence and presence of 1 x 10 ⁻⁴ M DIBMTPI at pH 9.2.....	68
Figure 3.8. Voltammograms for Ag° in the absence and presence of 1 x 10 ⁻⁴ M DIBMTPI at pH 9.2.....	69
Figure 3.9. FTIR reflection spectra of sodium DEDTPI, (DEDTPI) ₂ and AgDEDTPI.....	71
Figure 3.10. FTIR reflection spectra of (a) Au° at 750mV, (b) Ag° at 450 mV and (c) 50:50 Au-Ag alloy at 550 mV in 2 x 10 ⁻⁴ M DEDTPI.	72
Figure 3.11. The effect of potential on the IR signal intensity (2960 and 760 cm ⁻¹) of adsorbed DEDTPI for Au° in the presence of 2 x 10 ⁻⁴ M DEDTPI at pH 9.2.....	74

Figure 3.12.	The effect of potential on the IR signal intensity (2970 and 760 cm^{-1}) of adsorbed DEDTPI for Ag° in the presence of 2×10^{-4} M DEDTPI at pH 9.2.....	75
Figure 3.13.	The effect of potential on the IR signal intensity (2965 and 760 cm^{-1}) of adsorbed DEDTPI for 80:20 Au-Ag alloy in the presence of 2×10^{-4} M DEDTPI at pH 9.2.....	77
Figure 3.14.	The effect of potential on the IR signal intensity (2965 and 760 cm^{-1}) of adsorbed DEDTPI for 50:50 Au-Ag alloy in the presence of 2×10^{-4} M DEDTPI at pH 9.2.....	78
Figure 3.15.	FTIR reflection spectra of $\text{NH}_4\text{DIBDTPI}$, $(\text{DIBDTPI})_2$ and AgDIBDTPI	80
Figure 3.16.	FTIR reflection spectra of (a) Au° at 750 mV and (b) Ag° at 550 mV in 2×10^{-4} M DIBDTPI.....	82
Figure 3.17.	The effect of potential on the IR signal intensity (2960 cm^{-1}) of adsorbed DIBDTPI for Au° in the presence of 2×10^{-4} M DIBDTPI at pH 9.2.....	83
Figure 3.18.	The effect of potential on the IR signal intensity (2960 cm^{-1}) of adsorbed DIBDTPI for Ag° in the presence of 2×10^{-4} M DIBDTPI at pH 9.2.....	85
Figure 3.19.	FTIR reflection spectra of $\text{NH}_4\text{DIBMTPI}$, AgDIBMTPI , and Ag° at 500 mV in 1×10^{-4} M DIBMTPI.....	87
Figure 3.20.	The effect of potential on the IR signal intensity (2960 cm^{-1}) of adsorbed DIBMTPI for Au° in the presence of 2×10^{-4} M DIBMTPI at pH 9.2.....	88
Figure 3.21.	The effect of potential on the IR signal intensity (2960 cm^{-1}) of adsorbed DIBMTPI for Ag° in the presence of 2×10^{-4} M DIBMTPI at pH 9.2.....	90
Figure 3.22.	The effect of potential on the IR signal intensity (2960 cm^{-1}) of adsorbed DIBMTPI for 80:20 Au-Ag alloy in the presence of 1×10^{-4} M DIBMTPI at pH 9.2.....	91
Figure 3.23.	The effect of potential on the IR signal intensity (2960 cm^{-1}) of adsorbed DIBMTPI for 50:50 Au-Ag alloy in the presence of 1×10^{-4} M DIBMTPI at pH 9.2.....	92
Figure 3.24.	The effect of potential on the contact angle for Au° in the presence of 2×10^{-4} M (\square) and 1×10^{-3} M (\diamond) of DEDTPI at pH 9.2.....	93
Figure 3.25.	The effect of potential on the contact angle for Ag° in the presence of 2×10^{-4} M DEDTPI at pH 9.2.....	95
Figure 3.26.	The effect of potential on the contact angle for 80:20 Au-Ag alloy in the presence of 2×10^{-4} M DEDTPI at pH 9.2.....	96
Figure 3.27.	The effect of potential on the contact angle for 50:50 Au-Ag alloy in the presence of 2×10^{-4} M DEDTPI at pH 9.2.....	97

Figure 3.28.	The effect of potential on the contact angle for Au° in the presence of 2×10^{-4} M DIBDTPI at pH 9.2.....	99
Figure 3.29.	The effect of potential on the contact angle for Au° in the presence of 1×10^{-3} M DIBDTPI at pH 9.2.....	100
Figure 3.30.	The effect of potential on the contact angle for Ag° in the presence of 2×10^{-4} M DIBDTPI at pH 9.2.....	101
Figure 3.31.	The effect of potential on the contact angle for Au° in the presence of 1×10^{-4} M DIBMTPI at pH 9.2.....	103
Figure 3.32.	The effect of potential on the contact angle for Ag° in the presence of 1×10^{-4} M DIBMTPI at pH 9.2.....	104
Figure 3.33.	E_h -pH diagram for the silver/water/DTPI system for an initial collector concentration of 1×10^{-4} M.....	106
Figure 3.34.	E_h -pH diagram for the silver/water/MTPI system for an initial collector concentration of 1×10^{-4} M.....	107
Figure 4.1.	Cathodic scans for cyclic voltammograms for silver in solution of pH 9.2 containing 1×10^{-4} M ethyl xanthate. Scans at 20 mV/sec to different upper potential limits.....	113
Figure 4.2.	Schematic representation of the experimental set-up for the UV/Vis adsorption kinetic studies.....	117
Figure 4.3.	Voltammograms at 20 mV/sec for a silver electrode in pH 9.2 solution containing 1×10^{-4} M ethyl xanthate: (a) influence of upper potential limit in quiescent solution; (b) effect of stirring the solution.....	120
Figure 4.4.	Potential dependence of coverage of chemisorbed xanthate on silver in solutions of pH (a) 6.8 and (b) 9.2 containing various concentrations of ethyl xanthate (M/dm ³). The solid lines are the derived isotherm.....	122
Figure 4.5.	FTIR reflectance spectra of (a) a silver electrode held at different potentials in a pH 9.2 solution containing 1×10^{-4} M ethyl xanthate, and (b) silver ethyl xanthate.....	125
Figure 4.6.	Absorbance at 301 nm of a pH 9.2 solution initially containing 2×10^{-5} M ethyl xanthate being circulated through a silver wool electrode. Potential held at -0.43 V for 2 min then a triangular potential cycle at 1 mV/sec applied between -0.43 and 0.14 V.....	128
Figure 4.7.	UV/Vis spectra recorded for a pH 9.2 solution initially containing 2×10^{-5} M ethyl xanthate being circulated through a silver wool electrode (1) prior to, and (2) following a triangular potential cycle at 1 mV/sec applied between -0.43 and 0.14 V.....	129

- Figure 4.8. UV/Vis spectra recorded for a pH 9.2 solution initially containing 2×10^{-5} M ethyl xanthate being circulated through a silver wool electrode (1) at the initial potential of -0.45 V, (2) after stepping the potential to -0.11 V and holding for 4 min, and (3) after returning to -0.45 V.....131
- Figure 4.9. UV/Vis spectra recorded for a pH 9.2 solution initially containing 2×10^{-5} M ethyl xanthate being circulated through a silver wool electrode (1) at the initial potential of -0.42 V, (2) after holding at -0.13 V for 4 min and (3) after washing and drying the electrode, holding for 20 min under conditions simulating those used for FTIR spectroscopy, returning to the cell containing xanthate-free solution, and potentiostating at -0.42 V.....133
- Figure 4.10. Dependence of contact angle on potential for a silver electrode in pH 9.2 solution containing 1×10^{-4} M ethyl xanthate.....135
- Figure 4.11. Rest potential measurements for silver electrode in ethyl xanthate solutions at pH 9.2 and pH 6.8.....137
- Figure 4.12. E_h -pH diagram for the silver/water/ethyl xanthate system for an initial xanthate concentration of 1×10^{-4} M. Dashed lines are fractional surface coverages as indicated.....139
- Figure 4.13. Voltammograms at 50 mV/sec in pH 9.2 solution containing 1×10^{-3} M ethyl xanthate for (1) silver, (2) 50:50 and (3) 80:20 (weight %) gold-silver alloys.....144
- Figure 4.14. Potential dependence of fractional coverage of chemisorbed xanthate in solutions at pH 9.2 containing 1×10^{-3} M ethyl xanthate. Solid lines are isotherms for (1) silver, (2) calculated for 50:50 and (3) 80:20 gold-silver alloys. Points are experimental fractional coverages for 50:50 (o) and 80:20 alloys (Δ).....147
- Figure 4.15. Dependence of contact angle on potential in pH 9.2 solution containing 1×10^{-3} M ethyl xanthate for (1) silver, (2) 50:50, (3) 80:20 gold-silver alloys, and (4) gold.....149
- Figure 4.16. E_h -pH diagram for silver/water/ethyl xanthate system for an initial xanthate concentration of 1×10^{-3} M. Dashed lines are same fractional surface coverages as indicated in figure 4.12.....151
- Figure 4.17. E_h -pH diagram for 50:50 gold-silver alloy/water/xanthate system for an initial xanthate concentration of 1×10^{-3} M. Dashed lines are same fractional coverages as indicated in figure 4.12.....152
- Figure 4.18. E_h -pH diagram for 80:20 gold-silver alloy/water/ethyl xanthate system for an initial xanthate concentration of 1×10^{-3} M. Dashed lines are same fractional surface coverages as indicated in figure 4.12.....153
- Figure A.1. Schematic AES depth profile of Au-Ag (50:50) alloy at room temperature.....168

Figure A.2.	Voltammograms for 80:20 Au-Ag alloy in the absence and presence of 2×10^{-4} M DIBDTPI at pH 9.2.....	169
Figure A.3.	Voltammograms for 50:50 Au-Ag alloy in the absence and presence of 2×10^{-4} M DIBDTPI at pH 9.2.....	170
Figure A.4.	Voltammograms for 80:20 Au-Ag alloy in the absence and presence of 1×10^{-4} M DIBMTPI at pH 9.2.....	171
Figure A.5.	Voltammograms for 50:50 Au-Ag alloy in the absence and presence of 1×10^{-4} M DIBMTPI at pH 9.2.....	172
Figure A.6.	FTIR reflection spectra of (a) 80:20 Au-Ag alloy at 650 mV and (b) 50:50 Au-Ag alloy at 650 mV in 2×10^{-4} M DEDTPI.	173
Figure A.7.	The effect of potential on the IR signal intensity (2960 cm^{-1}) of adsorbed DIBDTPI for 80:20 Au-Ag alloy in the presence of 2×10^{-4} M DIBDTPI at pH 9.2.....	174
Figure A.8.	The effect of potential on the IR signal intensity (2960 cm^{-1}) of adsorbed DIBDTPI for 50:50 Au-Ag alloy in the presence of 2×10^{-4} M DIBDTPI at pH 9.2.....	175
Figure A.9.	FTIR reflection spectra of Ag° at different potentials in 2×10^{-4} M DEDTPI.....	176
Figure A.10.	FTIR reflection spectra of 80:20 Au-Ag alloy at different potentials in 2×10^{-4} M DEDTPI.....	177

List of Tables

Table 2.1. The wavenumbers of the corresponding bonding of dicresyl
monothiophosphate.....41

Table 3.1. Thiophosphate and thiophosphinate collectors.....54

Chapter 1. Introduction

1.1. General

Gold is widely distributed and the average content in the earth's crust is estimated to be 3.5 ppb (West, 1978; Glynn et al., 1979). The gold content of ocean water varies considerably with location. Reported values range from 40 ppb to 3 ppt (Putnam, 1953). However, recent investigations indicate that the average value is of the order of 10 ppt which is quite below the concentration (3 ppm) required for economic recovery. Larger local concentrations of gold - about 75-90% pure - in the metallic state occur in sedimentary and igneous rocks in combination with gangue minerals, usually quartz, and with silver and base metal sulfides, selenides, and tellurides. Gold is further obtained as a by-product in the electrolytic refining of copper and nickel.

Gold is produced in many countries, the leading one being the South Africa, followed by the USSR and Canada (Glynn, 1979). In the United States, about 60% of the gold production originates from ores and the remainder primarily from the refining of base metals, e.g., copper, zinc, lead and mercury. The largest United States gold producer is Homestake Mine at Lead, S. Dakota, which supplies around 30% of the U.S. production (West, 1978).

Beside being used as jewelry and for monetary standard, gold is used extensively for industrial use. To meet the increasing demands for gold, it is necessary to develop more efficient methods for producing gold. The cyanidation technique is used widely, but increasing environmental awareness and concerns necessitates new technology development. Of the various methods of producing gold, flotation is regarded the most

environmentally sound and economically acceptable technique.

The purpose of the present investigation is to study the reaction mechanisms between precious metals and modified thiol-type collectors. These reagents represent the most promising of the various new precious metals collectors that are being developed by mining chemicals companies. The reaction mechanisms will be studied using various electrochemical and spectroscopic techniques, and the results compared with appropriate thermodynamic data. The informations obtained from the present work will be useful not only for improving the recovery processes for gold and other precious metals but also for advancing the state of our knowledge on flotation chemistry in general.

1.2. Gold Recovery Processes

Placer mining is the oldest form of gold mining. Auriferous sand is swirled with water in a pan and gold, which settles out owing to its high density, is collected. On a large scale, the mixture of sand and water is passed through a sluice box fitted with transverse riffles behind which the gold accumulates (Gaudin, 1939). The technique is still in use but requires large quantities of water. It could become important again for dredging large alluvial and marine deposits (Harvey, 1973). Air classification also is possible but inefficient. At present, most gold is obtained by deep mining.

Mined gold ore is milled sufficiently to allow separation of the gold; recoveries usually are 92-96% of the ore's gold content (Jones, 1970). After milling, various recovery processes may be used such as amalgamation, cyanidation, gravity concentration, flotation, and roasting, or a combination of these processes. Roasting is carried out when the gold ore contains other metals, sulfides, and tellurides (Ramdohr, 1979). Gold in association with metals, such as copper, nickel and lead, follows

these metals in the concentration process and eventually can be separated and recovered in the anode slimes of electrolytic refining.

Amalgamation is carried out by passing a water slurry of the ground ore over mercury-coated copper plates to which the gold particles adhere. The amalgam of gold is scraped periodically. Much of the mercury can be removed and recycled; any remaining mercury can be removed by distillation (Parker, 1957).

In cyanidation, the ore (or tailings from amalgamation) is leached with a solution of sodium cyanide (0.02-0.05%) or an equivalent of calcium cyanide together with some lime. The leaching solution is aerated to provide oxygen and gold is dissolved with formation of $\text{Na}[\text{Au}(\text{CN})_2]$. The rate of dissolution is directly proportional to the oxygen content of the gas used for aeration (Norwood, 1969). The cyanide solution also dissolves silver and some of the base metals which may lead to high cyanide consumption. A recent development is heap leaching in which the cyanide solution is distributed over the top of an open mound or leveled heap of the finely ground ore (Seeton, 1979).

Although cyanidation is almost ubiquitous in gold-ore treatment, it is unlikely that this process will remain as the major method of processing gold-ore because of the environmental problems it causes. Therefore, environmentally more safe method should be emphasized and, in that sense, flotation will be the adequate technique which fulfills this needs. Also, in combination with roasting and cyanidation, it has been found that more gold was recovered when flotation is adopted in the processing flowsheet (Elvey, 1977). Thus, in the treatment of gold-ore, the importance of flotation will be more significant in the future.

1.3. Flotation of Precious Metals

Precious metals are found in ore and placer deposits in their native state and in the form of chemical compounds - as tellurides (gold and silver) and sulfides (silver). In addition, they form finely divided inclusions in sulfides, and sometimes precious metal sulfides form a solid solution in another sulfide (Subrahmanyam et al., 1988). Flotation is sometimes employed before further extraction of the precious metals; it is also used in a very wide range of combinations with hydrometallurgical and pyrometallurgical processing of material containing precious metals (Fraser et al., 1991). The extraction of gold and silver in flotation of lead-zinc and copper ores is of great importance and the extraction of gold-bearing pyrite concentrate is usually intended for the flotation of free gold and of gold associated with pyrite.

Flotation of precious metals has a number of peculiar features due to the properties of precious metals and their association with other minerals. The free grains which are not associated with sulfides have characteristic properties due to the state of the metal surface. In addition, flotation depends on the mineralogical characteristics of the precious metal ores, due to association with sulfides and other minerals; it is often necessary to float the associated (principally sulfide) minerals in order to concentrate the precious metals (Jha et al., 1984). This is due to the fineness of precious metal impregnation in sulfides. Sometimes, the precious metals are so finely disseminated that there is no economically acceptable and technically efficient method of exposing the precious metal grains.

1.3.1. Gold Flotation

Gold may be floated as the native metal telluride or as a constituent of gold-bearing minerals, principally copper and lead sulfides, pyrite or arsenopyrite. Native gold is encountered in ores and in sands from placer deposits as an alloy with silver (5-30%), copper (up to 8%), and with other metals. Gold tellurides are often encountered in an isomorphic mixture with silver such as calaverite, $(\text{Au,Ag})\text{Te}_2$, and petzite, $(\text{Au,Ag})_2\text{Te}$ (Henley, 1975). Gold prevails in the former and silver in the latter. Gold occurs in a wide range of particle sizes and only relatively small particles of gold are susceptible to flotation.

Gold in quartz can be readily floated, although this form of concentration is not widely used due to the great difficulty of producing a stable froth in the absence of sulfides. Also, the recovery is lower than when cyanidation is used. Flotation may be difficult in the presence of micaceous, graphitic or other lamellar minerals. The presence of free gold usually necessitates stronger collectors and an increased frother addition. The duration of reagent contact should be increased if the gold has a film of oxides on the surface.

Ethyl or butyl xanthates are used for collective flotation of gold-bearing quartz ores with sulfide mineralization. Amyl xanthate is added for ores which have been subjected to initial oxidation. One of the dithiophosphates (diisoamyl) may also be used as a second collector. Cresol, pine oil and dithiophosphates can be used as frothers (Kudryk, 1984).

1.3.2. Silver Flotation

Argentiferous minerals are usually encountered in the form of sulfides and complex sulfarsenides and sulfantimonides, and less often as

native silver and silver chloride. The usual silver minerals are: argentite, Ag_2S ; polybasite, $9(\text{Ag,Cu})\text{S}+(\text{Sb,As})_2\text{S}_3$; proustite, $3\text{Ag}_2\text{S}+\text{As}_2\text{S}_3$; pyrargyrite, $3\text{Ag}_2\text{S}+\text{Sb}_2\text{S}_3$; and stephanite, $5\text{Ag}_2\text{S}+\text{Sb}_2\text{S}_3$ (Henley, 1975). Silver is also found as an impurity in tetrahedrite, tennantite ($3(\text{Cu,Ag})_2\text{S}+\text{Sb}_2\text{S}_3$), and lead glance. Strong sulfhydryl collectors are used for extraction of silver sulfide minerals. Combinations of reagents are commonly used for the flotation of silver-bearing ores; these combinations include mixtures of dithiophosphates, creosote oil, and dithiophosphate and ethyl xanthate.

1.4. Reagents

Sulfhydryl collectors are commonly used for the flotation of native precious metals and the sulfides with which they are often associated; these include xanthate (ethyl, butyl, and amyl) and dithiophosphoric acid esters (diisoamyl, dicresyl) (Rao, 1971). In the present study, Monothiosphosphate (MTP), Mono- and Di-thiophosphinate (MTPI, DTPI) and Ethyl Xanthate (EX) have been chosen as collectors for the flotation of precious metals.

MTP is known as a selective collector for gold under certain pH conditions (Nagaraj et al., 1987). It is derived from its corresponding dithiophosphate by replacing one of the S atoms with O. This single change in the nature of the dithio acids is sufficient to alter its collector properties in view of the difference in electronegativities between S and O. Monothio acids have been found to be more stable, stronger acids, and stronger collectors than their dithio analogs (Nagaraj and Avotins, 1988). The dialkyl MTP was found to be truly acid circuit collectors in contrast to the dithio acids which are better collectors in the alkaline pH range. This fact results in savings in the lime consumption and, therefore, the operating cost. The reason for MTP being used as an acid circuit collector may be due to the tautomerism of the

molecule. It is known that the thiol form is stable in the acidic solution and the thione form in alkaline solutions (Kozachenko et al., 1976).

MTPI and DTPI are newly developed collectors by American Cyanamid Company for the flotation of base metal sulfides and precious metals. The differences in the collector properties between the thiophosphates and thiophosphinates are attributed to the differences in the bonding of the alkyl substituents to the central phosphorous atom. In thiophosphates, the alkyl groups are attached to the P through oxygens, whereas in the phosphinates, the alkyl groups are directly attached to the P. The thiophosphinates are found to be somewhat weaker acids than the thiophosphates, and they are neither truly acid circuit collectors nor truly alkaline circuit collectors (Nagaraj et al., 1989). MTP and MTPI are different from the conventional thiol collectors in that they contain O donors, in addition to the S donors. The O donors either participate directly in bond formation with the mineral species, or influence the pK of the reagent by changing the electron density distribution of the S donor (Somasundaran et al., 1986, Bogdanov et al., 1977). The difference between MTPI and DTPI lies in the number of S donors in polar head group. This difference results in difference in reactivity and, hence, requires different operating conditions.

The reason for the choice of these modified thiol collectors is that they are known to be very effective for the selective flotation of precious metals and to give improved recoveries. Further details of these collectors concerning molecular structure and industrial use will be presented in each chapter.

EX has been used most widely for the flotation of sulfide minerals and precious metals. In the present work, the reactivity of the conventional EX with precious metals has also been studied extensively and

compared with those of the modified thiol collectors.

1.5. Objectives of the Study

The main objective of this study is to study the adsorption mechanisms of MTP, MTPI, DTPI and EX with gold and silver. Since these precious metals commonly occur as alloys, the reaction mechanisms involving gold-silver alloys (80:20 and 50:50 wt.%) will also be studied. The adsorption mechanisms will be studied by means of contact angle measurements. Since the adsorption mechanisms will be critically dependent on the electrochemical properties of the system, the contact angle measurements will be conducted under carefully controlled potential conditions.

The adsorption mechanisms will also be studied by means of cyclic voltammetry. This technique will be useful for obtaining kinetic information. By comparing the results with thermodynamic data, it is possible to determine the reaction mechanisms.

The objectives of the present work will be met by studying the adsorption mechanisms, using an FTIR reflection technique under controlled potential conditions. Although the technique is based on *ex situ* measurements, it offers a convenient method of monitoring adsorbed species as functions of applied electrochemical potential, pH, collector concentration and contact time. By using polarized light as incident beam, one also obtains information concerning orientation of the adsorbed species.

Results of the contact angle, voltammetry and FTIR studies will be compared with the thermodynamic data. The E_h -pH diagrams for the silver/water, gold-silver alloy/water systems in the presence of the various collectors will be conducted using the SOLGASWATER computer program. Some of the thermodynamic data not available in literature will

be determined in the present work.

The adsorption mechanisms of EX on silver will be studied by monitoring the solution chemistry using a fast-scan UV/Vis spectrophotometer. This technique offers an *in situ* method of studying the adsorption mechanisms under controlled potential conditions. The xanthate adsorption mechanisms will be compared with those of the modified thiol collectors.

Chapter 2. Monothiophosphate System

2.1. Introduction

Xanthate is the most common collector used in the flotation of sulfide minerals and precious metals, and its reaction mechanisms with a variety of minerals have been studied extensively. It is well established that reaction of xanthate occurs via a mixed potential mechanism, involving anodic oxidation of xanthate and cathodic reduction of oxygen. When the reaction results in dixanthogen formation, the mineral itself does not participate in the reaction except offering a passage for the transfer of electrons. This would be the case for the adsorption of xanthates on gold, pyrite and pyrrhotite.

Xanthate reaction with some of the other sulfide minerals such as chalcocite, galena and silver results in the formation of metal xanthates, in which case the mineral itself is participating in the adsorption mechanism. The process of metal xanthate (MX_2) formation may be viewed as a two-step process, involving an initial electrochemical reaction (E);



followed by a chemical reaction (C),



The overall reaction then becomes:



which is a coupled electrochemical and chemical reaction. Such a mechanism is referred to as EC-mechanism and is commonly recognized in organic electrochemistry (Nicholson and Shain, 1964; Southampton Electrochemistry Group, 1985). The rate of reaction (2) often determines the electrochemical behavior of the electrode.

In the EC mechanism, the electrochemical reaction is controlled by the electrochemical potential (E_h) of the system, while the chemical step is controlled by its stability constant (pK), as suggested by the chemical theory of collector adsorption (Taggart et al., 1934). It may be stated, therefore, that the adsorption of thiol collectors on sulfides is controlled by both the E_h and pK values of the system. The E_h determines the availability of metal ions, while the pK of the metal thiol complex determines whether this complex can be formed or not. The interrelationship between E_h and pK may be best illustrated by the chalcopyrite-xanthate system. Since this mineral is relatively noble, not enough copper ions (Cu^+) become available to form copper xanthate during the initial potential scan of a chalcopyrite electrode, but as the potential scan continues xanthate is oxidized to dixanthogen. As the potential is further raised, the mineral eventually releases enough Cu^+ ions for reaction (2) to occur. Thus, both dixanthogen and copper xanthate are formed on chalcopyrite depending on the potential of the electrode (Leppinen et al., 1989).

In the previous work, the EC mechanism was used to explain the adsorption of modified thiol-type collectors, such as thionocarbamates and thioureas on copper and copper sulfides (Basilio et al., 1991). This work has been extended in the present chapter to precious metal-monothiophosphate systems using electrochemical and spectroscopic methods.

The monothiophosphate is derived from the corresponding dithiophosphate by replacing one of the sulfur atoms with oxygen. This

change affects the electron distribution on the donors and, hence, the pK and metal complexation properties (Nagaraj et al. 1988; Nagaraj and Basilio et al., 1989). The dialkyl monothiophosphate was found to be a true acid-circuit collector for sulfide minerals and was shown to improve precious metals recovery (Hensen and Killey, 1990).

2.2. Experiments

2.2.1. Materials

The silver and gold plates (0.5 mm thick, 99.9985% pure) were acquired from Johnson Matthey, while the gold-silver (Au-Ag) alloys were provided by Kultakeskus Oy (Gold Center), Finland. The same precious metal plates were used in both voltammetry and FTIR measurements. The dicresyl monothiophosphate (DCMTP, >98% pure) was provided by the American Cyanamid Company. The silver dicresyl monothiophosphate (AgDCMTP) complex was precipitated by mixing silver nitrate and DCMTP solutions at neutral pH conditions. Elemental analysis of the precipitate verified it to be AgDCMTP. That is, the ratio between Ag and DCMTP in the precipitated complex was 1 to 1.

The experiments were carried out in 0.5 M CH_3COOH /0.5 M CH_3COONa (pH 4.6) and 0.05 M $\text{Na}_2\text{B}_4\text{O}_7$ solutions (pH 9.2). For the FTIR spectroscopic and contact angle measurements, the solution pH was controlled by adding either 0.2 N HNO_3 or KOH solution. All reagents were of analytical grade, and all the solutions were prepared with 18 M Ω water. Prior to each series of electrochemical experiments, the solution was deoxygenated by purging with low-oxygen nitrogen gas (<0.05 ppm O_2) for at least one hour.

2.2.2. Voltammetry

Cyclic voltammetry experiments were carried out using a conventional three-electrode circuit with a working electrode holder constructed specially for the precious metal plates. Figure 2.1 shows the schematic diagram of the experimental set-up used for the linear sweep voltammetry. The electrode potential was controlled in the electrochemical and spectroscopic measurements with a Pine Instrument Co. Model RDE4 Potentiostat/Galvanostat and a PARC Model 175 Universal Programmer. Although an Ag/AgCl electrode was used as the reference electrode, the potentials reported here are all expressed on the standard hydrogen electrode (SHE) scale. A scan rate of 50 mV/sec was used in all the voltammetry experiments.

2.2.3. FTIR Spectroscopy

The spectra of the electrode surfaces were recorded using a Perkin Elmer Model 1710 FTIR Spectrometer equipped with a liquid nitrogen-cooled MCT detector. For this experiment, a plate-type specimen made to fit the specimen holder (about 1 cm x 4 cm) was used. In each experiment, a total of 100 spectra was recorded and signal-averaged with a spectral resolution of 4 cm⁻¹. The FTIR reflection spectroscopic measurements were done using a Barnes Model 501 Variable Angle Specular Reflectance accessory and a Harrick Wire Grid Polarizer.

2.2.4. Contact Angle Measurements

A modified electrochemical cell with parallel optical glass windows was used for the contact angle study. The schematic representation of this cell is shown in Figure 2.2. The electrode was made by mounting a small piece of precious metal using epoxy resin in a glass tube. Except

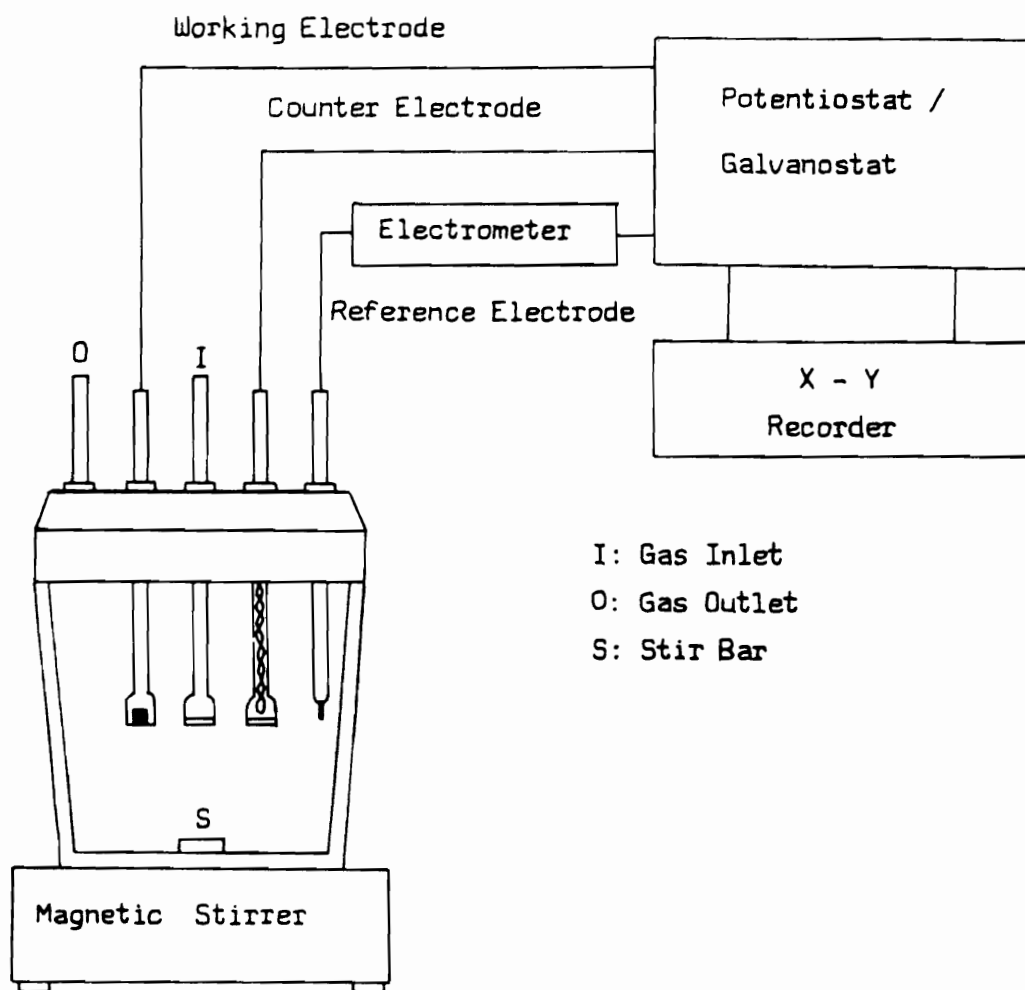


Figure 2.1. Schematic diagram showing the experimental set-up used for the linear sweep voltammetry.

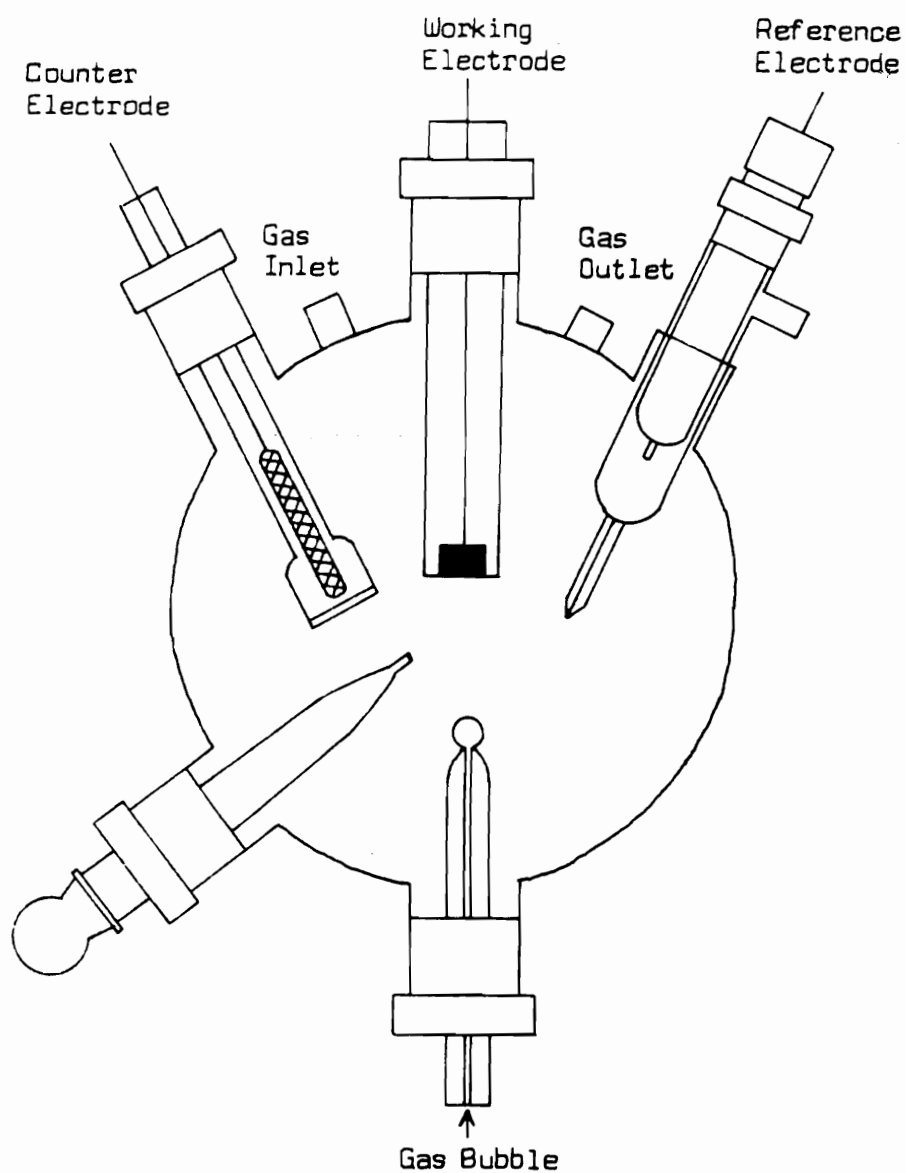


Figure 2.2. Schematic diagram of the modified electrochemical cell used for the contact angle measurements.

for the cell, the electrochemical set-up was similar to the one used for the voltammetric experiments. The contact angle was measured by depositing a nitrogen bubble on the electrode surface and using a Rame Hart Model 1000 Goniometer.

2.2.5. E_h -pH Diagram

In constructing the E_h -pH diagram for silver/water/monothiophosphate system, it was necessary to obtain the difference in standard Gibbs free energy of formation (ΔG°) between AgDCMTP precipitate and aqueous monothiophosphate ions. For this purpose, the solution containing a certain amount of Ag^+ ion was titrated by DCMTP solution while measuring the potential of the system. The end point was taken when the potential reached a constant value. It was possible to calculate the solubility product of the AgDCMTP complex from the volume of DCMTP solution required to reach the end point, the initial volume of silver nitrate solution, and the concentrations of both species. The pK value was verified by repeating the titration using a DCMTP solution of a different concentration with the same silver nitrate solution. The thermodynamic calculations used for the construction of the E_h -pH diagram were made using a version of the SOLGASWATER program developed by the Department of Chemistry, University of Umea, Sweden. This program is based on the free energy minimization technique (Eriksson, 1979) and can handle up to 80 species, including a maximum of 48 solid phases.

2.3. Results and Discussion

2.3.1. Voltammetry

The voltammograms of Ag^0 in the absence and presence of 1×10^{-4} M DCMTp at pH 4.6 and 9.2 are shown in Figure 2.3. At pH 4.6 in the absence of DCMTp, an anodic peak starting around 275 mV is found, which is due to the oxidation of Ag^0 to Ag^+ . At higher potentials, further oxidation of Ag^+ to AgO^+ is indicated by the continued increase in current. On the return scan, cathodic peaks are observed near 550 and 400 mV, which are due to the reverse of the oxidation reactions. The addition of DCMTp results in an anodic current rise above 100 mV. This is probably due to the following reaction:



The interaction of DCMTp with Ag^0 as proposed in reaction (4) could be the result of coupled chemical reactions of the EC-type. This explanation is similar to that proposed for the adsorption of modified thiol-type collectors, including DCMTp, on copper and sulfide minerals (Basilio et al., 1991). The electrochemical step (E) involves the oxidation of Ag^0 ;



while the chemical reaction (C) that follows is;



In this system, reaction (5) should be controlled by the E_h of the

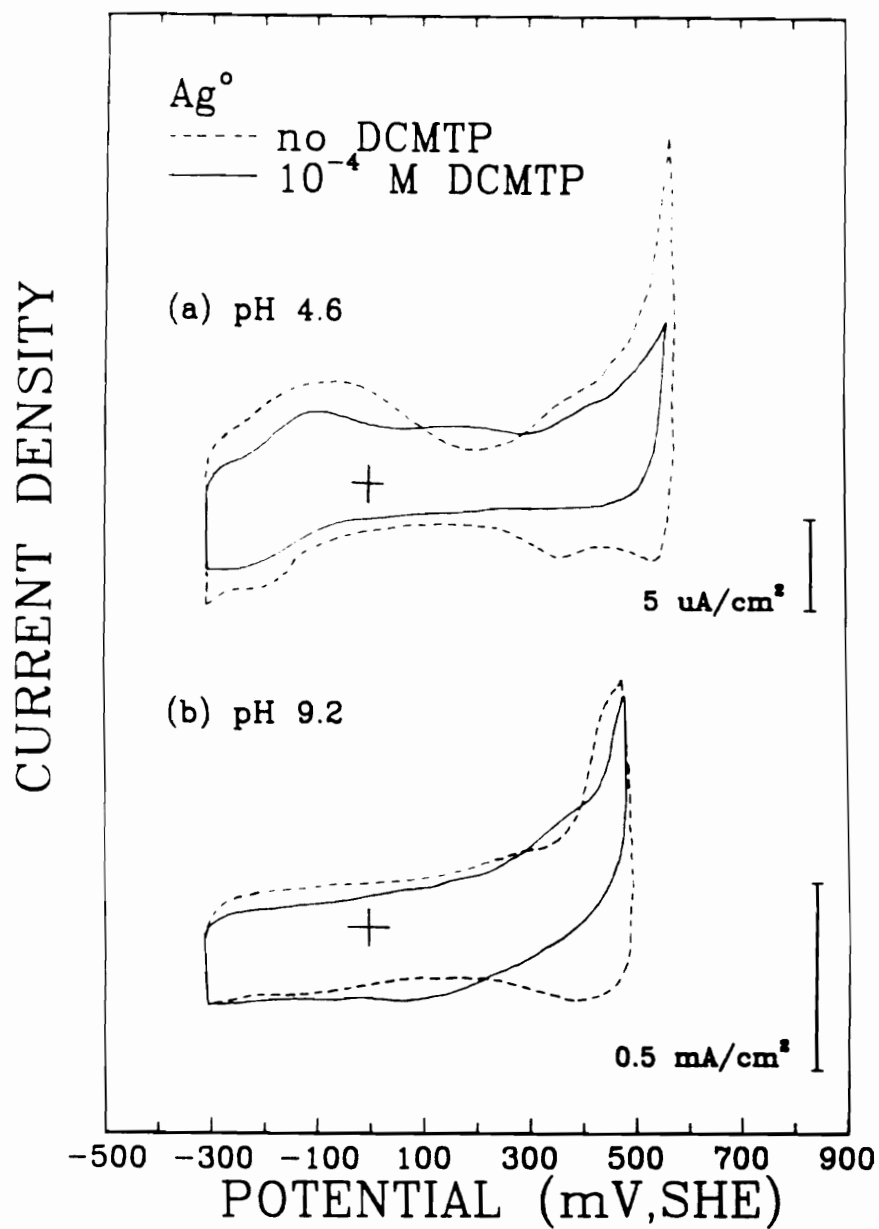


Figure 2.3. Voltammograms of Ag° at (a) pH 4.6 and (b) pH 9.2 in the absence and presence of $1 \times 10^{-4} \text{ M}$ DCMTP.

system, while reaction (6) should be controlled by the pK value of the AgDCMTP compound. Thus, both E_h and pK affect the adsorption of DCMTP on Ag^0 .

On the return scan, there were no reduction peaks corresponding to the reverse of DCMTP adsorption. This may be attributed to the slow kinetics of dissociation of the AgDCMTP complex which is the reverse of reaction (6). In cases where the kinetics of the chemical reaction step is fast (e.g., metal xanthate formation), the reverse of the anodic reactions may be more readily observed in the voltammograms.

It should be noted that although strong DCMTP interaction is observed only above 100 mV, passivation of the electrode is apparent at lower potentials. The electrode passivation may be attributed to a weak interaction of DCMTP, such as physisorption, at the starting potential. In the FTIR studies, which will be discussed later, there are some indications of slight DCMTP physisorption occurring at potentials lower than 100 mV.

At pH 9.2 and no collector addition, the oxidation of Ag^0 to Ag_2O is shown by the anodic current starting above 300 mV. On the return scan, the reduction of Ag_2O is indicated by the cathodic peak found near 390 mV. In the presence of 1×10^{-4} M DCMTP, passivation of the electrode surface is observed in the voltammogram (Figure 2.3(b)). The interaction of DCMTP with Ag^0 is indicated by the anodic peak starting above 250 mV, which is higher than that observed at pH 4.6. This potential shift may be attributed to the possible tautomerism in this collector (Nagaraj et al., 1989).

The tautomerism exhibited by monothioacids in non-aqueous solvents is well known (Kabachnik et al., 1955). This was suggested previously to be responsible for the change in the collector property of monothiophosphates at different pH conditions (Nagaraj, Basilio et al., 1989, Nagaraj, Brinen

et al., 1991). The thione form of DCMTP, as given below,



is expected to predominate in alkali conditions due to the high electronegativity of O compared with S. However, as the pH is decreased, the availability of excess protons is expected to favor the existence of the thiol form. In the flotation of sulfide minerals, the thiol form should be a much more powerful donor than the thione, which is why monothiophosphates are effective in acid circuits (Nagaraj et al., 1989). At the same time, the noble metals, such as Ag^0 , show considerably higher affinity for S donors; thus, Ag^0 can still form a complex with the thiol form (Cotton, 1980, Nagaraj, 1987).

The shift to a higher potential in the interaction of DCMTP with Ag^0 at pH 9.2 suggests that the Ag-thione complex has a lower pK value than the Ag-thiol complex. As the pK value becomes lower, a higher potential is required to liberate enough Ag^+ ions to form AgDCMTP complex. Thus, the shift in potential of the DCMTP adsorption shows how E_h and pK control the adsorption of the collector.

Figure 2.4 shows the voltammograms obtained for Au^0 in the absence and presence of 1×10^{-4} M DCMTP at pH 4.6 and 9.2. The addition of DCMTP results in the passivation of the electrode surface over the entire scan range. However, there are no indications of an electrochemical interaction between DCMTP and the Au^0 surface in these voltammograms. The results of the IR spectroscopic measurements carried out in 1×10^{-4} M DCMTP solutions (not shown here) also do not indicate DCMTP adsorption on Au^0 . The passivation of the electrode surface, therefore, may be

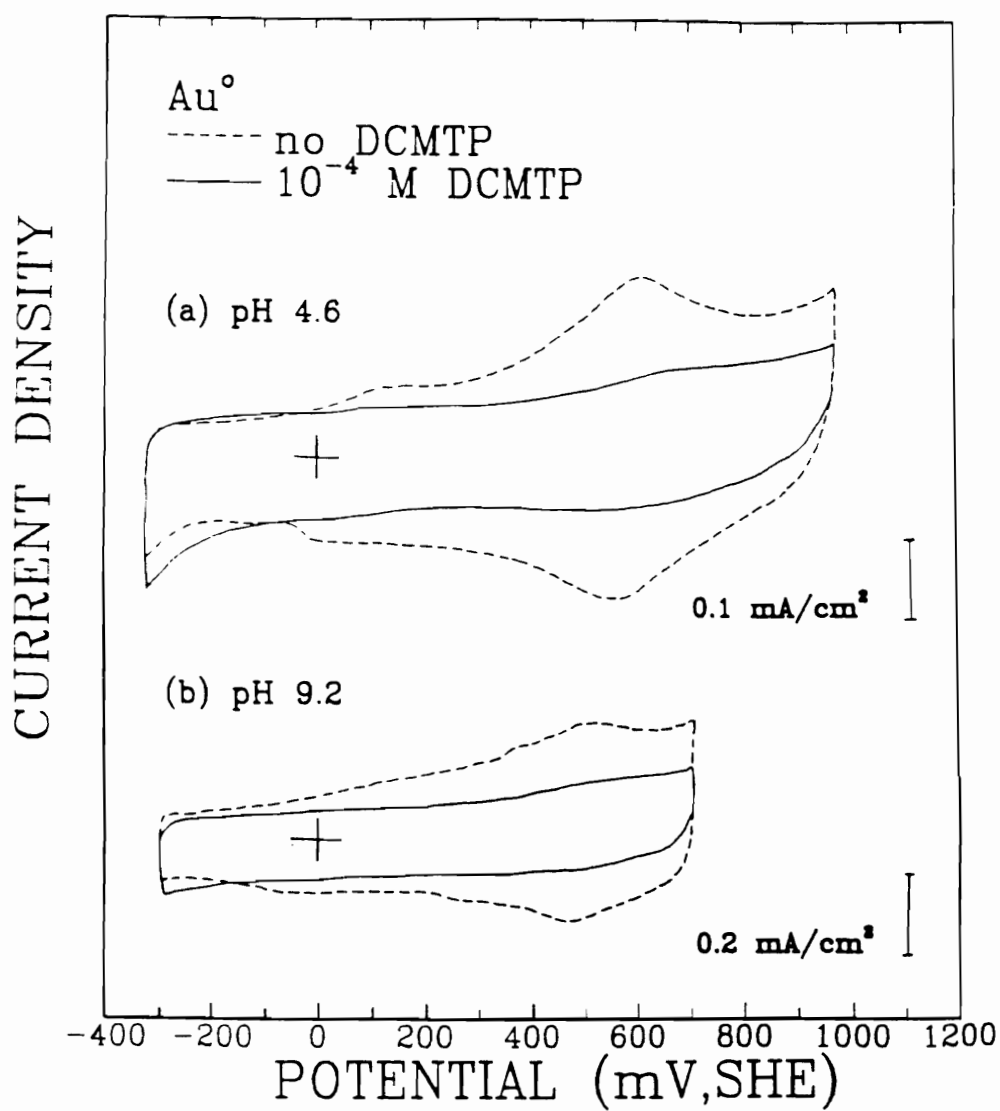


Figure 2.4. Voltammograms of Au° at (a) pH 4.6 and (b) pH 9.2 in the absence and presence of 1×10^{-4} M DCMTP.

attributed to the weak physisorption of DCMTF. The weakly physisorbed collector species on gold are probably desorbed when the electrode is rinsed prior to the *ex situ* IR measurements. *In situ* IR measurements similar to those employed previously (Leppinen, Basilio et al., 1989) may be necessary to detect such physisorbed species.

Contact angle measurements carried out under controlled-potential conditions in 1×10^{-4} M DCMTF solutions showed that the Au^0 electrode is completely hydrophilic over the entire potential range measured. This may suggest that even if there are any physisorbed species on gold, its orientation may be such that the surface is rendered hydrophilic. It may be concluded that the improved flotation recovery of gold from gold ores observed previously using DCMTF (Nagaraj, Brinen, et al., 1991) probably does not involve any Au-DCMTF interaction.

Other surface spectroscopic measurements such as XPS and SIMS (Nagaraj et al., 1991) also showed that DCMTF adsorption on gold is negligible. It should be pointed out that slight DCMTF adsorption was observed by Nagaraj et al. (1991) at very high collector concentrations and potentials greater than 500 mV. This is also observed in the IR spectroscopic measurements conducted in this work at very high DCMTF addition. However, the IR reflectance spectra (not presented here) showed only the peaks for the cresyl group vibrations, which may suggest that DCMTF is only physisorbed on the Au^0 surface. The absence of peaks of other bonding except that of cresyl group probably indicates that there is no chemical adsorption reaction between DCMTF and Au^0 .

The voltammograms of an Au-Ag alloy (80:20) with and without the addition of 1×10^{-4} M DCMTF at pH 4.6 and 9.2 are shown in Figure 2.5. In the presence of DCMTF, the interaction of the collector with the alloy is observed above 250 and 400 mV at pH 4.6 and 9.2, respectively. These potential values are significantly higher than those observed for DCMTF

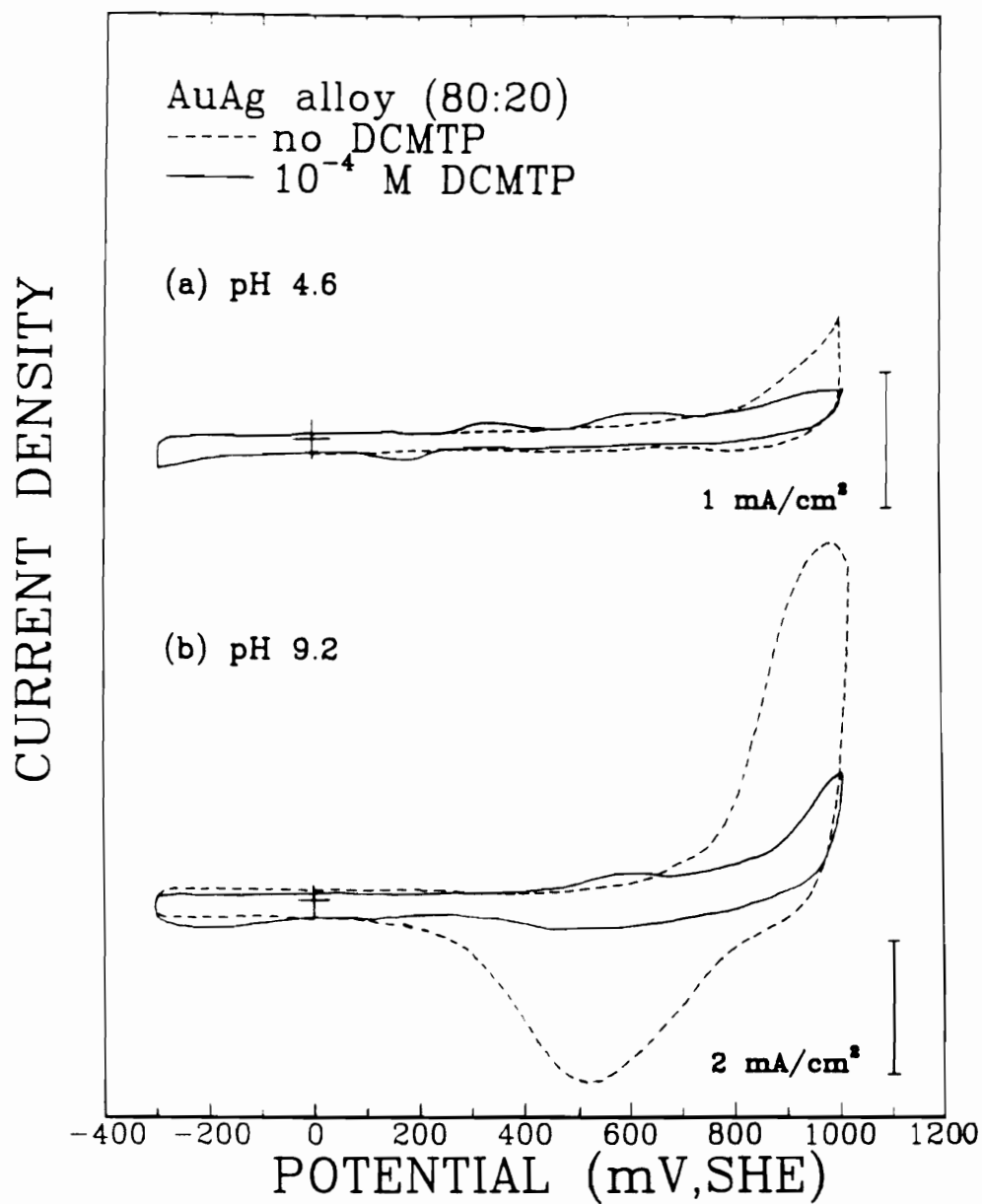


Figure 2.5. Voltammograms of AuAg alloy (80:20) at (a) pH 4.6 and (b) pH 9.2 in the absence and presence of 1×10^{-4} M DCMTP.

interaction with pure Ag° . The adsorption peaks observed here may be attributed to DCMTTP interacting with Ag° rather than with Au° .

Figure 2.6 shows the voltammograms obtained for the 50:50 Au-Ag alloy. The potentials at which DCMTTP interactions start are about 50 mV lower than those observed for the 80:20 Au-Ag alloy. Thus, increasing silver in Au-Ag alloys lowers the potential for the AgDCMTTP formation, providing further support that the reaction involves interaction with the Ag° .

2.3.2. FTIR Spectroscopy

2.3.2.1. Standard Spectra

The FTIR spectrum of DCMTTP given in Figure 2.7 shows a sharp band at 1507 cm^{-1} , which is due to the aromatic ring vibrations from the cresyl group of this collector (Katritzky, 1959). The signal observed at 1401 cm^{-1} is due to N-H stretching vibrations (Miller et al., 1952, Waldron, 1953), while those found in the region from $1225\text{--}1175\text{ cm}^{-1}$ may be attributed to both P=O and aromatic ring vibrations (Katritzky, 1959, Jones et al., 1960, Thomas, 1957, Bellamy, 1975). The strong band at 899 cm^{-1} is most likely due to P=O stretching vibrations (Jones and Katritzky, 1960, Thomas, 1957), while the P=S vibrations are found in the region below 722 cm^{-1} (Chittenden et al., 1964, Bellamy, 1968).

In the spectrum of AgDCMTTP (Figure 2.7), the N-H stretching vibrations found at 1401 cm^{-1} disappeared since the ammonium ion is removed from DCMTTP in aqueous solution. This fact was also verified by the NMR spectroscopy (not shown here). The P=O vibrations in the 1200 cm^{-1} region, as well as the P=S vibrations below 722 cm^{-1} , are both shifted to lower wavenumbers in the AgDCMTTP complex. These shifts can be attributed to the bonding of Ag° with DCMTTP through both sulfur and oxygen to form a four

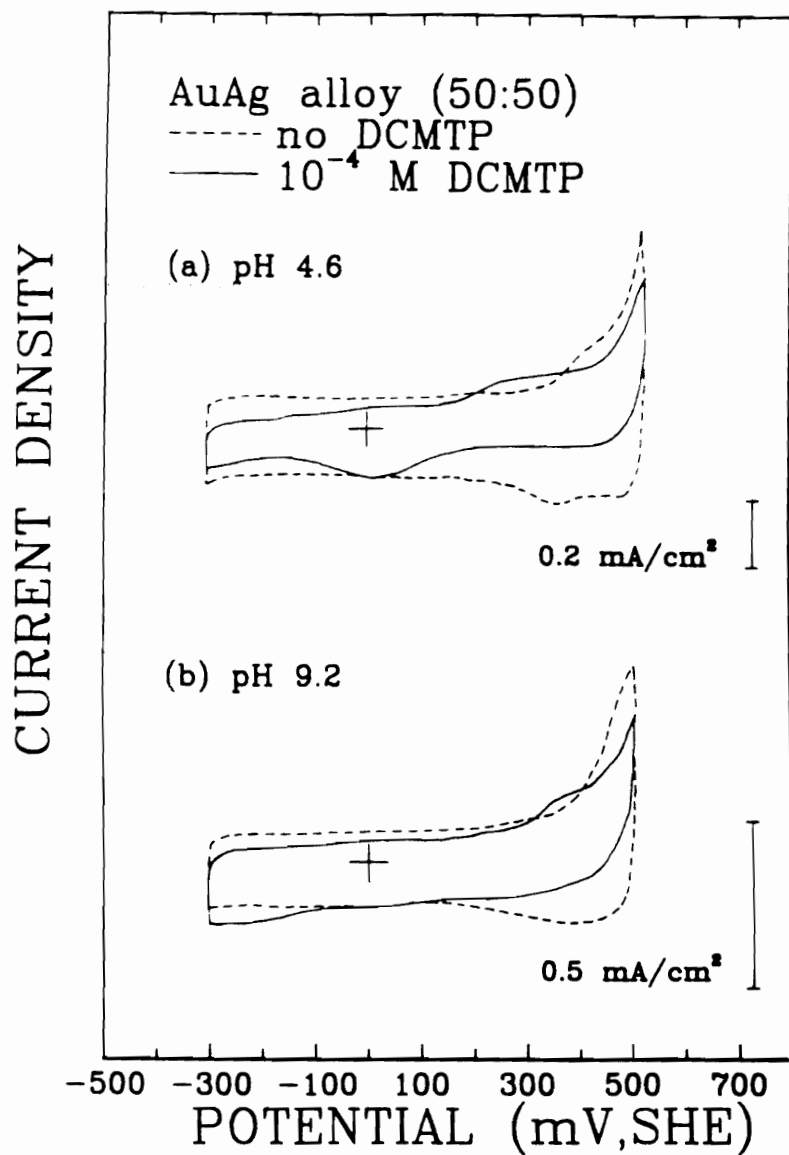


Figure 2.6. Voltammograms of AuAg alloy (50:50) at (a) pH 4.6 and (b) pH 9.2 in the absence and presence of 1×10^{-4} M DCMTTP.

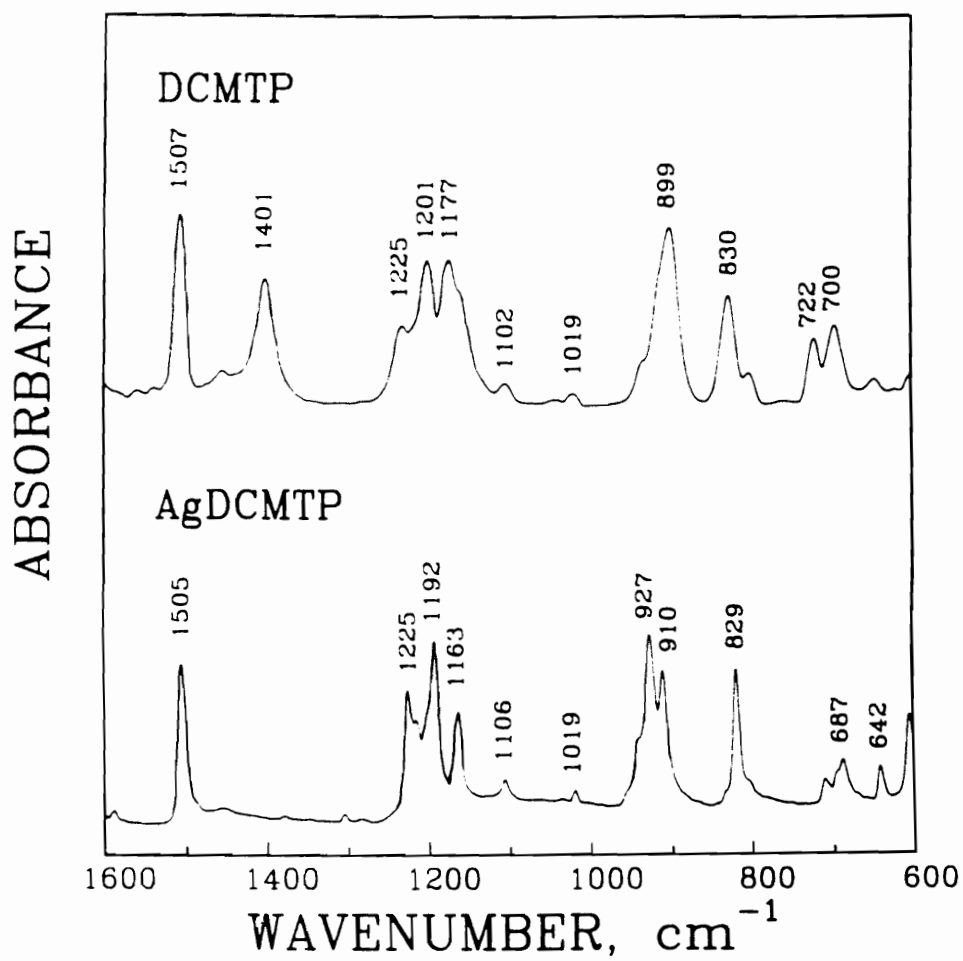


Figure 2.7. FTIR spectra of DCMTP and AgDCMTP.

membered ring compound. There was no spectrum obtained for a Au-DCMTP complex since there was no precipitate obtained after mixing gold(III) chloride and DCMTP solutions.

2.3.2.2. Effect of Potential

In the next series of experiments, The effect of potential on the adsorption of DCMTP on Ag° , Au° , and different Au-Ag alloys was investigated at pH 4.6 and 9.2. The precious metal plates were conditioned in 1×10^{-4} M DCMTP solutions and held under different potential conditions. The collector adsorption on Ag° and Au-Ag alloys is observed to be significantly lower at pH 9.2; hence, only the results obtained at pH 4.6 are presented here. Also, the IR reflectance data for Au° are not shown since there were no indications of DCMTP adsorption on Au° .

The IR reflection spectra of the surface DCMTP species adsorbed on Ag° at pH 4.6 and different potentials are shown in Figure 2.8. At potentials below 100 mV, there are indications of slight DCMTP adsorption. The observed signals have very low intensities and the spectra are similar to that of pure DCMTP. This would indicate that the species adsorbed at potentials below 100 mV is probably weakly physisorbed DCMTP. The spectra of DCMTP adsorbed on Ag° at higher potentials are quite different from that of DCMTP itself, but are similar to that of the AgDCMTP compound. Increasing the potential results in the shift of the characteristic peaks toward the direction of the bulk AgDCMTP compound. At potentials above 200 mV, the IR spectra are similar to that of the bulk AgDCMTP , indicating multi-layer formation of AgDCMTP . These findings suggest that the multi-layer formation is possible only when the Ag° electrode becomes sufficiently oxidized to release enough Ag^+ ions.

Figure 2.9 shows the effect of potential on the adsorption of DCMTP

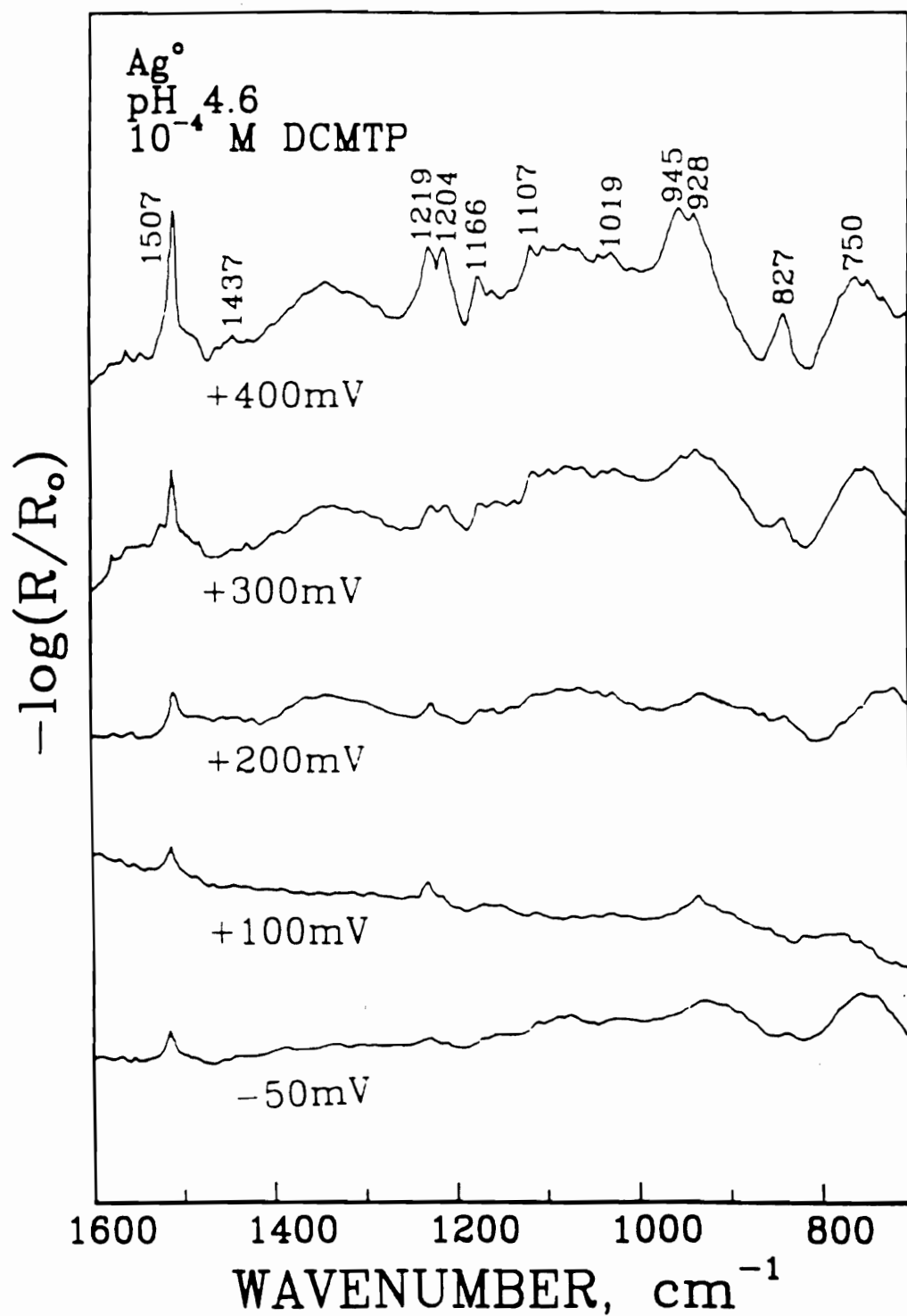


Figure 2.8. FTIR reflection spectra of Ag° conditioned in 1×10^{-4} M DCMTP at pH 4.6 and different potentials.

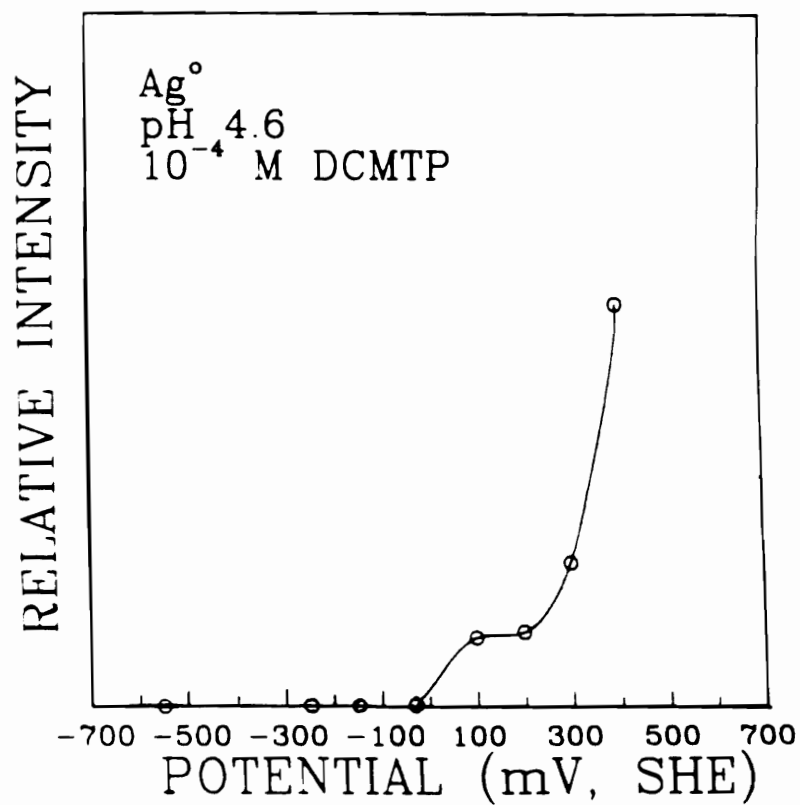


Figure 2.9. Effect of potential on the IR relative signal intensities of DCMTP adsorbed on Ag° at pH 4.6.

on Ag^0 at pH 4.6. The relative intensities were measured from the peak areas of the signals in the region between 1150 and 1250 cm^{-1} . The adsorption of DCMTp on Ag^0 starts above -50 mV and increases with increasing applied potential. There is a sharp increase in DCMTp adsorption above 200 mV, which may be attributed to multilayer formation associated with the release of Ag^+ ions. The data obtained from IR spectroscopy are in good agreement with the observations made from voltammetry.

The effect of potential on the adsorption of DCMTp on Au-Ag alloy (80:20) is shown in Figure 2.10. The IR reflection spectra obtained for this alloy are similar to that obtained for Ag^0 (Figure 2.8). Below 300 mV, there are no indications of DCMTp adsorption on the Au-Ag alloy (80:20). The signal intensities are very low and spectra are similar to that of pure DCMTp, indicating physisorption of DCMTp. At potentials \geq 300 mV, the chemisorbed DCMTp spectra similar to that found on Ag^0 are observed. As the potential is increased, the characteristic bands shift towards that of bulk AgDCMTp and the peak intensities increase. This is similar to the observations made for Ag^0 . At very oxidizing conditions, multi-layer formation of AgDCMTp is observed. Note that there are strong bands observed in the 1400-1450 cm^{-1} region at very high potentials. These bands may be attributed to acetate buffer adsorbing on the surface (Bellamy, 1975).

Figure 2.11 shows the plot of the relative IR intensity as a function of potential. The DCMTp adsorption starts at around 250 mV and then increases with increasing potential. This potential is higher than that observed for Ag^0 (Figure 2.9) and agrees well with the voltammetry results.

For the 50:50 Au-Ag alloy, the IR reflection spectra show that DCMTp chemisorption occurs at potentials above 200 mV (Figure 2.12). The spectra of the adsorbed species are similar to those obtained in the 80:20

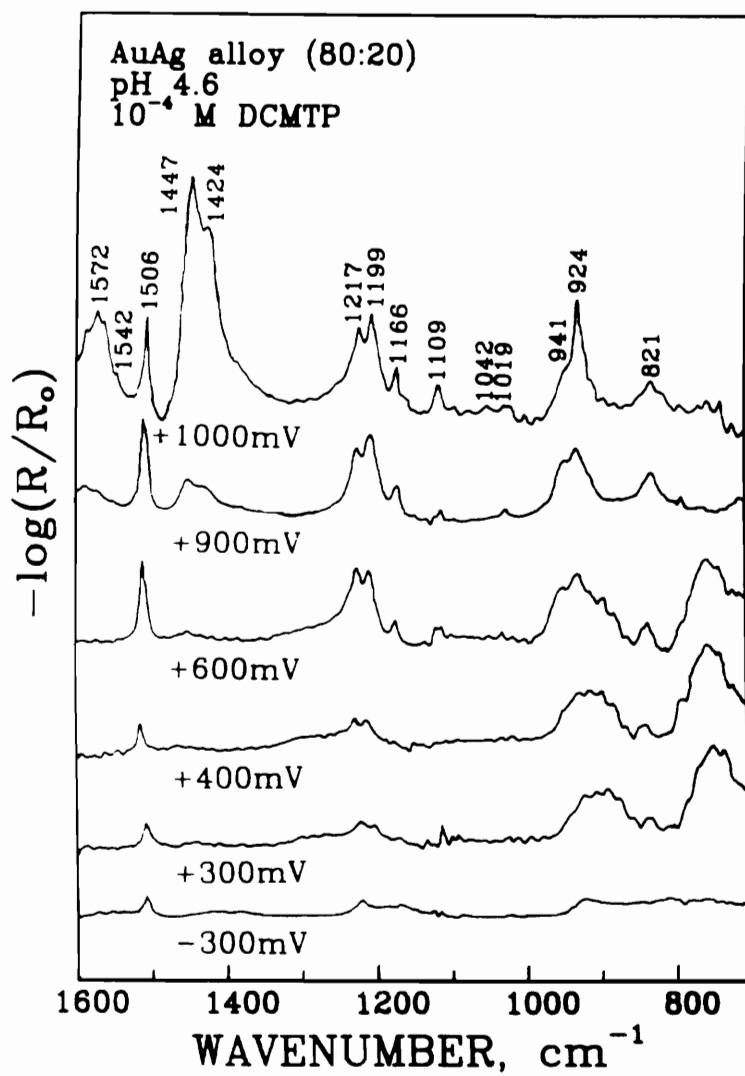


Figure 2.10. FTIR reflection spectra of AuAg alloy (80:20) conditioned in 1×10^{-4} M DCMTTP at pH 4.6 and different potentials.

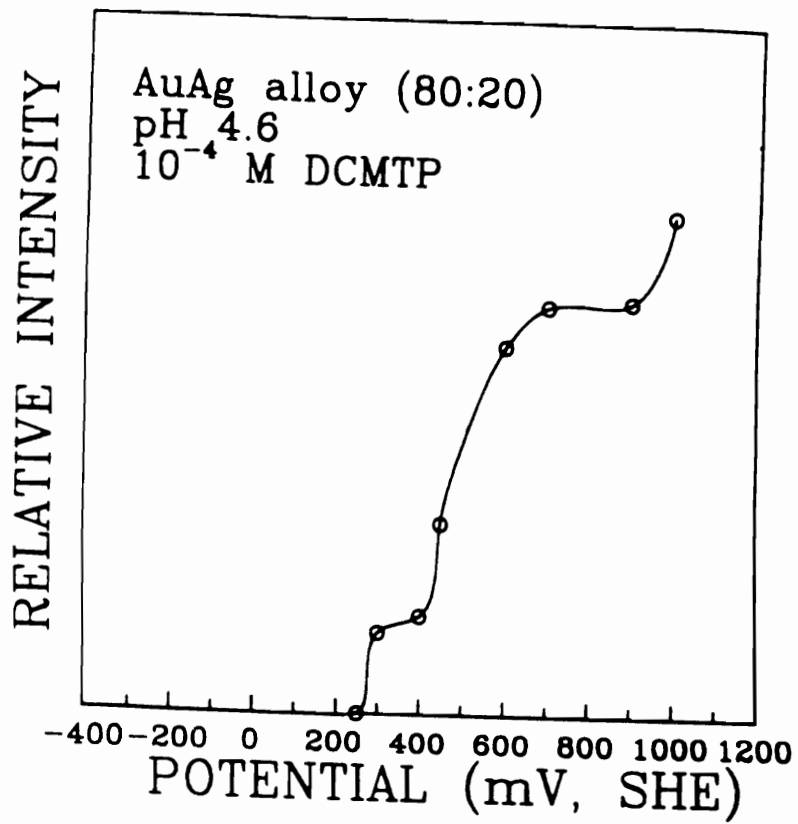


Figure 2.11. Effect of potential on the IR relative signal intensities of DCMTP adsorbed on AuAg alloy (80:20) at pH 4.6.

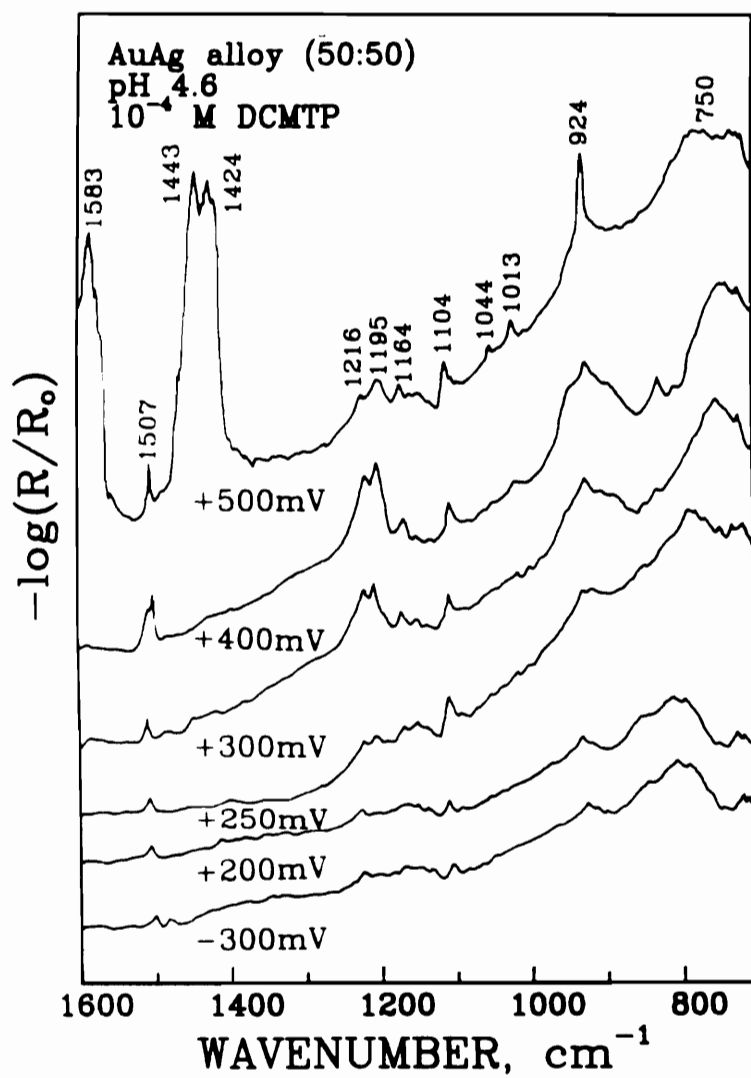


Figure 2.12. FTIR reflection spectra of AuAg alloy (50:50) conditioned in 1×10^{-4} M DCMTP at pH 4.6 and different potentials.

Au-Ag alloy and Ag° . At higher potentials, the absorption peaks shift in the direction of bulk AgDCMTP . This would indicate that the adsorbed species formed on the surfaces of the Au-Ag alloy is similar to that found on Ag° and on the other Au-Ag alloy. The bonding of DCMTP on this alloy is presumably through both oxygen and sulfur. The extraneous peaks attributed to acetate vibrations are also observed in this system at very high potentials.

Figure 2.13 shows that DCMTP adsorption on the 50:50 Au-Ag alloy occurs at a potential higher than that found for Ag° , but lower than the starting potential for adsorption on the 80:20 Au-Ag alloy. This suggests that the potential where DCMTP adsorption occurs on the Au-Ag alloy is dependent on the silver content of the alloy. Increasing the silver content results in the DCMTP adsorption occurring at lower potentials or closer to where they are observed on pure Ag° . This trend is also observed in the voltammograms obtained for these two Au-Ag alloy systems.

2.3.2.3. Effect of pH

The effect of pH on the adsorption of DCMTP on Ag° is given in Figure 2.14. The IR reflection spectra of silver metal conditioned in 1×10^{-4} M DCMTP solution were taken at different pH conditions. At acidic conditions, the IR spectra of the adsorbed species on Ag° are similar to that of AgDCMTP . This would indicate that both oxygen and sulfur are involved in the adsorption of the collector on the surface of Ag° . At higher pH values, the characteristic absorption bands are shifted toward the direction of pure DCMTP and the IR signal intensity decreases. This finding may suggest that as the pH becomes higher, DCMTP behaves increasingly as thione, which does not adsorb as strongly as the thiol form because of its low pK value. Above pH 10, the shift becomes more significant and the signal intensity is significantly lower, which would

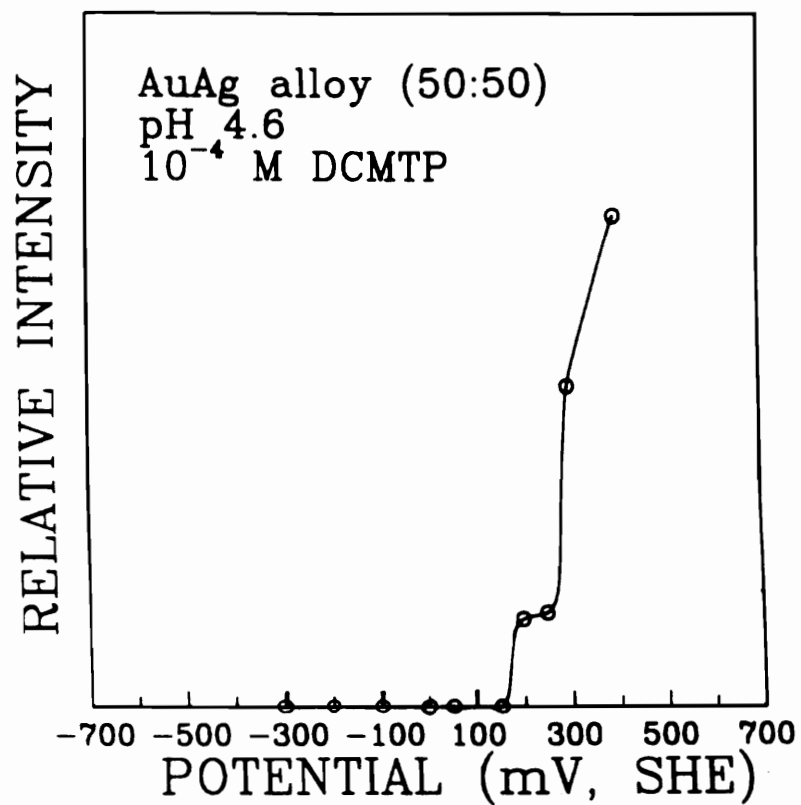


Figure 2.13. Effect of potential on the IR relative signal intensities of DCMTTP adsorbed on AuAg alloy (50:50) at pH 4.6.

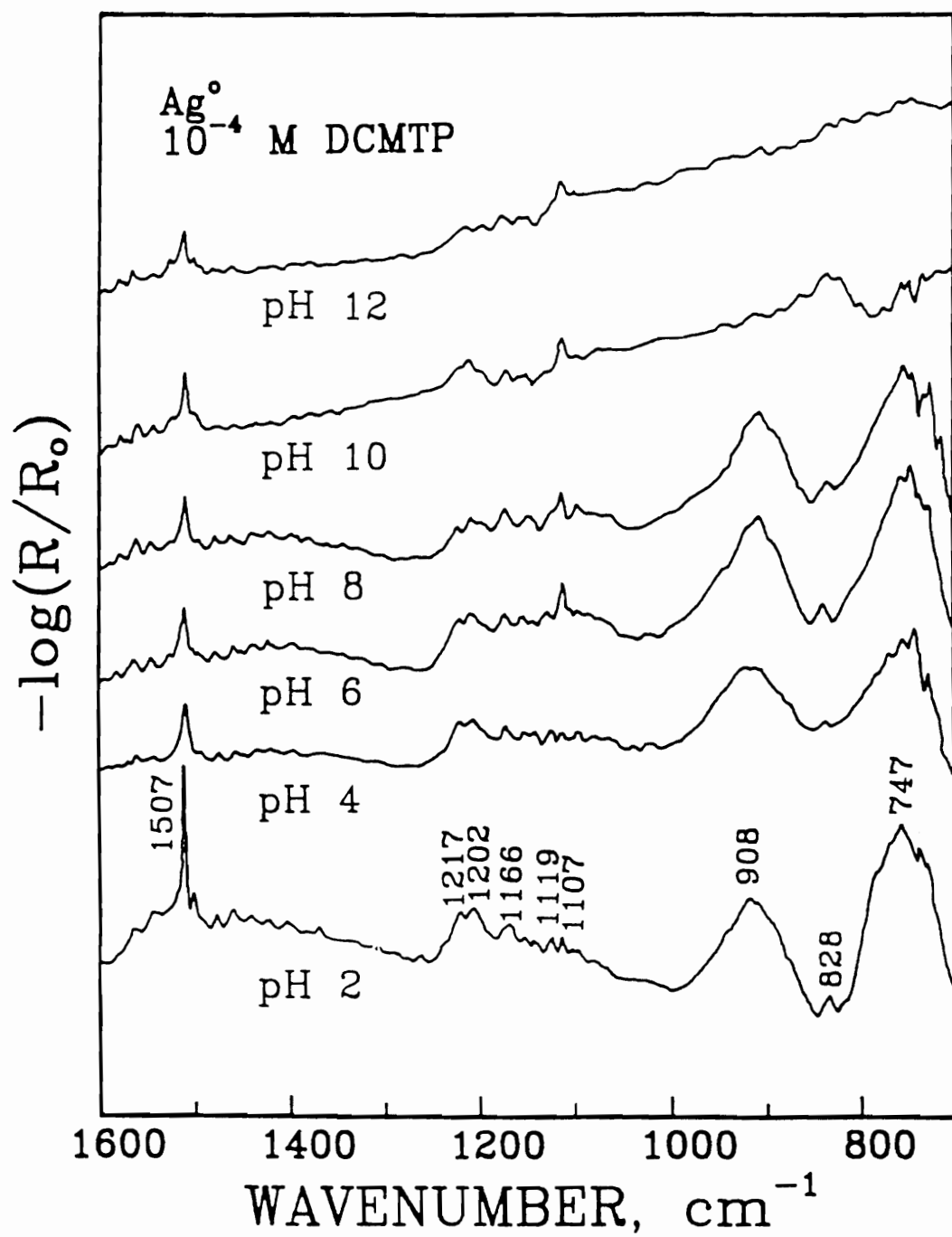


Figure 2.14. FTIR reflection spectra of Ag° conditioned in 1×10^{-4} M DCMTP at different pH's.

suggest that DCMTTP might be physisorbed.

Figure 2.15 shows the change in the IR peak area measured in the 1150-1250 cm^{-1} region. Assuming this to be a measure of the amount of DCMTTP adsorbed, it can be seen that DCMTTP adsorption on Ag^0 decreases with increasing pH. Above pH 10, the amount of collector adsorbed is almost negligible. This result represents well the tautomeric behavior of DCMTTP.

2.3.2.4. Effect of Conditioning Time

The FTIR spectrum of Ag^0 conditioned for different periods of time in the solution containing 1×10^{-4} M DCMTTP at pH 4.6 is presented in Figure 2.16. It shows that the intensity of each peak is increasing as the time increases and that the characteristic absorption bands are different as the conditioning time changes. The shape of the spectrum obtained after 30 sec is almost same as that obtained after 10 min and these spectra show three major bands at 1507 cm^{-1} , 1210 cm^{-1} and 920 cm^{-1} . On the other hand, the spectrum obtained after 1 min shows nearly same shape as those obtained after 2 min, 5 min, and 20 min. The wavenumbers of the peaks appearing in these spectra are 1507 cm^{-1} , 1210 cm^{-1} , 1100 cm^{-1} , 870 cm^{-1} , and 722 cm^{-1} .

The absorption bands observed may be attributed to the specific bonding of DCMTTP as shown in Table 2.1 (Meyrick and Thompson, 1950, Hudson, 1965, Chittenden and Thomas, 1968, Katritzky, 1959). The band at 920 cm^{-1} is due to the acetate buffer (pH 4.6).

Figure 2.17 shows how a DCMTTP molecule may be oriented on the surface of silver. It is shown that the collector is bonded to the Ag^0 on the surface through S and O forming a four-membered chelate. It also shows that the DCMTTP molecule lies flat on the surface of Ag^0 at low coverages (Fig. 2.17 (a)), and as the coverage increases with time, the DCMTTP stands

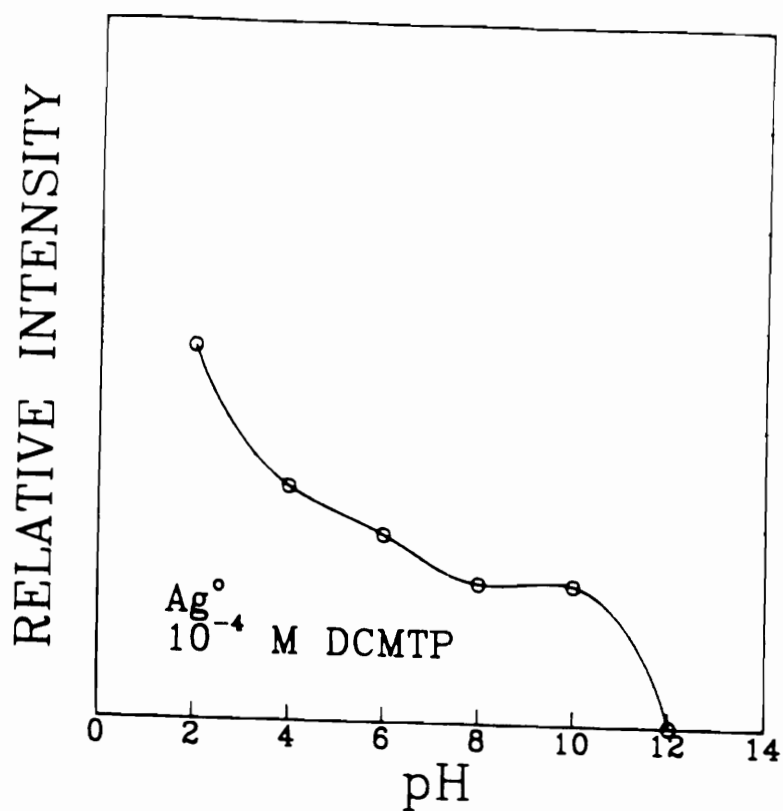


Figure 2.15. Effect of pH on the IR relative signal intensities of DCMTP adsorbed on Ag° .

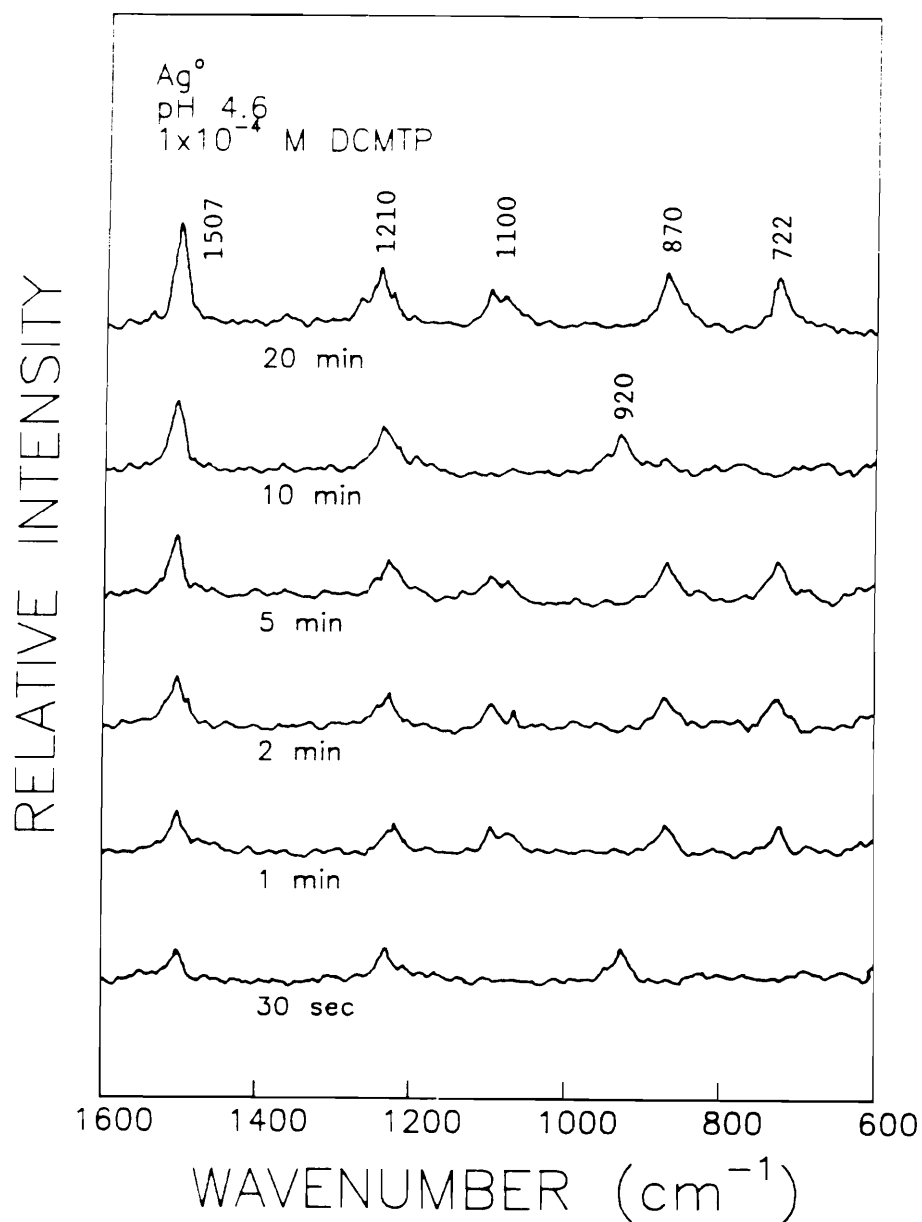
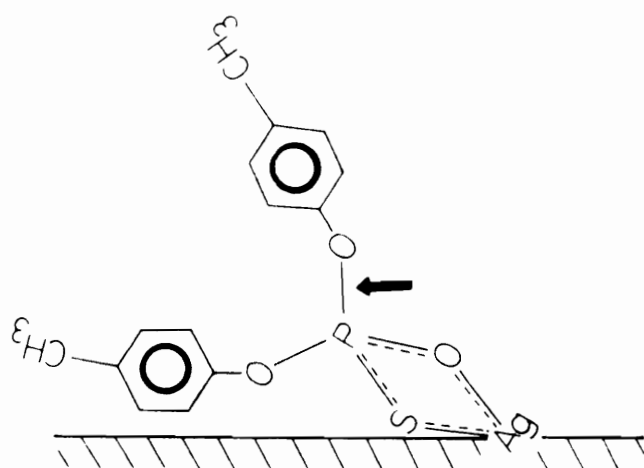
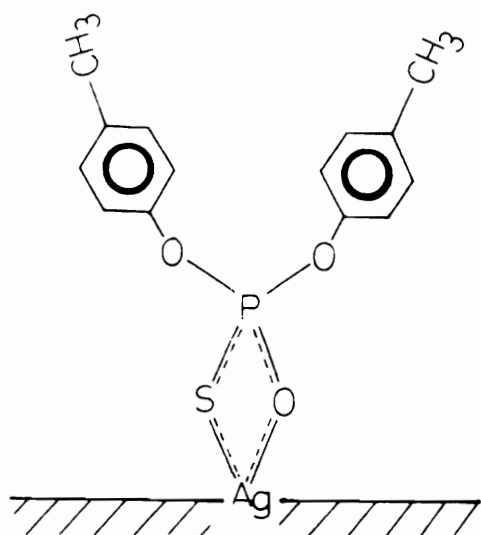


Figure 2.16. FTIR reflection spectra of Ag° conditioned in 1x10⁻⁴ M DCMTp for different periods. (722; P-S, 870 & 1100; 1:4 substitution in aromatic ring, 922; acetate buffer, 1210; aromatic ring or P-O, 1507; aromatic ring)



(a)



(b)

Figure 2.17. Schematic representation of molecular structure of DCMTTP adsorbed on silver. Plane (a) shows the initial stage of adsorption and, plane (b) shows the stage for the formation of close-packed monolayer.

Table 2.1 The wavenumbers corresponding to the bonding of dicresyl monothiophosphate.

Wavenumber (cm ⁻¹)	Corresponding Bonding
722	P-S
870	1:4 substitution in aromatic ring (para-type)
1100	1:4 substitution in aromatic ring (para-type)
1210	aromatic ring/P-O
1507	aromatic ring

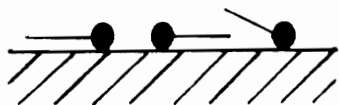
upright on the Ag° surface (Fig. 2.17 (b)).

Because the IR beam used in this experiment was P-polarized, it detects only the bonds showing a significant angle relative to the electrode surface. The bonds with a significant angle relative to the surface at the initial stage of adsorption are presumably P-O (see Figure 2.17) and the aromatic ring group. The spectra obtained after 30 sec of contact time show only these bonds; therefore, it may be considered that the DCMTTP molecules are lying flat on Ag° surface after 30 sec, as shown in Fig. 2.17 (a). At this stage, the adsorption layer probably do not form a close-packed monolayer, allowing acetate ions incorporated in the monolayer as indicated by their characteristic band at 920 cm^{-1} .

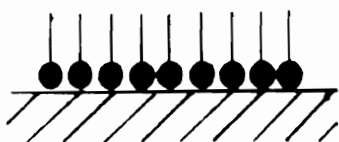
As the collector adsorbs further on the surface, the molecules would stand upright as shown in Fig. 2.17 (b). In this case, the bonds of cresyl group and P-O and P-S will have significant angle to the surface and, therefore, are shown in the spectra. The spectra obtained after 1 min show characteristic absorption bands for the P-O and P-S bands. Such an orientation may represent a close-packed monolayer. Under this condition, the surface is sufficiently hydrophobic that the acetate buffer solution would not adhere on the surface.

Figure 2.18 represents the proposed model for the adsorption of DCMTTP on Ag° . Step (i) is the initial stage of adsorption on the Ag° surface and DCMTTP molecules are considered to lie flat. Step (ii) shows the stage of a close-packed monolayer of DCMTTP. At this stage, DCMTTP molecule may be bonded to the Ag° surface through S and O forming a four-membered chelate. Therefore, P-S and P-O bonds have significant angle relative to the Ag° surface and show their characteristic bands in the IR spectra. Step (iii) is the initial stage of second layer formation on the first monolayer. The orientation of this second layer is probably random, and the molecules are in the form of AgDCMTTP . The multi-layer adsorption of AgDCMTTP renders

i)



ii)



MONOLAYER

iii)

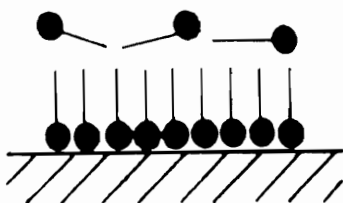


Figure 2.18. Adsorption model of collector (DCMTP) on the substrate depending on time.

the surface hydrophobic because AgDCMTP is naturally hydrophobic.

2.3.3. Contact Angle Measurements

2.3.3.1. Effect of Potential

The effect of potential on the hydrophobicity of Ag° , Au° , and Au-Ag alloys (80:20 and 50:50) was studied in the presence of 1×10^{-4} M DCMTP at pH 4.6 and 9.2. The electrode was held under different potential conditions and the contact angles measured. The contact angles on Ag° and Au-Ag alloys are observed to be nearly zero at pH 9.2. Although the IR spectra show adsorption at pH 9.2, apparently the amount of DCMTP adsorbed may not be enough to make the electrode surface hydrophobic. Therefore, only the results obtained at pH 4.6 are shown here. Also, the contact angle data obtained with Au° indicate that the electrode is completely hydrophilic over the entire potential range investigated and, therefore, not shown here.

Figure 2.19 shows the effect of potential on the contact angles measured on Ag° at pH 4.6. The electrode becomes hydrophobic above -50 mV and the hydrophobicity increases with increasing potential and levels off above 300 mV. These results are in agreement with those of IR experiments (Fig. 2.9) and voltammetry (Fig 2.3).

Fig. 2.20 shows the contact angle measurements obtained with 80:20 Au-Ag alloy. The contact angle starts at around 250 mV and, then, increases with increasing potential. This is in excellent agreement with the observations made from IR spectroscopy (Fig. 2.11) and voltammetry (Fig. 2.5). The starting potential observed for this alloy is higher than that for pure Ag° due to the decreased activity of silver in the alloy.

With the 50:50 Au-Ag alloy, the potential at which DCMTP adsorbs is further reduced as shown in Figure 2.21. This potential is higher than

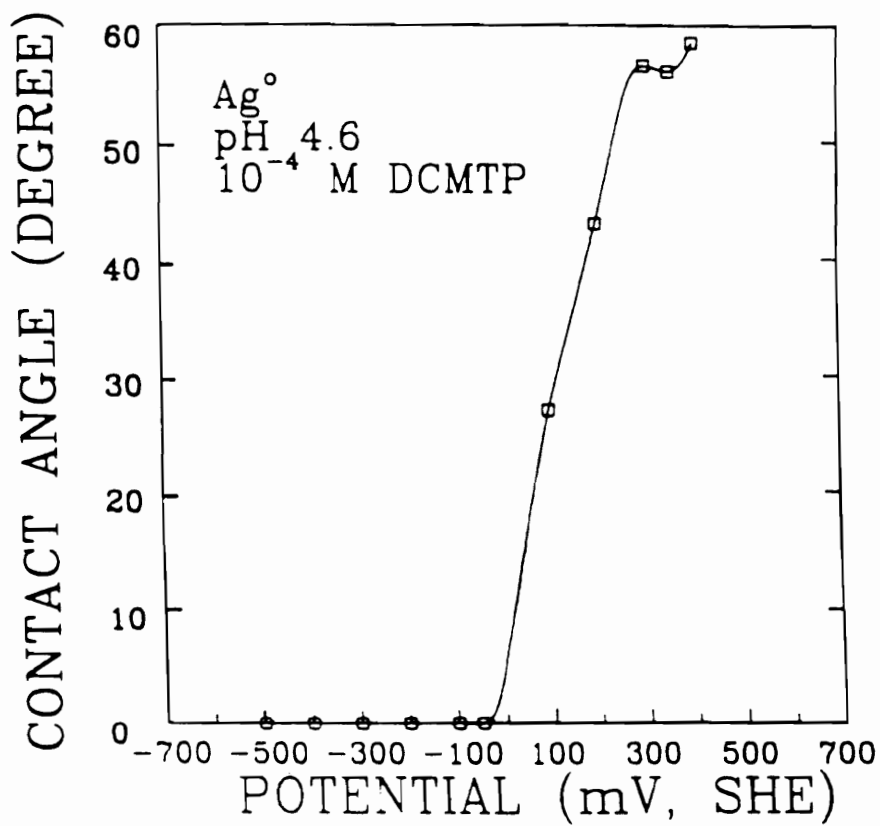


Figure 2.19. Effect of potential on the contact angle of DCMTP adsorbed on Ag° at pH 4.6.

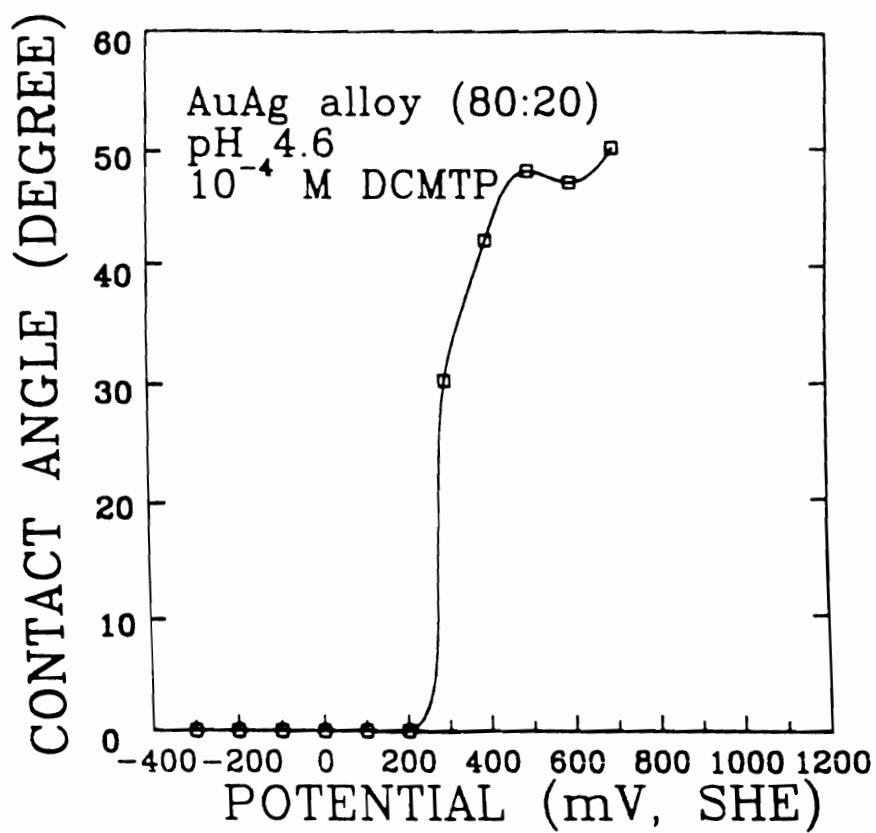


Figure 2.20. Effect of potential on the contact angle of DCMTTP adsorbed on AuAg alloy (80:20) at pH 4.6.

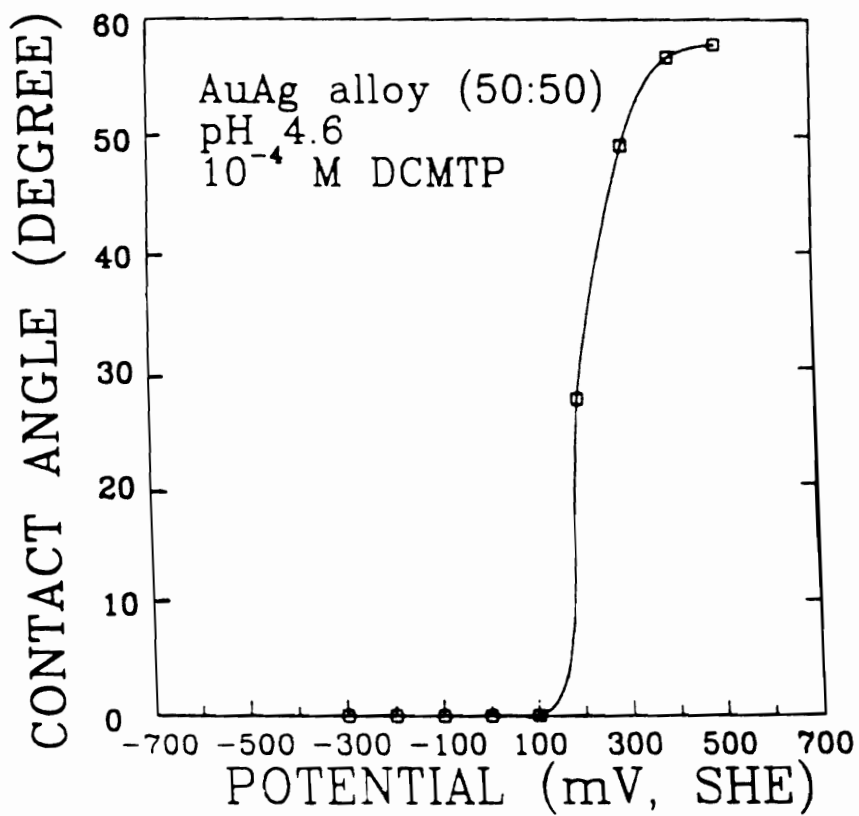


Figure 2.21. Effect of potential on the contact angle of DCMTP adsorbed on AuAg alloy (50:50) at pH 4.6.

that observed for pure Ag° , but lower than the onset potential for DCMTP adsorption on the 80:20 Au-Ag alloy. Therefore, it can be said that the starting potential where adsorption occurs on the alloy is dependent on the silver content in that alloy; the higher the Ag content, the closer the potential where adsorption starts to that observed for pure Ag° . The data obtained from contact angle measurements are in good agreement with the findings from voltammetry (Fig. 2.6) and IR spectroscopy (Fig. 2.13).

2.3.3.2. Effect of pH

Figure 2.22 shows the effect of pH on the contact angle of Ag° electrode in 1×10^{-4} M DCMTP. As shown, the contact angle decreases with increasing pH, which is in agreement with that of IR measurements. As shown in Fig. 2.15, the adsorption of DCMTP decreases with increasing pH. These findings suggest that the active form of DCMTP is thiol rather than thione.

2.3.4. E_h -pH Diagram

Figure 2.23 represents E_h -pH diagram for the silver/water/monothiophosphate (1×10^{-4} M) system, which was constructed by employing computer program using the thermodynamic data obtained in the present work. The pK value was determined to be 1.2×10^{-16} , from which ΔG° of AgDCMTP was calculated to be -13.8 kJ/mol. The concentration of MTP is 1×10^{-4} M and the pH of system right after titration was slightly higher than 5. Since the pH of the water used for the preparation of DCMTP solution and silver nitrate solution for the titration experiment was around 5.2, the effect of DCMTP^- , Ag^+ and NO_3^- ions on the pH of the system was found to be negligible.

It can be seen from the diagram that AgMTP starts to form at about

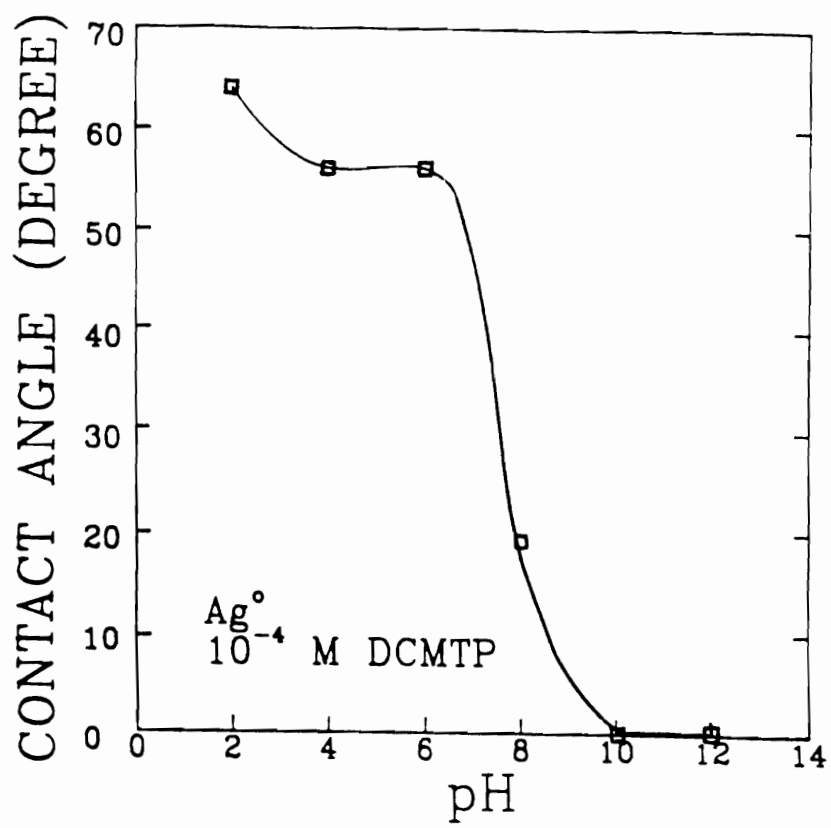


Figure 2.22. Effect of pH on the contact angle of DCMTP adsorbed on Ag°.

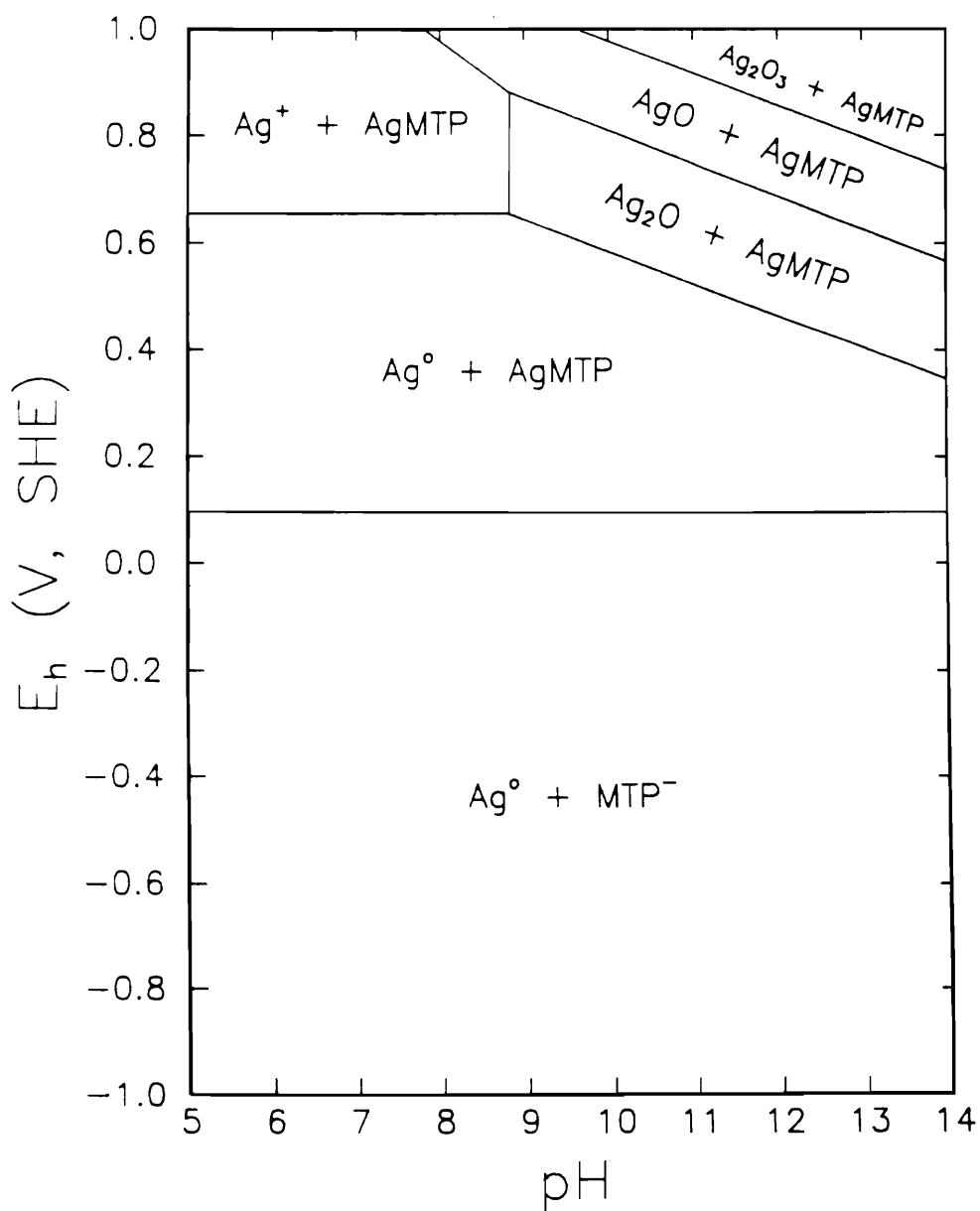


Figure 2.23. E_h -pH diagram for silver/water/MTP system for an initial DCMTTP concentration of 1×10^{-4} M.

0.1 V. Since the conditions used for constructing E_h -pH diagram are nearly the same as those for the electrochemical experiments conducted under acidic environment (1×10^{-4} M/l of MTP, pH 4.6), it would be meaningful to compare both results. The voltammogram for Ag^0 at pH 4.6 (Figure 2.3) showed that the addition of DCMTTP results in an anodic current rise above 100 mV and this was considered to be due to the formation of $AgDCMTTP$ on the electrode surface. This onset potential is consistent with the value for $AgMTP$ formation in the E_h -pH diagram. Also, there is a good correlation between the results of IR spectroscopy, contact angle measurements and the thermodynamic calculation. As the potential increases, Ag^0 is shown to be oxidized to Ag^+ or silver-oxides depending on the pH of the system.

2.4. Summary

The fundamental mechanisms of DCMTTP adsorption on gold, silver, and gold-silver alloys have been investigated. The voltammetry data indicate that the interaction of DCMTTP on Ag^0 and Au-Ag alloys (80:20, 50:50) involves a coupled chemical reaction of the EC-type. In this mechanism, an initial electrochemical reaction involving the oxidation of silver is followed immediately by the formation of the $AgDCMTTP$ compound. The adsorption of DCMTTP is then controlled by the E_h of the system and the pK value of the $AgDCMTTP$ compound.

The FTIR reflection spectra and contact angle data show that the adsorption of DCMTTP on Ag^0 and Au-Ag alloys (80:20, 50:50) occurs at potentials close to where they are observed in the voltammograms. Increasing the silver content of the Au-Ag alloy lowers the potentials for the DCMTTP adsorption.

The adsorption behavior of DCMTTP changes with pH, which may be attributed to the tautomerism exhibited by monothioacids. As the pH of

the system increases, the DCMTTP adsorption decreases, which may suggest that the thiol form is the more active form of DCMTTP.

The FTIR studies show that the orientation of DCMTTP changes with contact time. At short contact times, the DCMTTP molecules adsorb on the surface with flat orientation. At longer contact times, the collector forms a well oriented monolayer. After very long contact times, the adsorption layer becomes randomly oriented again. The collector species adsorbed in the multi-layer are in the form of AgDCMTTP.

E_h -pH diagrams constructed for Ag/water/MTP system support the findings of contact angle, IR and voltammetry experiments. There are no indications that DCMTTP reacts with gold. This suggests that the interaction of DCMTTP with silver is important in the flotation of Ag-containing gold ores.

Chapter 3. Thiophosphinate System

3.1. Introduction

The sulfur analogues of phosphinic acids have recently found wide acceptance as selective collectors for the flotation separation of base metal sulfides and precious metals, specially from complex sulfide ores (Wang and Avotins, 1982, Mingione, 1991). The dithiophosphinate (DTPI) is structurally similar to dithiophosphate (DTP), as shown in Table 3.1, but has collector properties that are quite different from that of DTP. The metal complexes of DTPI are several orders of magnitude more stable than those of DTP (Wang and Avotins, 1982). The DTPI is also more resistant to aqueous oxidation than DTP. The dialkyl DTPI is a far superior collector for galena, chalcopyrite, and precious metal values, as well as more selective against sphalerite and iron sulfides, than the corresponding DTP.

The monothiophosphinate (MTPI) is a new collector derived from the corresponding dithiophosphinate by replacing one of the sulfur atoms with oxygen (Table 3.1). This change results in a more stable and stronger collector under certain pH conditions (Nagaraj and Avotins, 1988, Nagaraj et al., 1988, Nagaraj et al., 1989).

As in the case of the dithio-analogues, there are differences in collector properties between MTPI and monothiophosphate (MTP). The MTPI, being a weaker acid than MTP, is more effective in the neutral and mildly alkaline pH conditions. The use of MTPI has also been shown to provide increased precious metals recoveries from ores.

Table 3.1. Thiophosphate and thiophosphinate collectors.

Dithiophosphate (DTP)	Dithiophosphinate (DTPI)
$\begin{array}{c} \text{S} \\ \\ \text{R-O} >\text{P} - \text{S}^- \\ \\ \text{R-O} \end{array}$	$\begin{array}{c} \text{S} \\ \\ \text{R} >\text{P} - \text{S}^- \\ \\ \text{R} \end{array}$
Monothiophosphate (MTP)	Monothiophosphinate (MTPI)
$\begin{array}{c} \text{S} \\ \\ \text{R-O} >\text{P} - \text{O}^- \\ \\ \text{R-O} \end{array}$	$\begin{array}{c} \text{S} \\ \\ \text{R} >\text{P} - \text{O}^- \\ \\ \text{R} \end{array}$

In Chapter 2, the EC mechanism was used to explain the adsorption of MTP on precious metals. For the reaction of DTPI with copper and copper sulfides, this mechanism was also adopted to explain the adsorption mechanism in other investigation (Basilio et al., 1991a). According to the EC mechanism, the process of copper-DTPI formation on copper may be viewed as a two-step process, involving an initial electrochemical reaction (E):



followed by a chemical reaction (C),



The overall reaction then becomes:



However, relatively little is known about the mechanism of interaction of thiophosphinates with precious metals. In this chapter, the mechanism of DTPI adsorption on gold, silver and its alloys are studied in view of the EC-mechanism.

3.2. Experiments

3.2.1. Materials

The sodium diethyl dithiophosphinate (DEDTPI) was prepared from tetraethyl phosphine and sodium sulfite according to the procedure of

Kuchen et al. (1963). The ammonium diisobutyl dithiophosphinate (DIBDTPI) and ammonium diisobutyl monothiophosphinate (DIBMTPI) were provided by the American Cyanamid Company. The silver diethyl dithiophosphinate (AgDEDTPi) complex was precipitated by mixing silver nitrate and DEDTPI solutions at neutral pH conditions. Elemental analysis of the precipitate verified it to be AgDEDTPi. A similar procedure was used in making the silver diisobutyl dithiophosphinate (AgDIBDTPI) and silver diisobutyl monothiophosphinate (AgDIBMTPI) complexes. The dimers of DTPI were prepared through oxidation with aqueous iodine-potassium iodide solution. The experiments were carried out in 0.05 M $\text{Na}_2\text{B}_4\text{O}_7$ solutions (pH 9.2). The experimental procedures for voltammetry, FTIR spectroscopy, contact angle measurements, and construction of E_b -pH diagrams are similar to that for monothiophosphate system.

3.3. Results and Discussion

3.3.1. Voltammetry

3.3.1.1. Diethyl Dithiophosphinate

The voltammograms of Au^0 in the absence and presence of 2×10^{-4} M DEDTPI at pH 9.2 are shown in Figure 3.1. In the absence of DEDTPI, the anodic peak shown at above 700 mV is presumably associated with the oxidation of Au^0 . The addition of DEDTPI results in the passivation of the electrode surface, as indicated by the decrease in the current above 250 mV. However, FTIR spectroscopic measurements carried out under similar conditions do not indicate DEDTPI adsorption in the region where the electrode is passivated. The presence of DEDTPI on the Au^0 surface is observed only at the larger concentration of DEDTPI (10^{-3} M). Therefore, the passivation of the electrode may be due to weak physisorption of

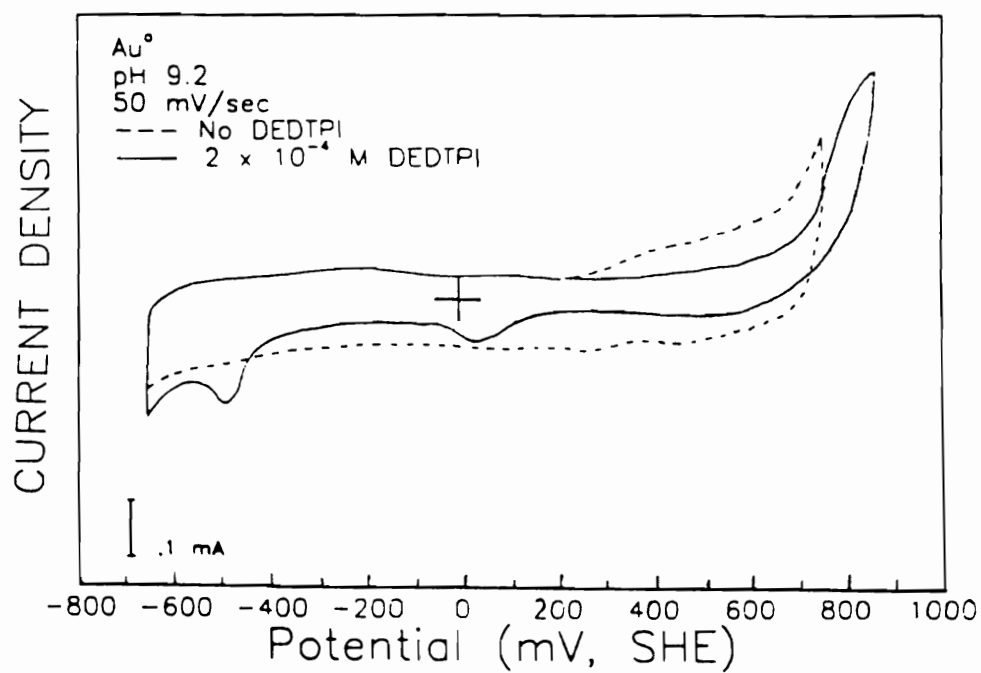


Figure 3.1. Voltammograms for Au° in the absence and presence of 2 x 10⁻⁴ M DEDTPI at pH 9.2.

DEDTPI, which is presumably removed when the sample is rinsed prior to the *ex situ* FTIR measurements.

At potentials above 500 mV, an anodic current rise is observed. This may be attributed to the oxidation of DEDTPI according to the reaction;



The cathodic peak observed at around 0 mV is probably due to the reverse of this reaction. As will be shown later (Fig. 3.10), the formation of $(\text{DEDTPI})_2$ is also verified by the IR reflectance spectra obtained at these potentials. There is no evidence for the formation of a Au-DEDTPI complex on the electrode surface.

Figure 3.2 shows the voltammograms of Ag^0 without and with the addition of 2×10^{-4} M DEDTPI at pH 9.2. In the absence of DEDTPI, the oxidation of Ag^0 to Ag_2O is shown by the anodic current starting above 300 mV. The reduction of the oxidation product is indicated by the cathodic peak near 400 mV. The starting potential of the oxidation of Ag^0 is much lower than the oxidation potential of Au^0 , which is well presented in these voltammograms. The addition of DEDTPI results in the appearance of a new anodic peak starting above 0 mV. This is probably due to the following reaction;



The proposed DEDTPI adsorption reaction could be the result of coupled reactions of the EC-type, which has also been suggested for monothiophosphate interaction with Ag^0 (Basilio et al., 1991b). The electrochemical reaction (E) involves the oxidation of Ag^0 ;

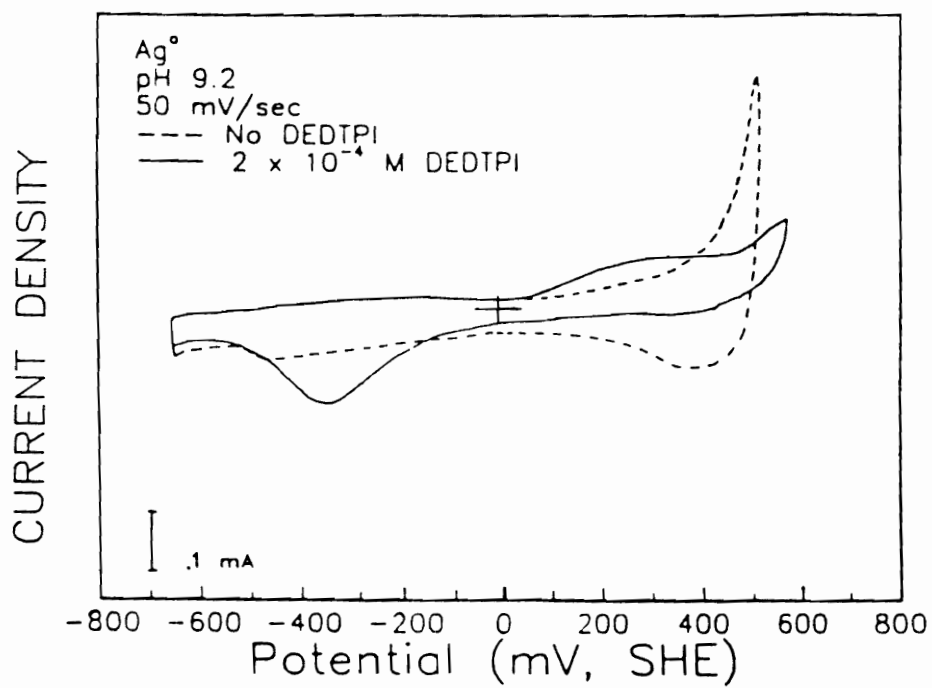


Figure 3.2. Voltammograms for Ag° in the absence and presence of 2 x 10⁻⁴ M DEDTPI at pH 9.2.



followed by the chemical step (C);



The cathodic current rise starting at -150 mV in the cathodic scan is probably associated with the reduction of AgDEDTPI. The passivation of the electrode is also observed below 0 mV with the addition of DEDTPI. This may be attributed to the weak physisorption of DEDTPI on the electrode surface. However, the IR reflectance measurements were not able to detect any physisorbed species under similar conditions because the physisorbed DEDTPI may be removed when the sample is rinsed prior to the FTIR measurement.

The voltammograms for an 80:20 Au-Ag alloy in the absence and presence of 2×10^{-4} M DEDTPI are shown in Figure 3.3. Without any DEDTPI addition, the oxidation of Ag^0 is observed starting at around 350 mV, while oxygen adsorption on this alloy is indicated by the increase in current above 600 mV. Since the alloy contains 80% of Au^0 by weight, it shows a characteristics quite similar to pure Au^0 . As mentioned before, the oxidation potential for Ag^0 is much lower than for Au^0 . Therefore, the potential at which oxygen adsorption starts on the alloy is higher compared with that of Ag^0 .

In the presence of DEDTPI, Ag^0 is passivated below 250 mV. The interaction of DEDTPI with the alloy, via the EC mechanism proposed for Ag^0 (Reactions (6) and (7)), is indicated by the anodic current rise above 250 mV. This potential is higher than that observed for the onset of DEDTPI adsorption on pure Ag^0 due to the lower activity of silver in the alloy.

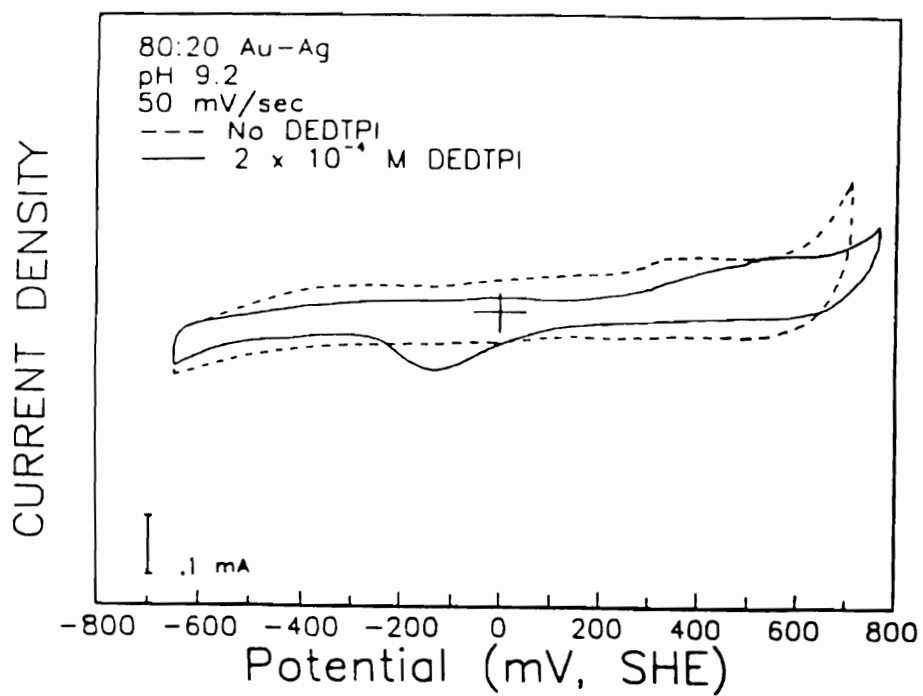


Figure 3.3. Voltammograms for 80:20 Au-Ag alloy in the absence and presence of 2×10^{-4} M DEDTPI at pH 9.2.

The cathodic current rise starting at around 0 mV, which is also higher than the case of pure Ag° , is presumably due to the reduction of this oxidized species. The oxidation of DEDTPI to $(\text{DEDTPI})_2$ is shown by the current rising above 550 mV. The anodic current at higher potentials is due to the oxidation of Ag° .

Figure 3.4 shows the results of the voltammetry obtained for the 50:50 Au-Ag alloy-DEDTPI system. The voltammograms show that the addition of 2×10^{-4} M DEDTPI results in the passivation of the electrode at low potentials. The interaction of DEDTPI on Ag° is indicated by the anodic current rising above 150 mV. This value is lower than that for the 80:20 Au-Ag alloy, but higher than that for Ag° . Therefore, the onset of DEDTPI adsorption is dependent on the silver content of the alloy; the higher the silver content, the closer the adsorption potential moves towards that observed for pure Ag° . The anodic peak observed at this potential may be attributed to an EC-type reaction mechanism given by reactions (6) and (7). The cathodic current rise starting at around -100 mV is associated with the reverse of reaction (7) and this potential also shows the value between those for 80:20 Au-Ag alloy and pure Ag° . At potentials higher than 550 mV, the oxidation of DEDTPI to a dimer (reaction (4)) is indicated by the increase in anodic current.

Except for differences in the potentials where the oxidation and reduction of DEDTPI occurs, the general shape of this voltammogram is similar to that for Ag° . Since this alloy contains 50% of silver by weight, the actual atomic ratio of Ag° is more than 0.64. Therefore, the silver activity on the surface of electrode is high and this alloy shows similar characteristic to that of pure Ag° in voltammetry.

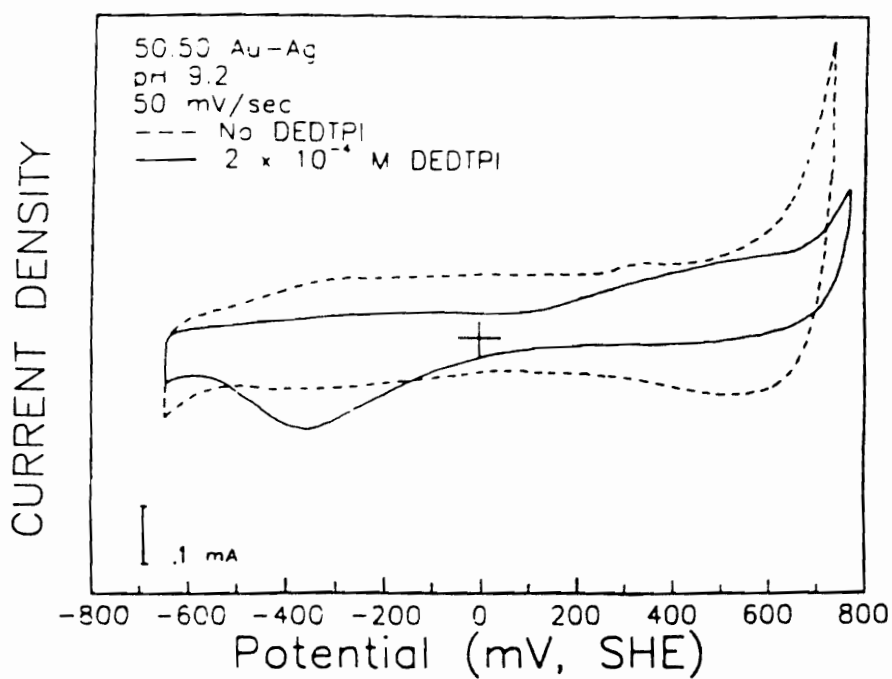


Figure 3.4. Voltammograms for 50:50 Au-Ag alloy in the absence and presence of 2×10^{-4} M DEDTPI at pH 9.2.

3.3.1.2. Diisobutyl Dithiophosphinate

The voltammograms for Au^0 in the absence and presence of 2×10^{-4} M DIBDTPI at pH 9.2 are shown in Figure 3.5. The electrochemical behavior of Au^0 represented in this voltammogram is similar to that observed for the Au^0 -DEDTPI system. The addition of DIBDTPI results in the passivation of the electrode surface, as indicated by the decrease in the current above 50 mV. However, the IR spectroscopic measurements carried out under similar conditions do not indicate DIBDTPI adsorption in the region where the electrode is passivated. The presence of DIBDTPI on the Au^0 surface is observed only at DIBDTPI additions of more than 10^{-3} M. The passivation of the electrode observed in this voltammogram, therefore, may be associated with the weak physisorption of DIBDTPI, which is probably removed from the surface when the sample is rinsed prior to the *ex situ* IR measurements.

At potentials around 550 mV, the anodic current starts to rise. This may be attributed to the oxidation of DIBDTPI according to the following reaction;



Apparently, this reaction is not reversible as there is no well-defined reduction peak shown on the return scan.

Figure 3.6 shows the voltammograms for Ag^0 in the absence and presence of 2×10^{-4} M DIBDTPI at pH 9.2. In the absence of DIBDTPI, the anodic current rise starting above 300 mV is due to the oxidation of Ag^0 to Ag_2O . The reduction of this oxidation product is observed by the cathodic peak around 400 mV. The electrode is passivated in the presence of DIBDTPI, as

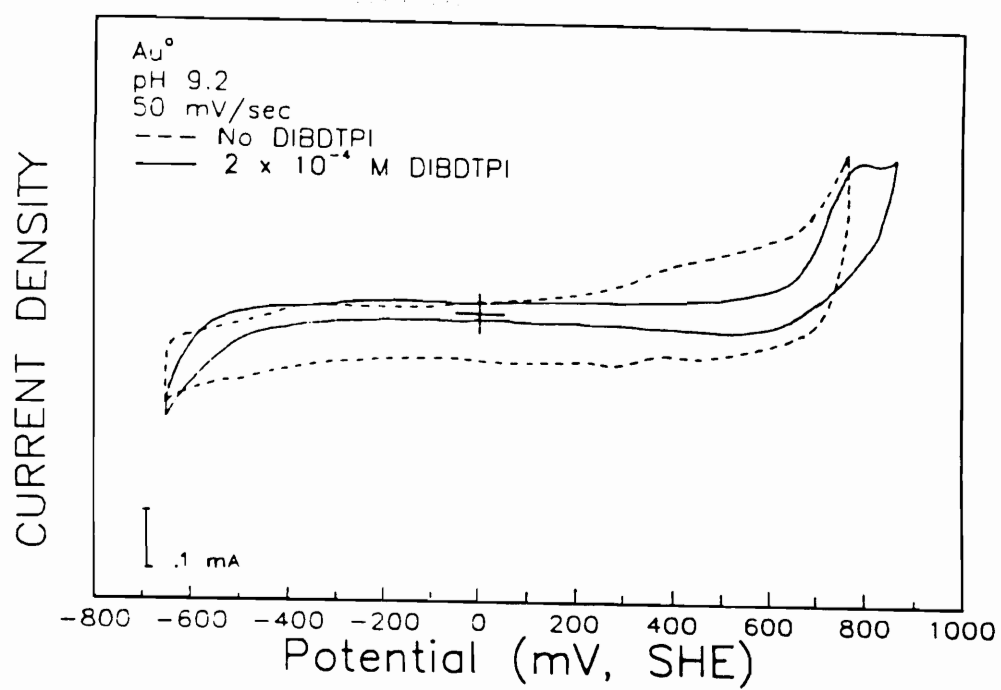


Figure 3.5. Voltammograms for Au⁺ in the absence and presence of 2 x 10⁻⁴ M DIBDTPI at pH 9.2.

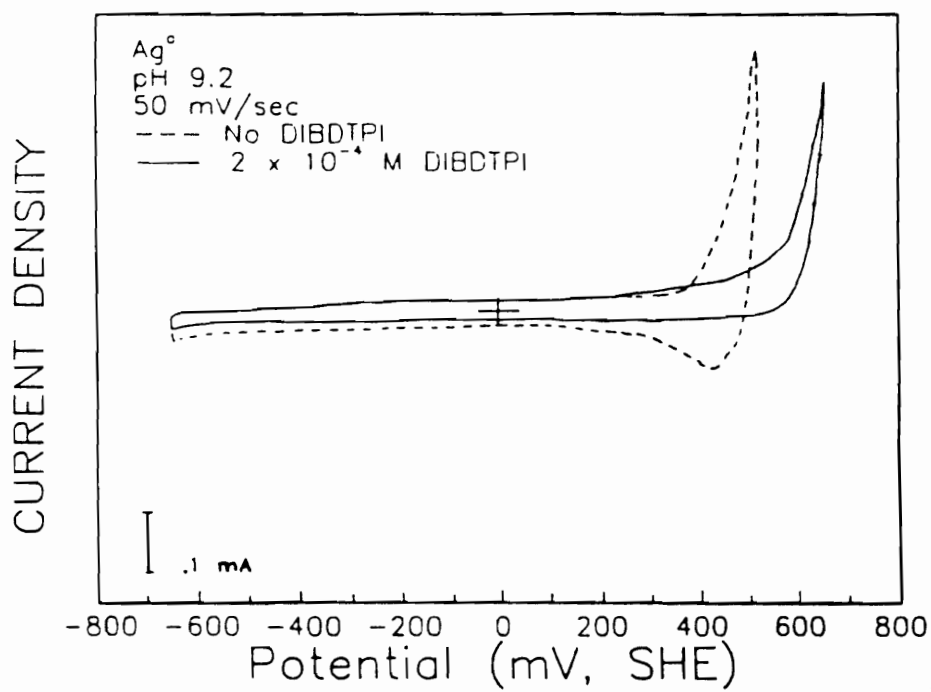


Figure 3.6. Voltammograms for Ag⁺ in the absence and presence of 2 × 10⁻⁴ M DIBDTPI at pH 9.2.

shown by the decrease in current. The adsorption of DIBDTPI, which starts at about 250 mV, may be attributed to an EC mechanism involving Ag^0 and DIBDTPI to form AgDIBDTPI . The adsorption mechanism suggested is similar to that proposed above for the Ag-DEDTPI system (reaction (6) and (7)). That is, the electrochemical reaction (E) is followed by the chemical step (C).

The results of voltammetry obtained for the two Au-Ag alloys are similar to those obtained for EDTPI and indicate the formation of AgDIBDTPI , followed by $(\text{DIBDTPI})_2$ (shown in Appendix). As in the case of EDTPI, the potential for the onset of adsorption is directly related to the silver content of the alloy. DIBDTPI adsorption is found at a lower potential for the 50:50 Au-Ag alloy than for the 80:20 Au-Ag alloy because the activity of silver diminishes as the gold content increases in the alloy.

3.3.1.3. Diisobutyl Monothiophosphinate

The voltammograms for Au^0 without and with the addition of 1×10^{-4} M DIBMTPI are shown in Figure 3.7. Similar to the findings for the Au^0 -DTPI systems, passivation of the electrode is observed. However, there are no indications of the oxidation of DIBMTPI on the electrode surface, which is opposite to that observed for the corresponding dithio analogue. The FTIR spectroscopic measurements do not indicate the presence of adsorbed species on the Au^0 surface over the entire potential range measured. The passivation observed in this voltammogram may be attributed to the weak physisorption of DIBMTPI, which the *ex situ* IR reflectance measurement is unable to detect. This finding suggests that monothiophosphinate is more stable than its dithio homologue.

Figure 3.8 shows the voltammograms for Ag^0 in the absence and presence

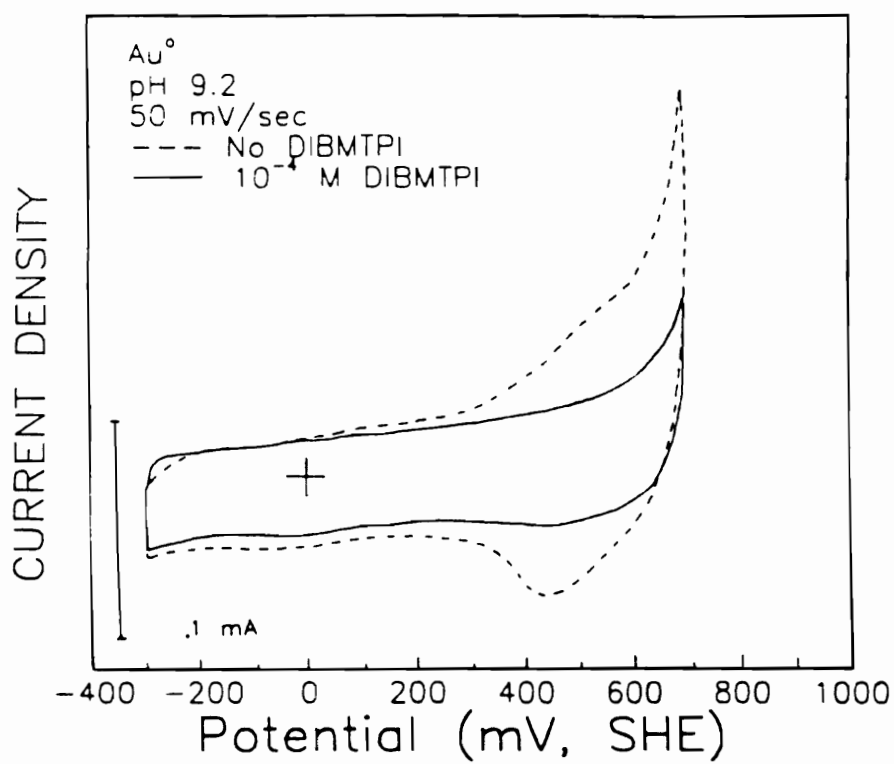


Figure 3.7. Voltammograms for Au° in the absence and presence of 1×10^{-4} M DIBMTPI at pH 9.2.

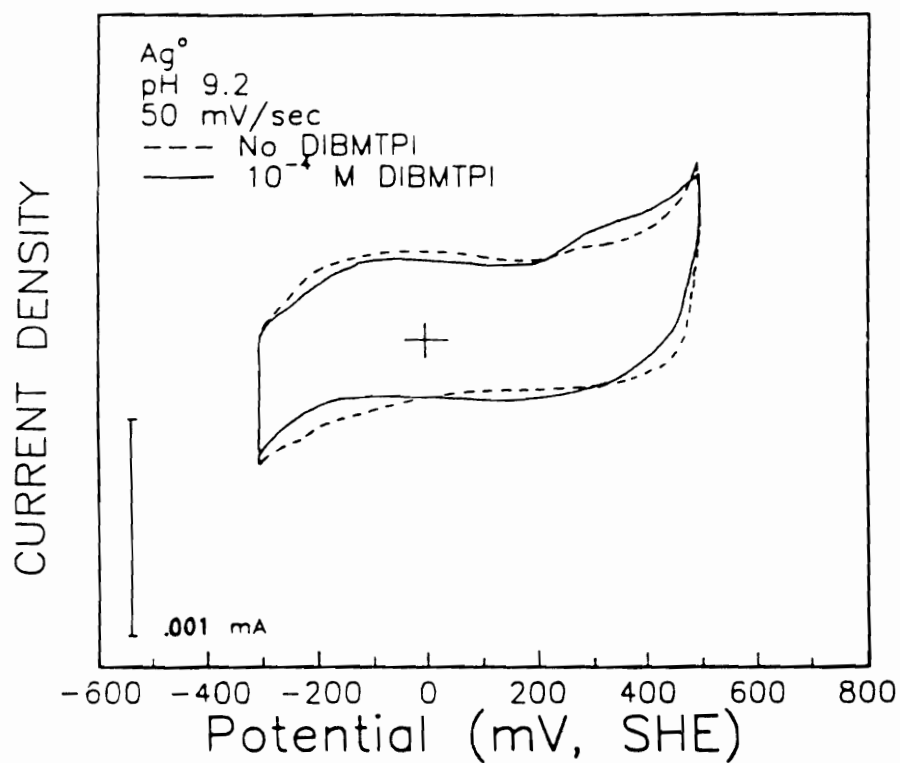


Figure 3.8. Voltammograms for Ag° in the absence and presence of 1×10^{-4} M DIBMTPI at pH 9.2.

of 1×10^{-4} M DIBMTPI at pH 9.2. The adsorption of DIBMTPI is indicated by the anodic current rise which starts at around 250 mV. The interaction of DIBMTPI with Ag^0 may be explained by the EC mechanism, which is similar to that given above for DTPI. The results for the Au-Ag alloys (80:20, 50:50) are similar to those found for DTPI except that the formation of $(\text{DIBMTPI})_2$ is not observed for this collector (shown in Appendix).

3.3.2. FTIR Spectroscopy

3.3.2.1. Diethyl Dithiophosphinate

3.3.2.1.1. FTIR Spectra

The FTIR spectra of NaDEDTPI, $(\text{DEDTPI})_2$, and AgDEDTPI are given in Figure 3.9. $(\text{DEDTPI})_2$ was prepared by oxidizing DEDTPI in iodine-potassium iodide solution. The major absorption bands that are characteristic for the pure reagent are observed at 2987, 2974, 2941, 2878, 1044, 1023, 768 and 740 cm^{-1} . The peaks that are characteristic of $(\text{DEDTPI})_2$ are found at 2973, 2932, 2892, 1010, 767, and 732 cm^{-1} . For the AgDEDTPI compound, the bands are observed at 2970, 2932, 2873, 1109, 1028, 761 and 709 cm^{-1} . The signals observed in the $3000\text{--}2800 \text{ cm}^{-1}$ region may be attributed to C-H vibrations coming from the alkyl group (Bellamy, 1975). The bands in the $770\text{--}700 \text{ cm}^{-1}$ region is probably due to the P-S vibrations (Kabachnik, 1965; Bellamy, 1968). The spectrum for AgDEDTPI shows that the signals due to the P-S vibrations are shifted. This may indicate that the sulfur is involved in the bonding with silver.

Figure 3.10 shows some of the IR reflectance spectra obtained for the different precious metals held at different potentials. For Au^0 conditioned in 2×10^{-4} M DEDTPI solution and held at a potential of 750 mV, the spectrum is similar to that for $(\text{DEDTPI})_2$. The spectrum obtained

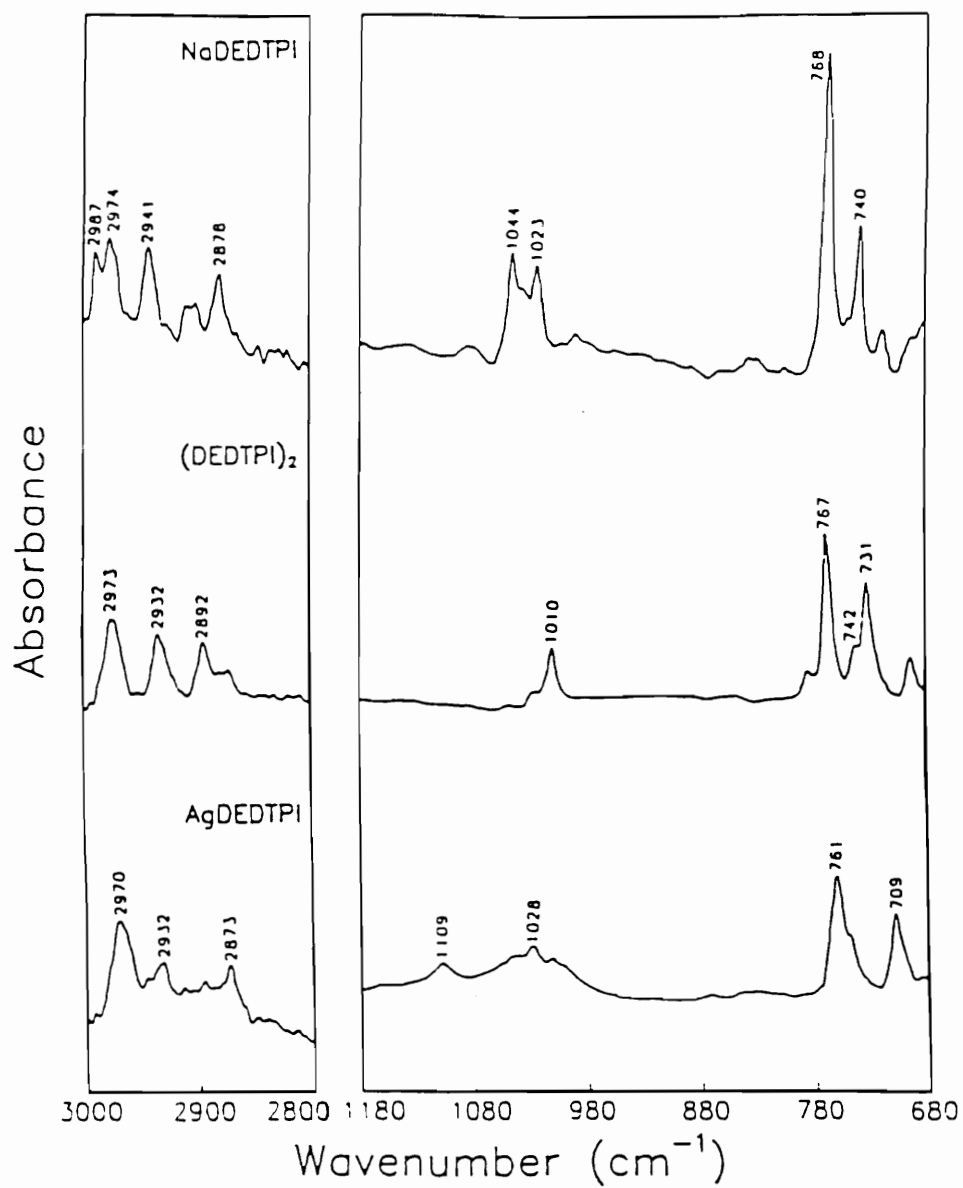


Figure 3.9. FTIR reflection spectra of sodium DEDTPI, (DEDTPI)₂ and AgDEDTPI.

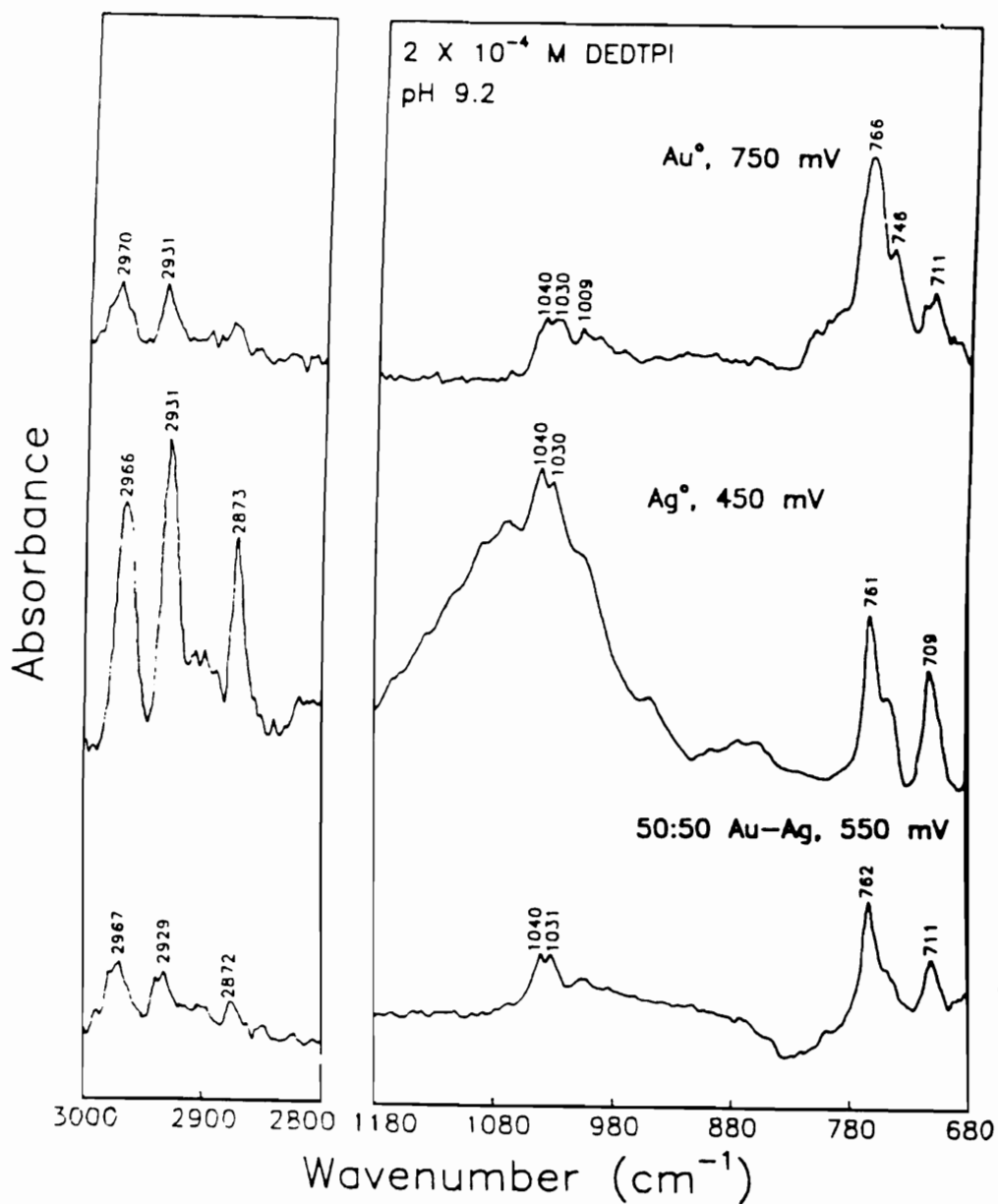


Figure 3.10. FTIR reflection spectra of (a) Au° at 750mV, (b) Ag° at 450 mV and (c) 50:50 Au-Ag alloy at 550 mV in 2 x 10⁻⁴ M DEDTPI.

for Ag° conditioned at 450 mV shows characteristic peaks which are similar to that for the bulk AgDEDTPI compound. The broad band observed between 1180 and 980 cm^{-1} is probably due to the oxidation product of Ag° , which is expected at this high potential. The 50:50 Au-Ag alloy conditioned at 550 mV gives a spectrum similar to that for the Ag° - DEDTPI system, which indicates the formation of AgDEDTPI . The spectra obtained at higher potentials (shown in Appendix) confirm the presence of both AgDEDTPI and $(\text{DEDTPI})_2$ on both alloy surfaces. These results from IR spectroscopy support the observations made from voltammetry.

3.3.2.1.2. Effect of Potential

Figure 3.11 shows the change in the IR peak intensity measured at 2960 and 760 cm^{-1} for Au° in the presence of 2×10^{-4} M DEDTPI at pH 9.2. The adsorption of DEDTPI starts at around 550 mV and increases with increasing potential. The initial adsorption potential corresponds with that where an anodic current rise is observed on the voltammogram. The FTIR spectroscopic measurements carried out between 250 mV and 500 mV, where the electrode is passivated, indicates no adsorption of DEDTPI . The passivation of the electrode, therefore, may be due to the weak physisorption of DEDTPI , which is presumably removed from the surface when the sample is rinsed prior to the *ex situ* IR measurements. However, the presence of DEDTPI on the Au° surface is observed when a large amount of DEDTPI was added (1×10^{-3} M) to the solution.

The effect of potential on the adsorption of DEDTPI on Ag° is shown in Figure 3.12. The adsorption of DEDTPI starts at 0 mV and increases with increasing potential. This is probably due to the formation of AgDEDTPI from the reaction of Ag° and DEDTPI^- via EC-type reaction mechanism. Above 350 mV, there is a sharp increase in DEDTPI adsorption,

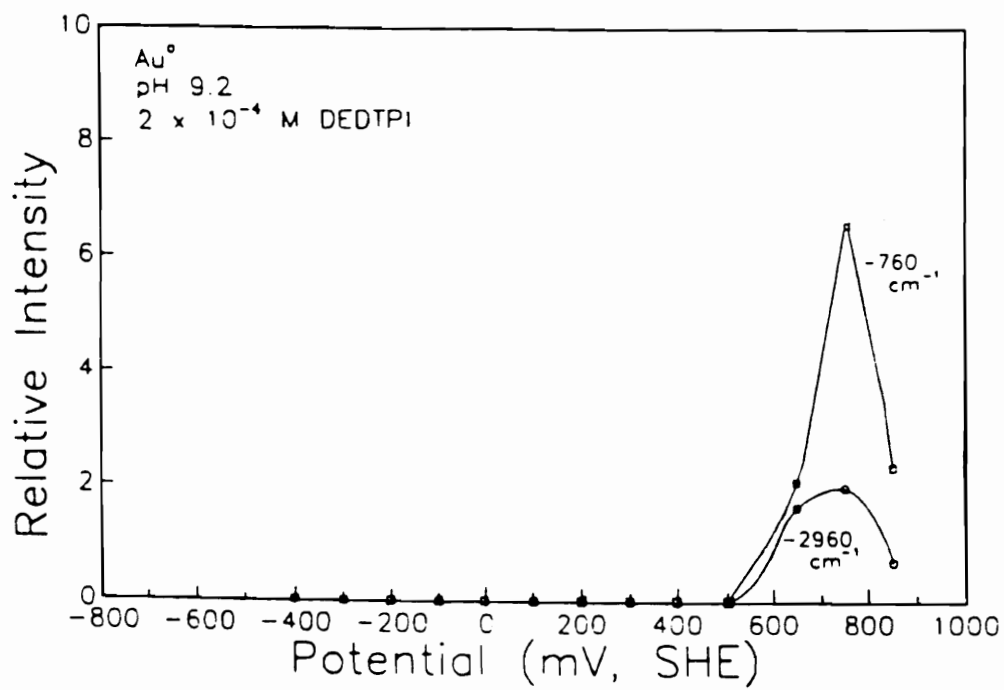


Figure 3.11. The effect of potential on the IR signal intensity (2960 and 760 cm^{-1}) of adsorbed DEDTPI for Au^0 in the presence of $2 \times 10^{-4} \text{ M DEDTPI}$ at pH 9.2.

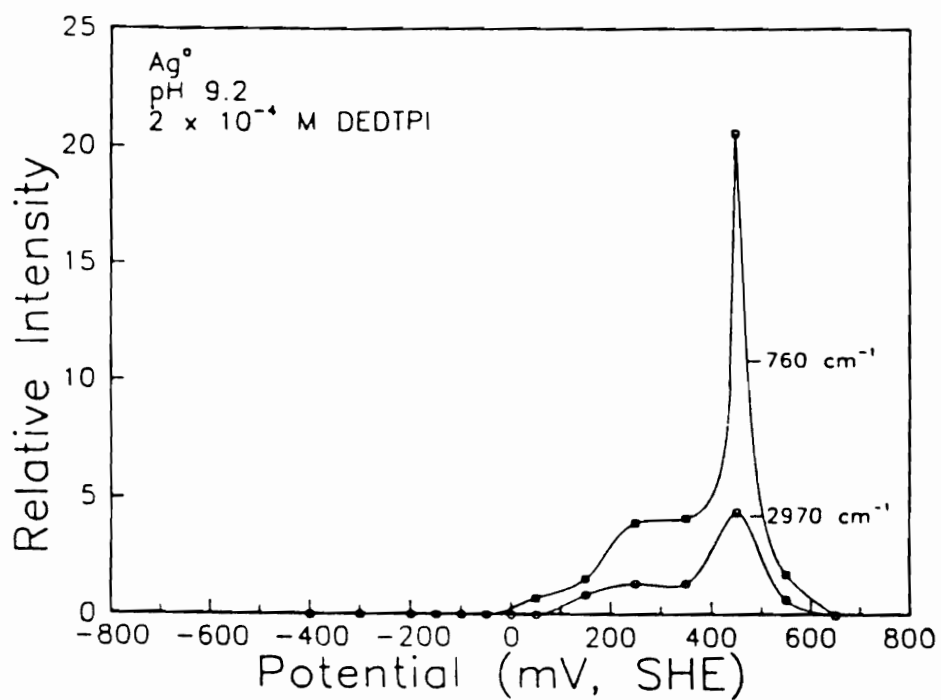


Figure 3.12. The effect of potential on the IR signal intensity (2970 and 760 cm^{-1}) of adsorbed DEDTPI for Ag^0 in the presence of 2×10^{-4} M DEDTPI at pH 9.2.

which is believed to be due to multilayer formation associated with the release of Ag^+ ions. The start of the oxidation of Ag^0 is also observed in the voltammogram at around the same potential. Thus, there is a good agreement between the results of electrochemical and spectroscopic measurements. There is a sharp decrease in the amount of DEDTPI adsorbed above 450 mV. This can be attributed to the formation of Ag_2O , which passivates the electrode.

The FTIR reflectance measurements for an 80:20 Au-Ag alloy in the presence of 2×10^{-4} M DEDTPI at pH 9.2 are shown in Figure 3.13. DEDTPI adsorption starts above 250 mV, as indicated by the increase in the relative intensity of the band at 760 cm^{-1} . The anodic current rise in the voltammogram is also observed at this potential. This potential is higher than that observed for the onset of DEDTPI adsorption on pure Ag^0 due to the diminished activity of silver in the alloy. Similar to the results obtained from voltammetry, the onset potential of DEDTPI adsorption on the electrode surface for this alloy lies between those for Au^0 and Ag^0 . Thus, the results of voltammetry and IR reflectance experiments are in agreement with each other. The amount adsorbed increases slightly up to 600 mV and then increases sharply at higher potentials. The sharp increase above 600 mV may be attributed to the formation of multilayers of AgDEDTPI and $(\text{DEDTPI})_2$, as indicated by the spectra obtained at high potentials.

Figure 3.14 shows the results of FTIR spectroscopy obtained for the 50:50 Au-Ag alloy-DEDTPI system. In the voltammetry, the addition of 2×10^{-4} M DEDTPI results in the passivation of the electrode at low potentials. However, the result of IR reflectance measurements shown here does not indicate any adsorption on the electrode at these potentials. This is because that the passivation observed in the voltammogram at low potentials is due to the weak physisorption of DEDTPI. This physisorbed DEDTPI is presumably removed from the electrode surface when the sample is

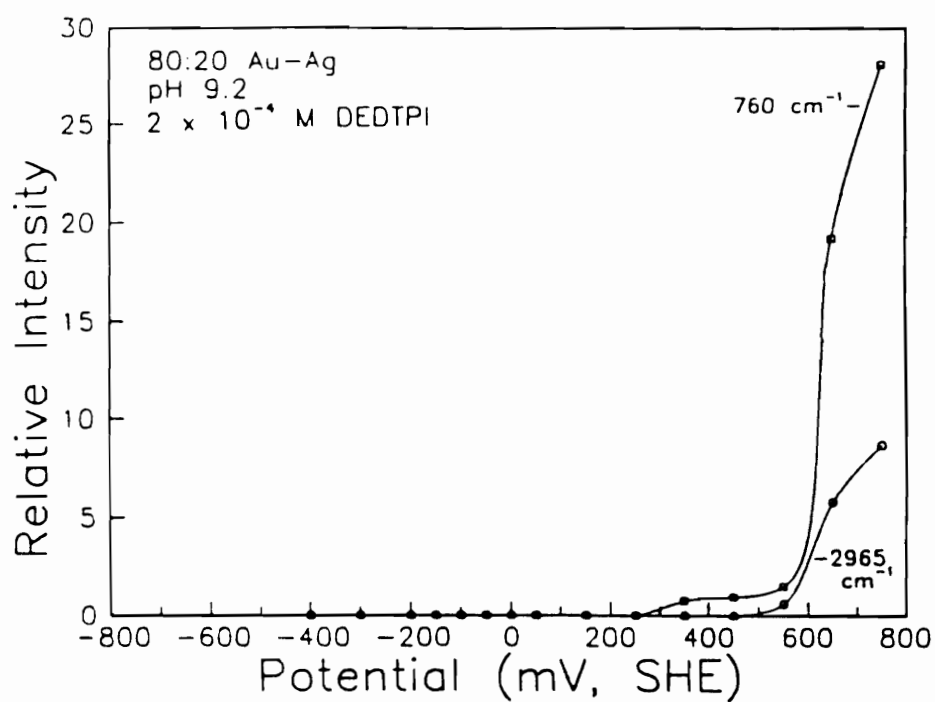


Figure 3.13. The effect of potential on the IR signal intensity (2965 and 760 cm^{-1}) of adsorbed DEDTPI for 80:20 Au-Ag alloy in the presence of 2×10^{-4} M DEDTPI at pH 9.2.

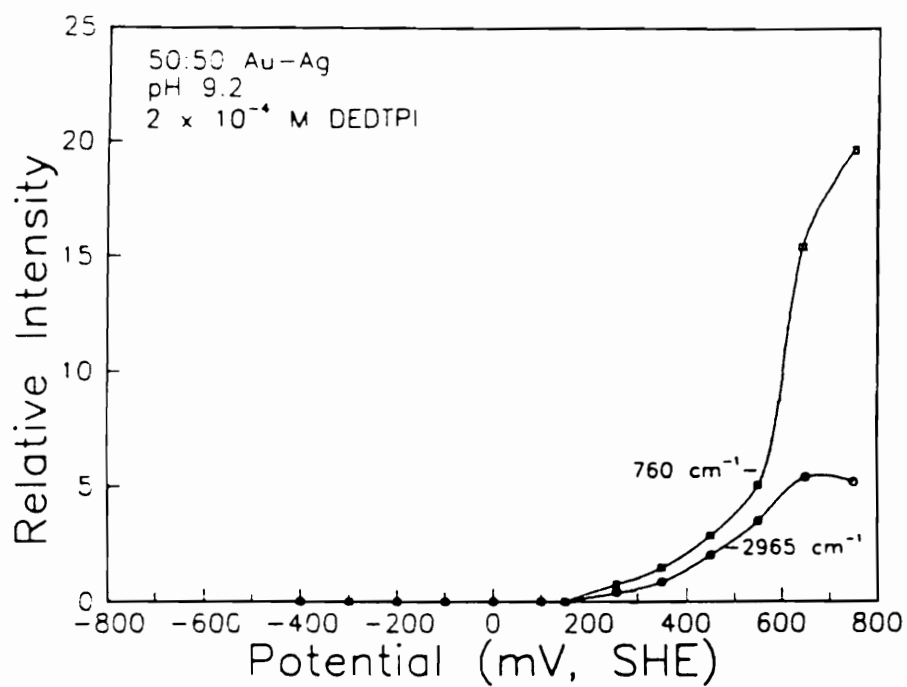


Figure 3.14. The effect of potential on the IR signal intensity (2965 and 760 cm^{-1}) of adsorbed DEDTPI for 50:50 Au-Ag alloy in the presence of 2×10^{-4} M DEDTPI at pH 9.2.

rinsed before taking the *ex situ* IR spectrum and, therefore, no adsorption peak is detected at these potentials.

The FTIR reflectance measurements show the start of DEDTPI adsorption above 150 mV. This value is lower than that for the 80:20 Au-Ag alloy, but higher than that for pure Ag°. Thus, the onset of DEDTPI adsorption is dependent on the silver content of the alloy; the higher the silver content, the closer the potential where adsorption starts to that observed for pure Ag°. The adsorption of DEDTPI observed on the electrode above 150 mV may be attributed to an EC-type reaction mechanism given by reactions (6) and (7). There is a sharp increase in the relative intensity at potentials above 550 mV. This is probably associated with the oxidation of DEDTPI to a dimer as given by reaction (4). The increase in anodic current is also observed in the voltammograms. Therefore, the results of spectroscopic measurements show a good agreement with those of electrochemical experiments.

3.3.2.2. Diisobutyl Dithiophosphinate

3.3.2.2.1. FTIR Spectra

The IR spectra obtained for NH₄DIBDTPI, (DIBDTPI)₂, and AgDIBDTPI are given in Figure 3.15. (DIBDTPI)₂ was prepared by oxidizing DIBDTPI in iodine-potassium iodide solution. The major absorption peaks which are characteristic for the NH₄DIBDTPI are observed at 2956, 2868, 1165, 1106, 1060, 921, 838, 813, 797, 745 and 710 cm⁻¹. The bands that are characteristic for (DIBDTPI)₂ are found at 2958, 2928, 2868, 1161, 1104, 1064, 1055, 851, 819, 783, 749, and 725 cm⁻¹. For the AgDIBDTPI compound, the characteristic bands are observed at 2953, 2868, 1164, 1106, 1065, 840, 808, 799, 759, 731, and 711 cm⁻¹. The bands observed between 3000-2800 cm⁻¹, which may be associated with the C-H vibrations of the alkyl

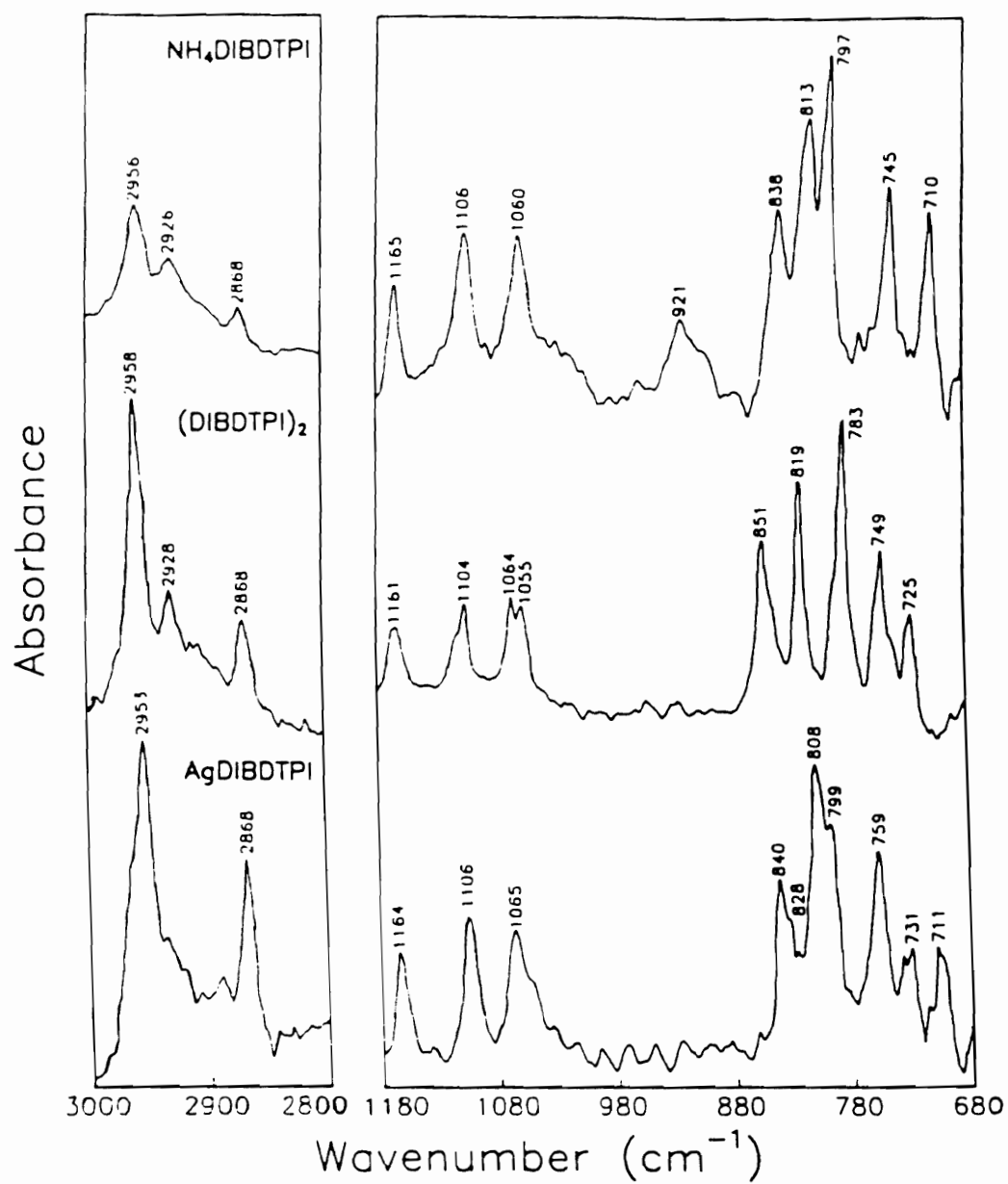


Figure 3.15. FTIR reflection spectra of $\text{NH}_4\text{DIBDTPI}$, $(\text{DIBDTPI})_2$, and AgDIBDTPI .

group (Bellamy, 1975), are the same for the three DIBDTPI. However, the absorption peaks found below 900 cm^{-1} are shifted for $(\text{DIBDTPI})_2$ and AgDIBDTPI as compared with those for $\text{NH}_4\text{DIBDTPI}$. The signals that may be due to P-S vibrations (Kabachnik, 1965; Bellamy, 1968) are shifted in both cases. This suggests that the sulfur is involved in the bonding, i.e., a S-S bond for $(\text{DIBDTPI})_2$ and a S-Ag bond for AgDIBDTPI .

Some of the spectra obtained for Au^0 and Ag^0 in the presence of $2 \times 10^{-4}\text{ M}$ DIBDTPI at different potentials are shown in Figure 3.16. The spectrum for Au^0 conditioned at 750 mV probably indicates the formation of the $(\text{DIBDTPI})_2$ species on the electrode surface. For Ag^0 at a potential of 550 mV, the spectrum is similar to that for AgDIBDTPI , suggesting that the species formed on the surface is AgDIBDTPI . The presence of silver oxidation products on the electrode surface, which is expected at this potential, is indicated by the broad band in the $1080\text{--}880\text{ cm}^{-1}$ region.

3.3.2.2.2. Effect of Potential

The results of IR reflectance spectroscopy for Au^0 in the presence of $2 \times 10^{-4}\text{ M}$ DIBDTPI at pH 9.2 are shown in Figure 3.17. Assuming the peak intensity to be the measure of DIBDTPI adsorbed on the surface, it can be seen that the amount of collector adsorption increases as the applied potential increases. In the voltammetry, the oxidation of DIBDTPI to $(\text{DIBDTPI})_2$ was observed to start at around 550 mV, which is in good agreement with the results of spectroscopic experiments shown here. Although the electrode was also passivated at potentials below 550 mV, IR spectra do not show any absorption in this potential region. The weakly physisorbed DIBDTPI may be removed from the surface when the electrode is rinsed before taking the *ex situ* FTIR spectrum. The IR signal intensities measured here for DIBDTPI are higher than those for DEDTPI. This may be

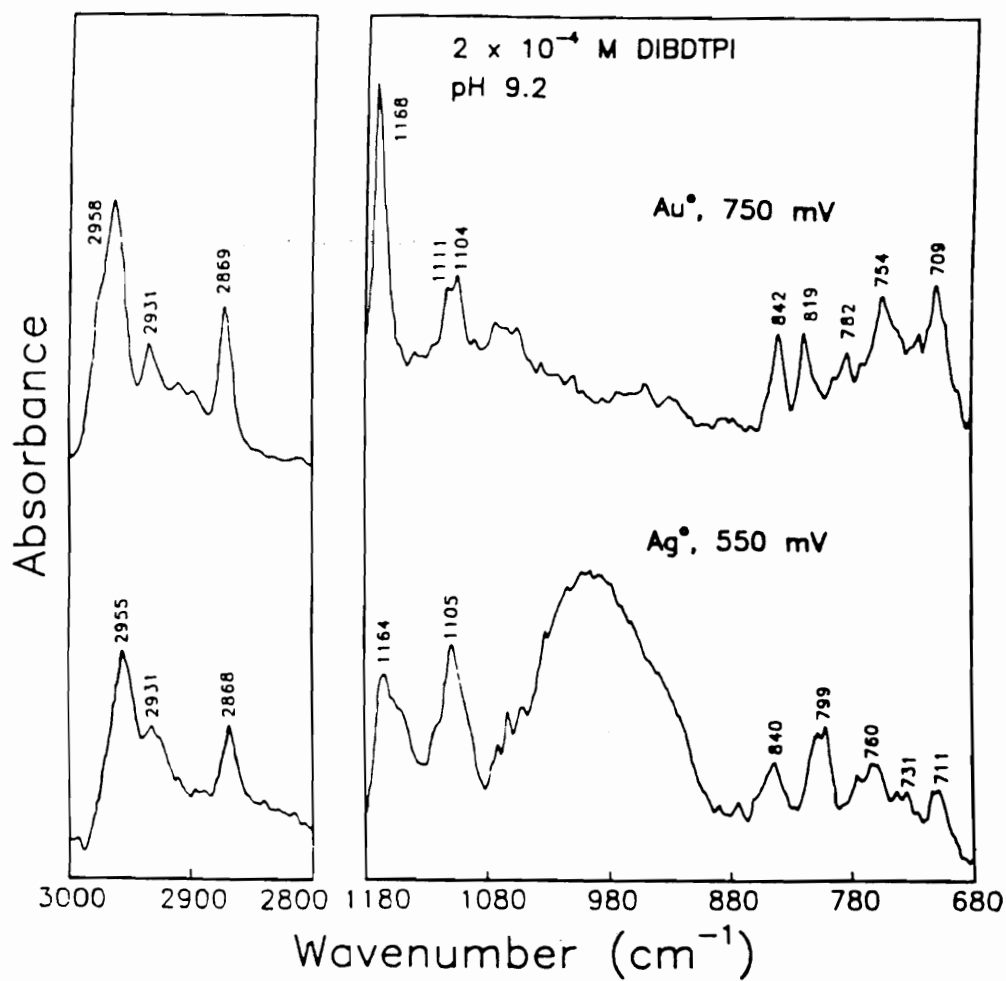


Figure 3.16. FTIR reflection spectra of (a) Au° at 750 mV and (b) Ag° at 550 mV in 2×10^{-4} M DIBDTPI.

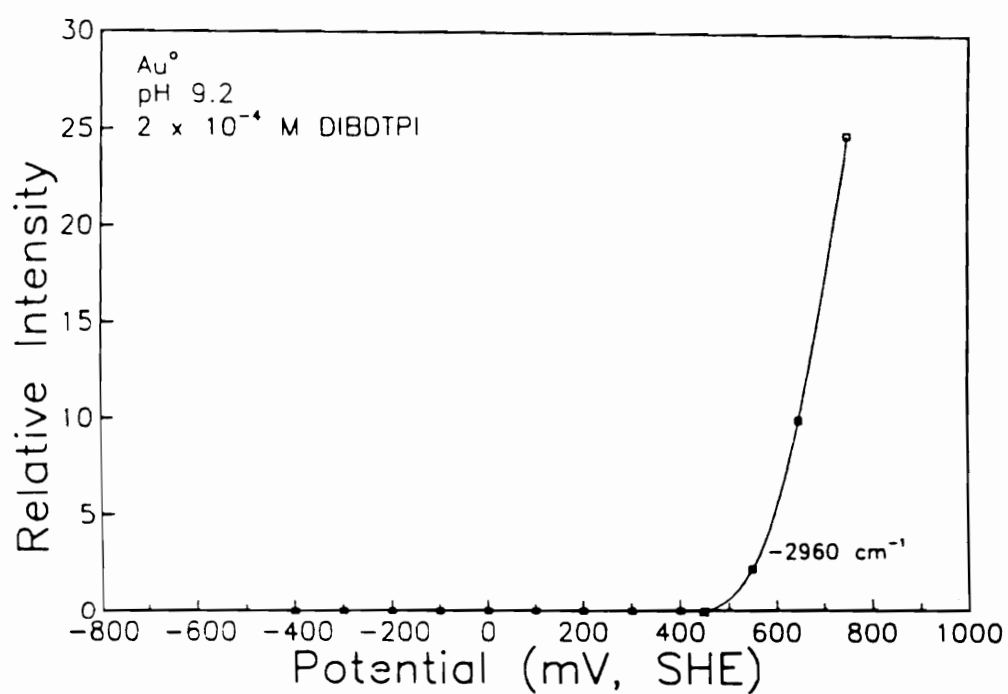


Figure 3.17. The effect of potential on the IR signal intensity (2960 cm^{-1}) of adsorbed DIBDTPI for Au° in the presence of $2 \times 10^{-4}\text{ M}$ DIBDTPI at pH 9.2.

attributed to the longer chain length of the alkyl group in DIBDTPI.

Figure 3.18 shows the IR intensities of DIBDTPI adsorbed on Ag° . These results are consistent with that of voltammetry and show an increase in adsorption with applied potential. The adsorption peak intensity starts to increase at around 250 mV, which is presumably associated with the EC-type reaction mechanism involving Ag° and DIBDTPI to form AgDIBDTPI . The reaction mechanism suggested here is similar to that for Ag-DEDTPI system. That is, the electrochemical step (E) is followed by a chemical reaction step (C). Above 350 mV, the adsorption intensity increases sharply, which may be due to multilayer formation associated with the release of Ag^+ ions. The start of oxidation of Ag° is also observed in the voltammogram at around the same potential.

There is a decrease in the intensity of DIBDTPI adsorption above 450 mV. At high potentials, Ag° oxidizes to Ag_2O passivating the electrode and, hence, limiting the adsorption. The potential at which DIBDTPI begins to adsorb on Ag° is higher than that observed for DEDTPI . The reason for this difference is not known at present.

The IR reflectance spectroscopy obtained for the two Au-Ag alloys (80:20 and 50:50) showed similar results to those obtained for DEDTPI and represents the formation of AgDIBDTPI , followed by $(\text{DIBDTPI})_2$ formation (shown in Appendix). The potential where the collector adsorption starts is directly related to the Ag content in the alloy. DIBDTPI adsorption starts at a lower potential for the 50:50 Au-Ag alloy than for the 80:20 Au-Ag alloy; however, it starts at a higher potential for the 50:50 Au-Ag alloy compared with that for pure Ag° . This is due to the diminished activity of Ag as the silver content decreases in the alloy.

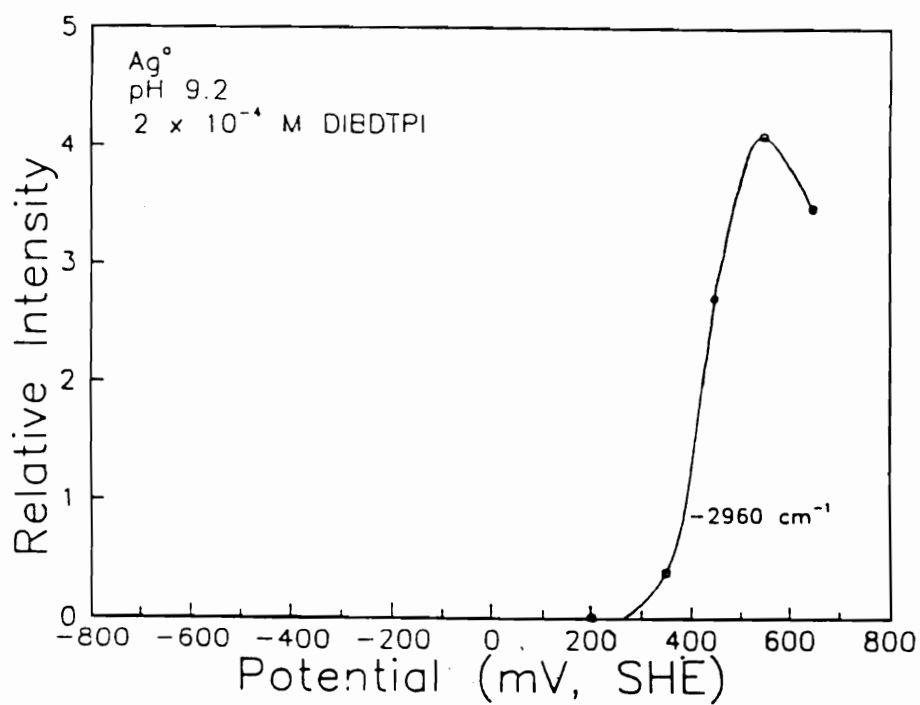


Figure 3.18. The effect of potential on the IR signal intensity (2960 cm^{-1}) of adsorbed DIBDTPI for Ag° in the presence of $2 \times 10^{-4} \text{ M}$ DIBDTPI at pH 9.2.

3.3.2.3. Diisobutyl Monothiophosphinate

3.3.2.3.1. FTIR Spectra

Figure 3.19 shows the FTIR spectra of $\text{NH}_4\text{DIBMTPI}$ and AgDIBMTPI , and the spectrum obtained for Ag° conditioned at 500 mV. The major absorption bands that are characteristic for the pure reagent are observed at 2957, 2872, 1167, 1107, 1067, 1026, 936, 846, 816, and 773 cm^{-1} . For the AgDIBMTPI , the characteristic peaks are observed at 2960, 2869, 1166, 1119, 1052, and 804 cm^{-1} . The bands observed in the 3000–2800 cm^{-1} range, which may be due to the C-H vibration of the alkyl group, do not represent any shift for these two species. On the contrary, the absorption bands observed below 900 cm^{-1} , which is presumably attributed to the P-S vibrations, are shifted for AgDIBMTPI . This implies that sulfur is involved in the bonding between silver and DIBMTPI to form AgDIBMTPI .

The spectrum obtained for Ag° conditioned at 500 mV in the presence of 1×10^{-4} M DIBMTPI shows characteristic peaks which are similar to that for the bulk AgDIBMTPI compound. Therefore, the surface species present on the electrode is thought to be AgDIBMTPI .

3.3.2.3.2. Effect of Potential

The IR reflectance spectroscopy for Au° with the addition of 1×10^{-4} M DIBMTPI is shown in Figure 3.20. As seen from this result, the spectroscopic measurements do not indicate the presence of adsorbed species on the Au° surface over the entire potential range investigated. In the voltammograms, the passivation of the electrode is observed, which is similar to the findings for the Au° -DTPI systems. However, there is no indication for the oxidation of DIBMTPI, which is unlike the case with

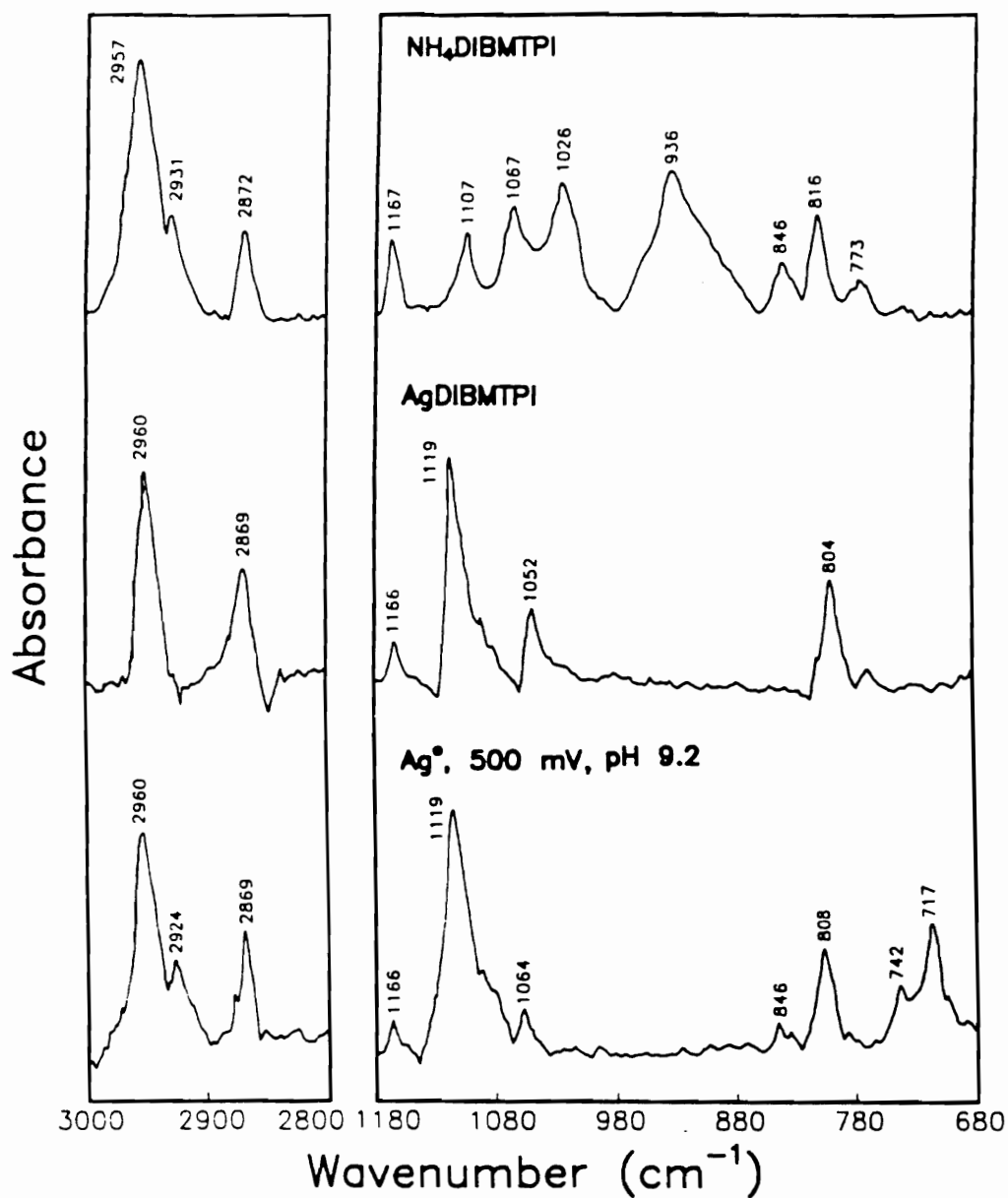


Figure 3.19. FTIR reflection spectra of NH₄DIBMTPI, AgDIBMTPI, and Ag° at 500 mV in 1 x 10⁻⁴ M DIBMTPI.

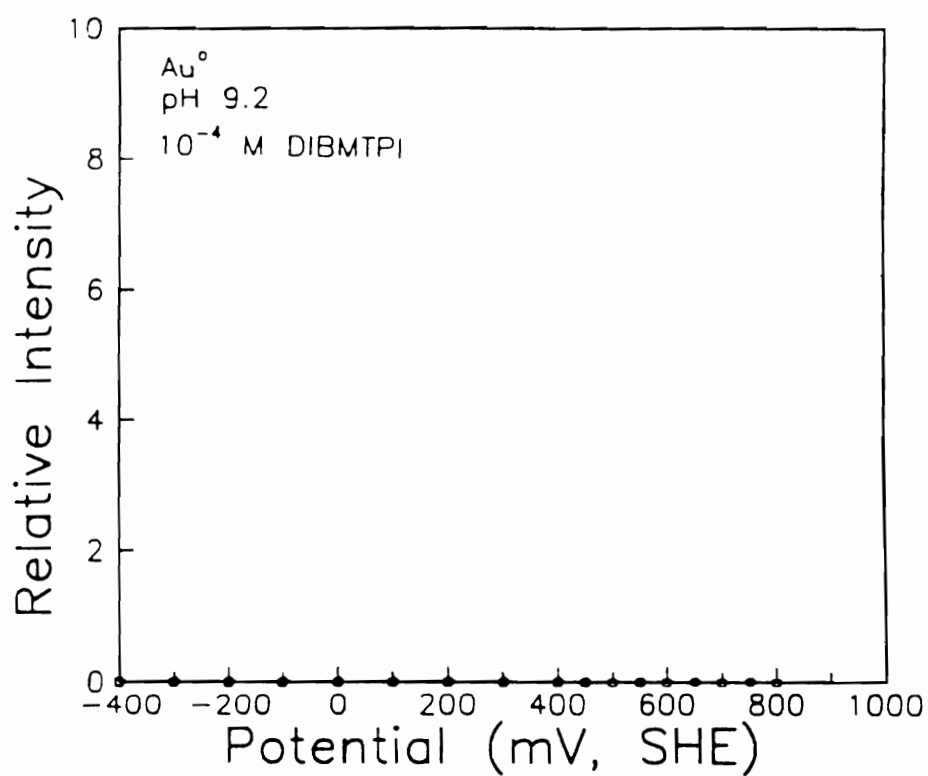


Figure 3.20. The effect of potential on the IR signal intensity (2960 cm⁻¹) of adsorbed DIBMTPI for Au⁰ in the presence of 2 x 10⁻⁴ M DIBMTPI at pH 9.2.

dithio analogue. Therefore, it may be said that the passivation observed in the voltammograms is presumably due to the weak physisorption of DIBMTPI, which the *ex situ* IR reflectance measurements cannot detect. The adsorption of DIBMTPI on Au^0 is observed only at higher reagent additions.

Figure 3.21 shows the IR reflectance measurements for Ag^0 at pH 9.2. It indicates that adsorption of DIBMTPI on the surface starts at potentials above 250 mV, with the amount adsorbed increasing with the applied potential. This result shows a good agreement with voltammetry. The interaction of DIBMTPI with silver may be explained by the EC-type reaction mechanism, which is similar to that given for Ag^0 -DTPI system. The IR experiments for the two Au-Ag alloys (80:20, 50:50) shows similar results to those observed for DTPI (Figures 3.22 and 3.23). However, the formation of dimer is not observed for DIBMTPI in the spectroscopic measurements.

3.3.3. Contact Angle Measurement

3.3.3.1. Diethyl Dithiophosphinate

The contact angle data obtained for Au^0 in the presence of 2×10^{-4} M DEDTPI (\square) at pH 9.2 is shown in Figure 3.24. The results show that there is no change in the hydrophobicity of Au^0 over the entire potential range measured. This is contrary to the observations made in the voltammetry and IR spectroscopic measurements. However, at higher concentrations (1×10^{-3} M) of DEDTPI (\diamond), the contact angle results are in good agreement with the IR data. The observed hydrophobicity may be attributed to the formation of $(\text{DEDTPI})_2$ on the electrode surface according to reaction (4). The fact that Au^0 becomes hydrophobic only at high concentrations indicates that reaction (4) occurs at concentrations above certain threshold value of $[\text{DEDTPI}]$. This is analogous to xanthate oxidation to dixanthogen.

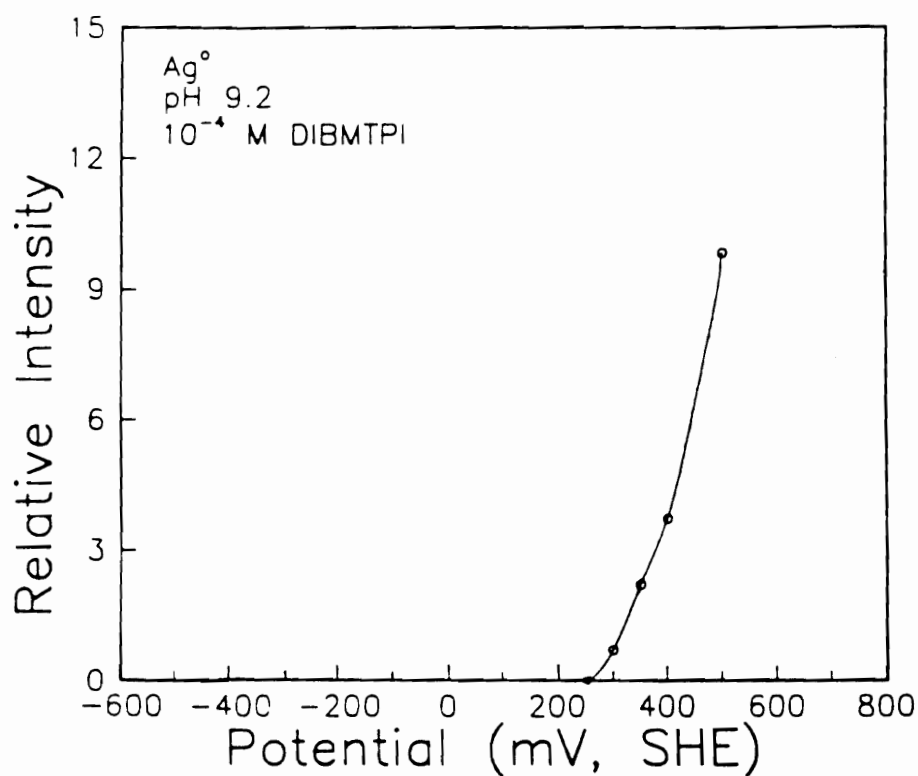


Figure 3.21. The effect of potential on the IR signal intensity (2960 cm⁻¹) of adsorbed DIBMTPI for Ag° in the presence of 2 x 10⁻⁴ M DIBMTPI at pH 9.2.

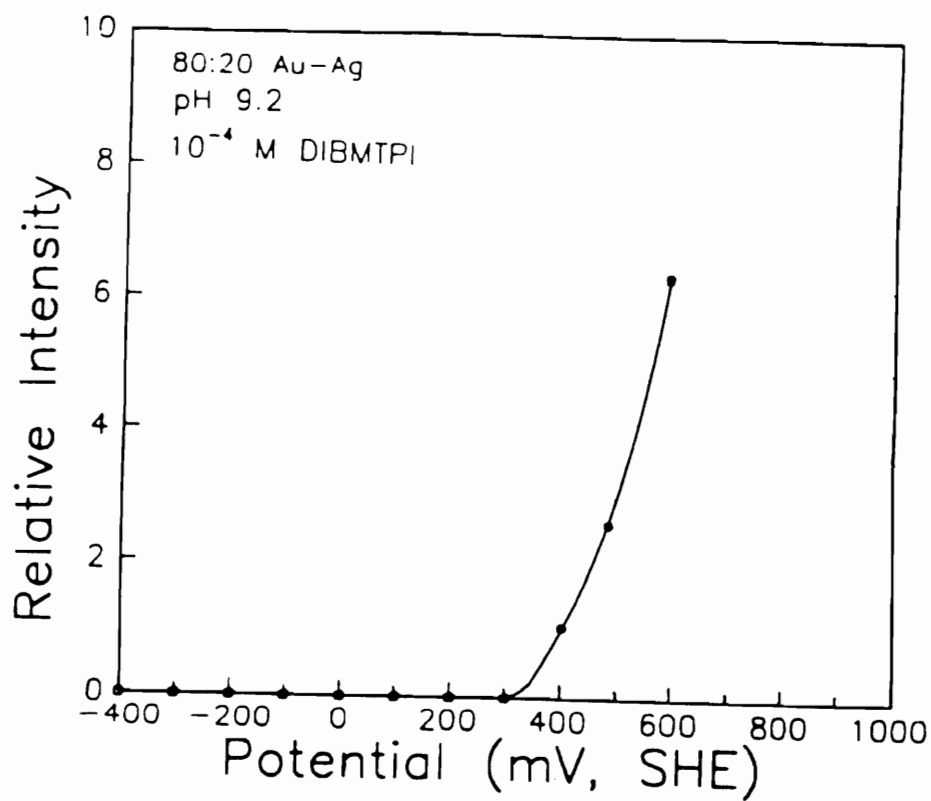


Figure 3.22. The effect of potential on the IR signal intensity (2960 cm^{-1}) of adsorbed DIBMTPI for 80:20 Au-Ag alloy in the presence of 1×10^{-4} M DIBMTPI at pH 9.2.

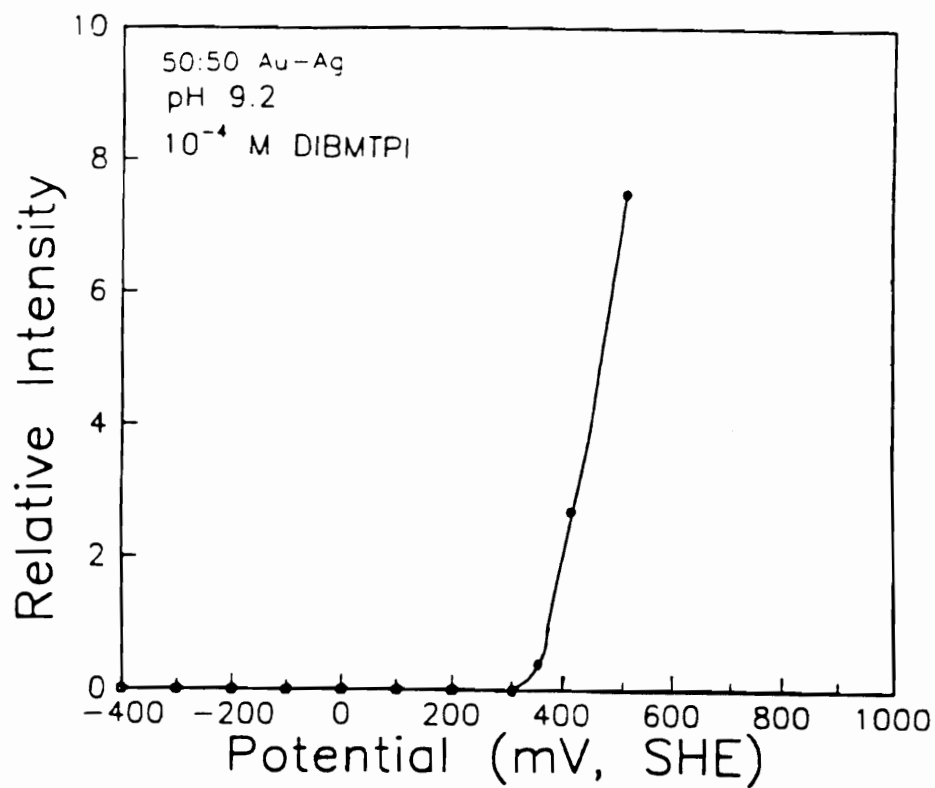


Figure 3.23. The effect of potential on the IR signal intensity (2960 cm^{-1}) of adsorbed DIBMTPI for 50:50 Au-Ag alloy in the presence of 1×10^{-4} M DIBMTPI at pH 9.2.

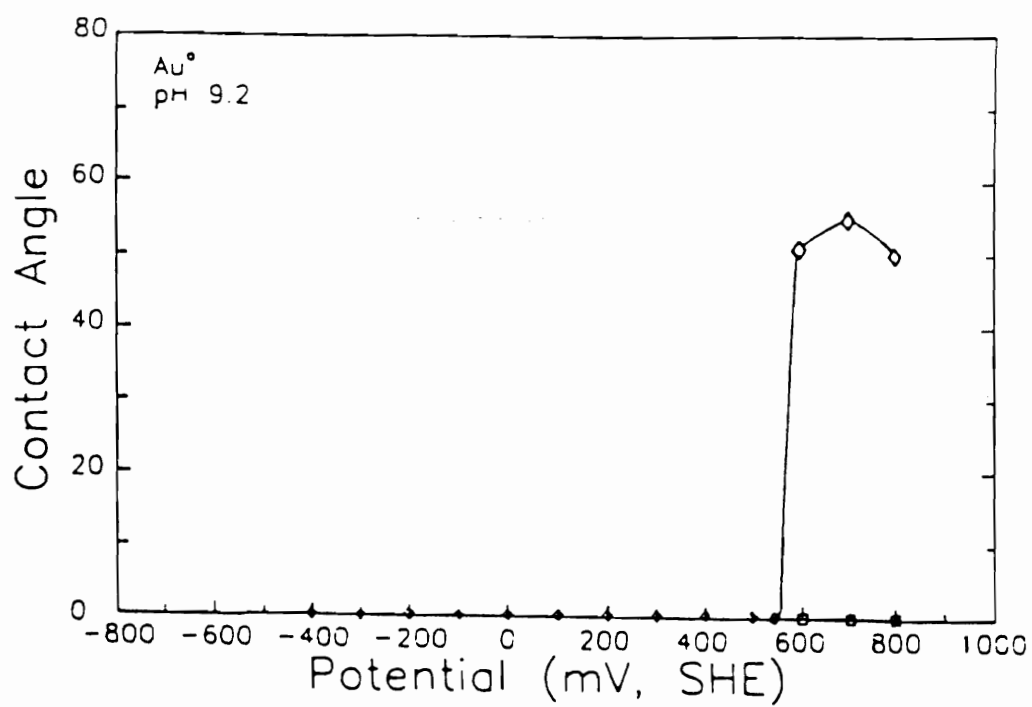


Figure 3.24. The effect of potential on the contact angle for Au° in the presence of $2 \times 10^{-4} \text{ M}$ (\square) and $1 \times 10^{-3} \text{ M}$ (\diamond) of DEDTPI at pH 9.2.

Figure 3.25 represents the contact angle measurements for Ag°. It can be seen that Ag° becomes hydrophobic at about 0 mV. The potentials, at which a new anodic peak starts in the voltammograms and the adsorption peak intensity begins to increase in IR measurements, show the same value. Therefore, the data obtained from contact angle and IR spectroscopy measurements are in good agreement with the findings from voltammetry. The formation of AgDEDTPI according to the coupled reactions of EC-type is probably responsible for the hydrophobicity observed in the presence of DEDTPI. The contact angle remains constant above 100 mV, probably indicating that a monolayer coverage is obtained.

In the IR reflectance measurements, there is a sharp increase in DEDTPI adsorption above 350 mV (Fig. 3.12), which has been attributed to multilayer formation. However, there is no changes in contact angle even above this potential. Thus, it may be said that multilayer formation of collector on the electrode does not increase the hydrophobicity.

The influence of potential on the contact angle for the 80:20 Au-Ag alloy - DEDTPI system is represented in Figure 3.26. The contact angle measurements show that the electrode becomes hydrophobic above 450 mV. There is no significant increase in the contact angle at potentials where (DEDTPI)₂ is formed on the electrode (above 550 mV). Therefore, the interaction of DEDTPI with the silver in the Au-Ag alloy is responsible for making this alloy hydrophobic. It should be pointed out that the results of contact angle and IR measurements support the findings in voltammetry.

Figure 3.27 shows the results of contact angle measurements obtained for the 50:50 Au-Ag alloy in the presence of 2×10^{-4} M DEDTPI. It is shown that DEDTPI begins to adsorb above 150 mV. This value is lower than that for the 80:20 Au-Ag alloy, but higher than that for Ag°. Therefore,

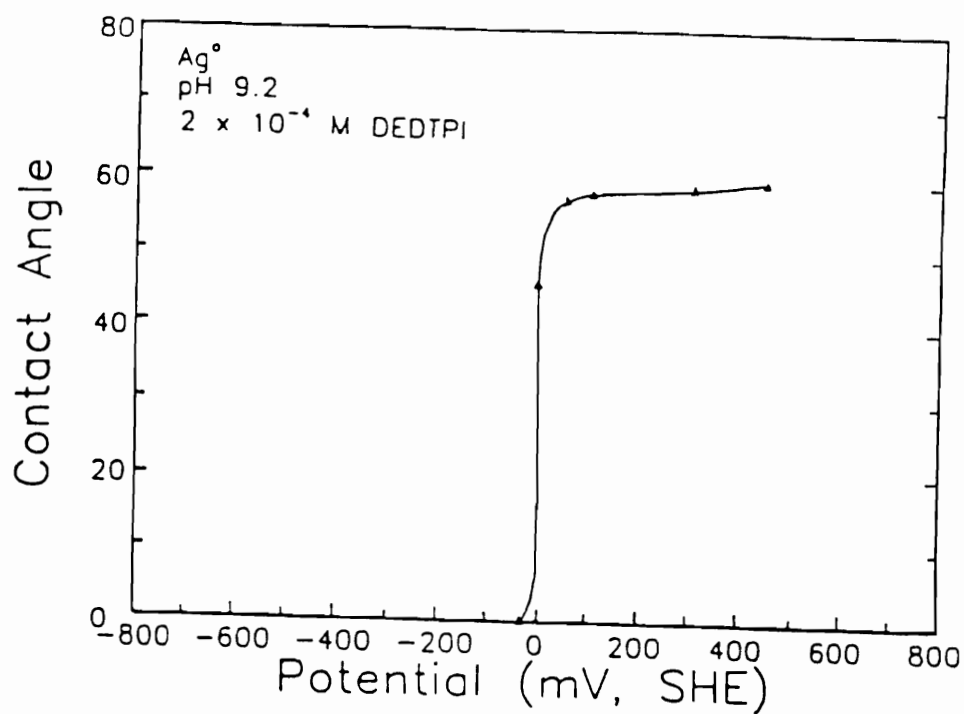


Figure 3.25. The effect of potential on the contact angle for Ag° in the presence of 2×10^{-4} M DEDTPI at pH 9.2.

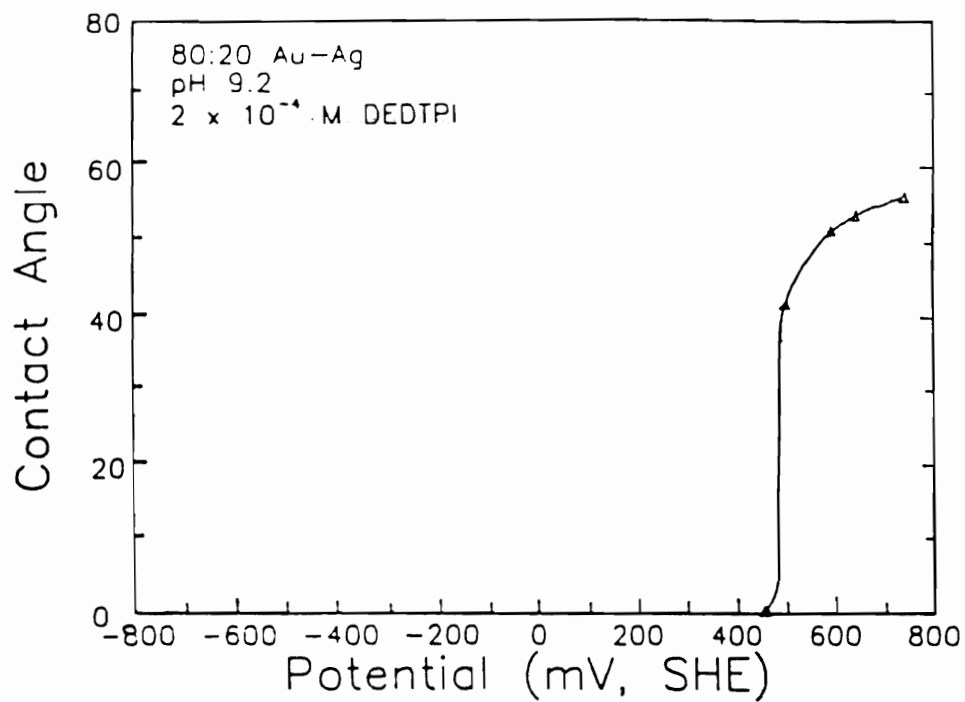


Figure 3.26. The effect of potential on the contact angle for 80:20 Au-Ag alloy in the presence of 2×10^{-4} M DEDTPI at pH 9.2.

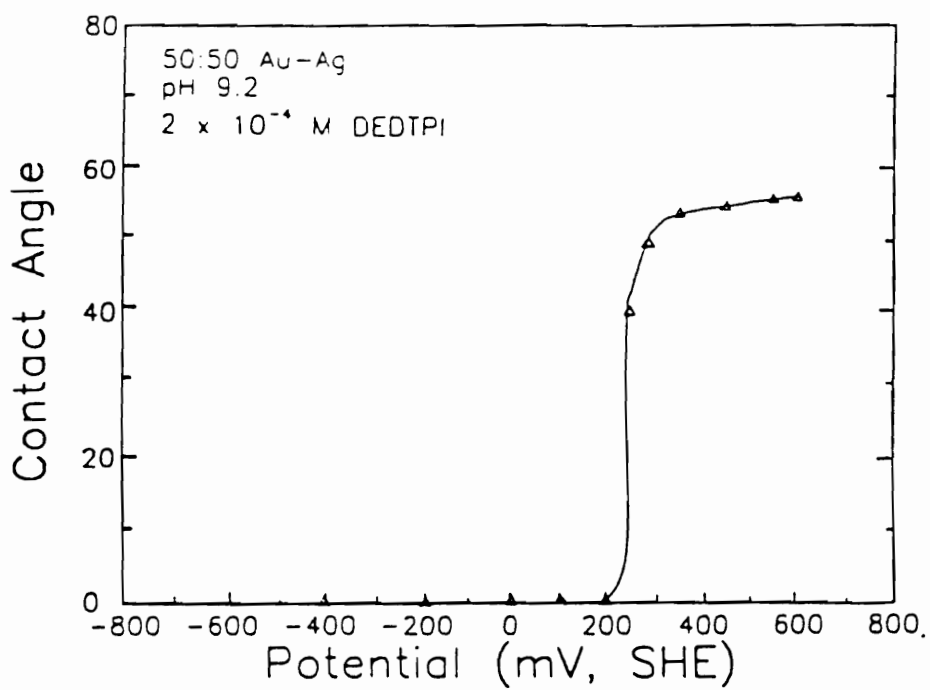


Figure 3.27. The effect of potential on the contact angle for 50:50 Au-Ag alloy in the presence of 2×10^{-4} M DEDTPI at pH 9.2.

the onset of DEDTPI adsorption is directly dependent on the activity of silver in the alloy. The higher the silver content, the closer the onset potential approaches that of pure Ag° .

At potentials above 550 mV, the oxidation of DEDTPI to $(\text{DEDTPI})_2$ has been indicated by the increase in anodic current in voltammetry (Fig. 3.4). However, no increase in the contact angle is observed in this potential range. Thus, the formation of AgDEDTPI may be sufficient to render the electrode hydrophobic.

3.3.3.2. Diisobutyl Dithiophosphinate

The contact angle measurements conducted with the Au° electrode in the presence of 2×10^{-4} M DIBDTPI are shown in Figure 3.28. Similar to those observed for the Au° -DEDTPI system, no bubble contact was observed over the entire potential range at this concentration. According to voltammetry results, the oxidation of DIBDTPI to dimer starts at approximately 550 mV. At higher collector additions (10^{-3} M), significant contact angles are observed at potentials close to that observed with voltammetry (Fig. 3.29). Therefore, the hydrophobicity of Au° electrode in the presence of DIBDTPI is most likely due to the formation of $(\text{DIBDTPI})_2$. The contact angle and voltammetry data are in good agreement with those of the IR measurements.

Figure 3.30 shows the effect of potential on the surface hydrophobicity of Ag° at pH 9.2. According to this result, the adsorption of DIBDTPI starts at about 250 mV, which may be attributed to an EC mechanism involving Ag° and DIBDTPI to form AgDIBDTPI . This mechanism is similar to that proposed for the Ag -DEDTPI system. The contact angle measured on the electrode increases with increasing potential and levels off above 350 mV. Since the contact angle does not increase significantly at higher potentials, the multilayer formation of reagent may not

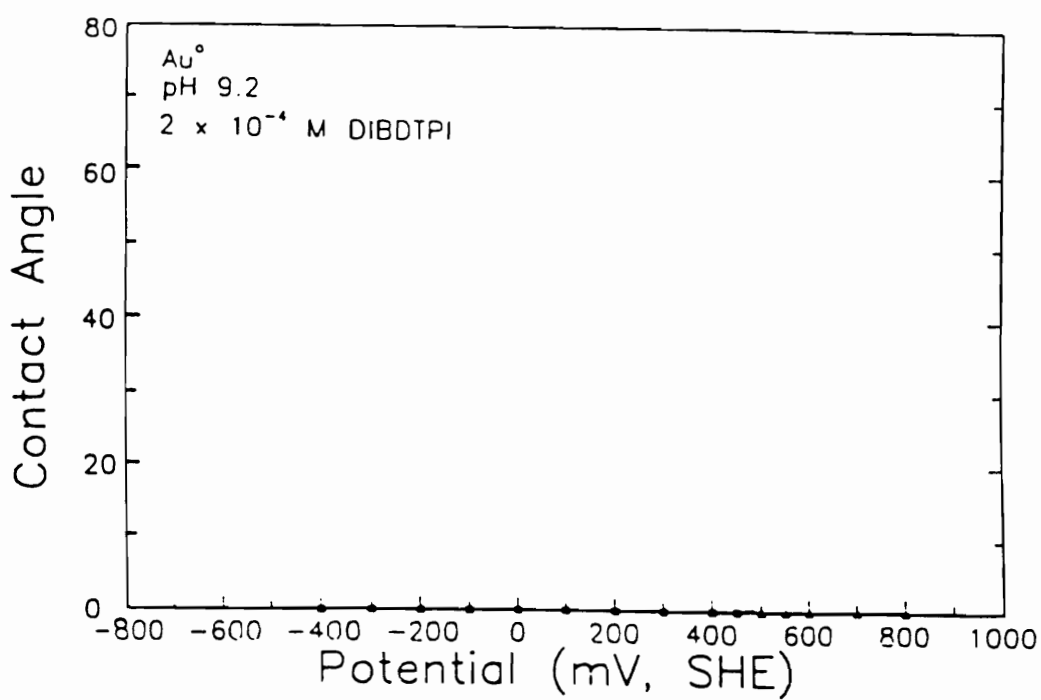


Figure 3.28. The effect of potential on the contact angle for Au° in the presence of 2×10^{-4} M DIBDTPI at pH 9.2.

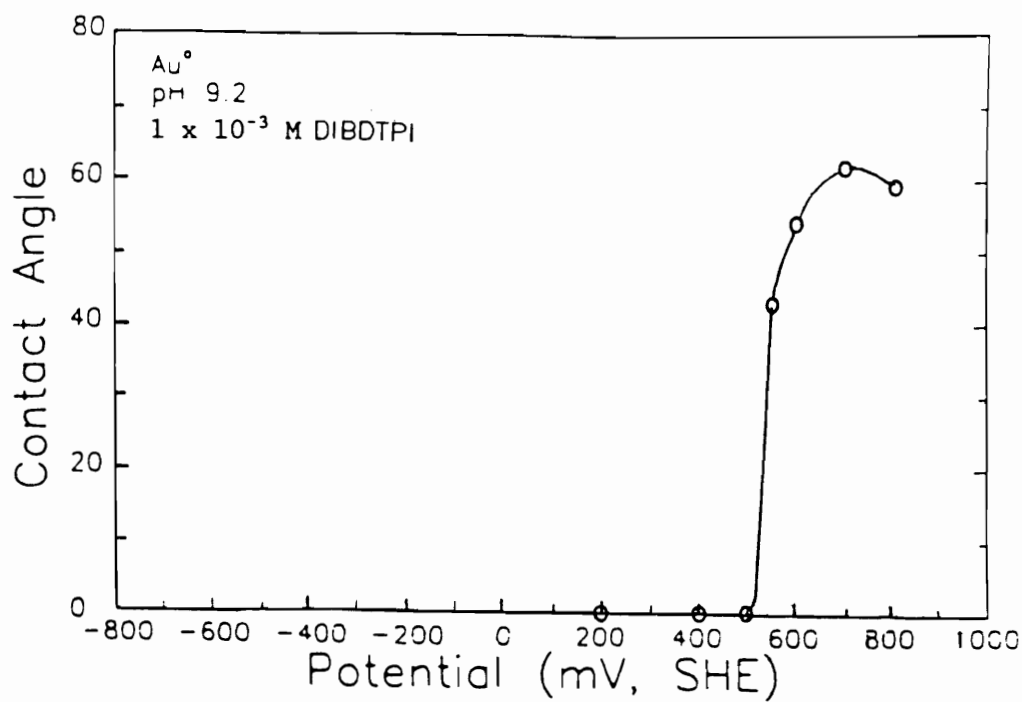


Figure 3.29. The effect of potential on the contact angle for Au° in the presence of 1 x 10⁻³ M DIBDTPI at pH 9.2.

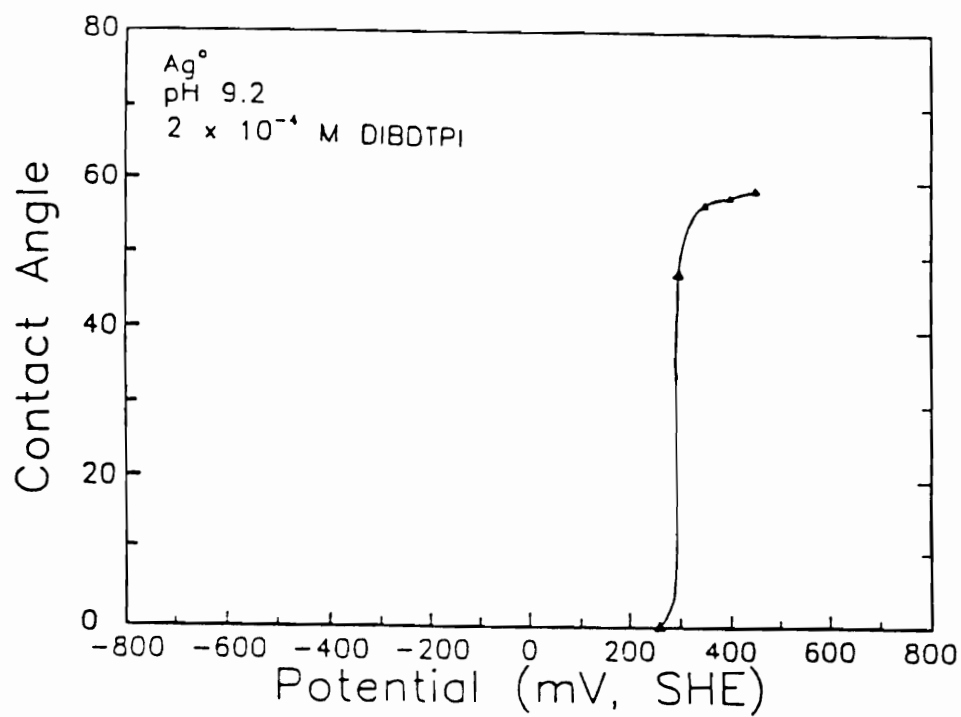


Figure 3.30. The effect of potential on the contact angle for Ag° in the presence of 2 x 10⁻⁴ M DIBDTPI at pH 9.2.

contribute to the surface hydrophobicity.

During the voltammetry experiments, the electrode is passivated in the presence of DIBDTPI in the potential range observed in the contact angle measurements (Fig. 3.6). Therefore, the contact angle data are consistent with that observed in the voltammetry.

3.3.3.3. Diisobutyl Monothiophosphate

The contact angle data for Au^0 in the presence of 1×10^{-4} M DIBMTPI at pH 9.2 are shown in Figure 3.31. It does not show any appreciable contact angle over the entire potential range measured. Similar observations have been also made for the Au^0 -MTP systems (Basilio et al., 1991b). Neither the IR spectra show the presence of adsorbed species on the electrode surface. The dissimilarity between DIBMTPI and the other dithio-reagents studied presumably comes from the different structure in head group. That is, two sulfur atoms in dithiophosphate presumably provide more favorable conditions for the reaction with Au^0 than DIBMTPI, which contains only one sulfur atom in head group.

Figure 3.32 shows the change in hydrophobicity of the Ag^0 electrode with changing potential. The result shows that Ag^0 becomes hydrophobic above 300 mV. According to the voltammetry experiments (Fig. 3.8), the adsorption of DIBMTPI is indicated by the anodic current rise at approximately the same potential as observed in contact angle measurements. The FTIR reflectance measurements also show the onset of collector adsorption above 250 mV (Fig. 3.21). Therefore, it may be said that the formation of AgDIBMTPI is responsible for the hydrophobicity observed in the contact angle measurements.

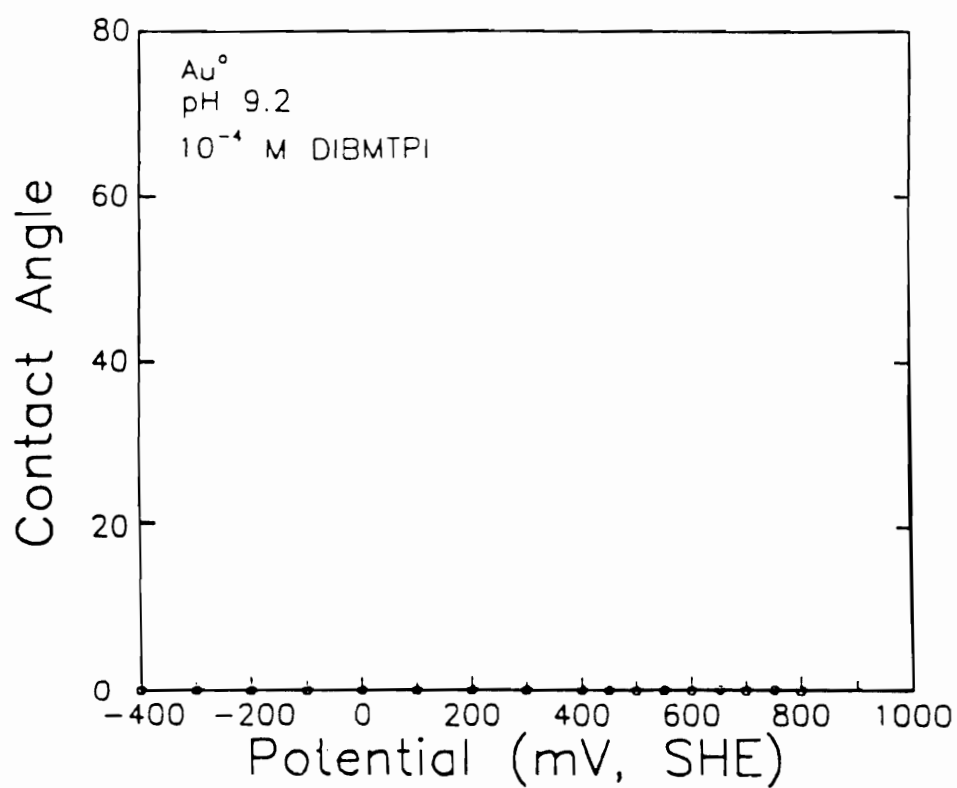


Figure 3.31. The effect of potential on the contact angle for Au° in the presence of 1×10^{-4} M DIBMTPI at pH 9.2.

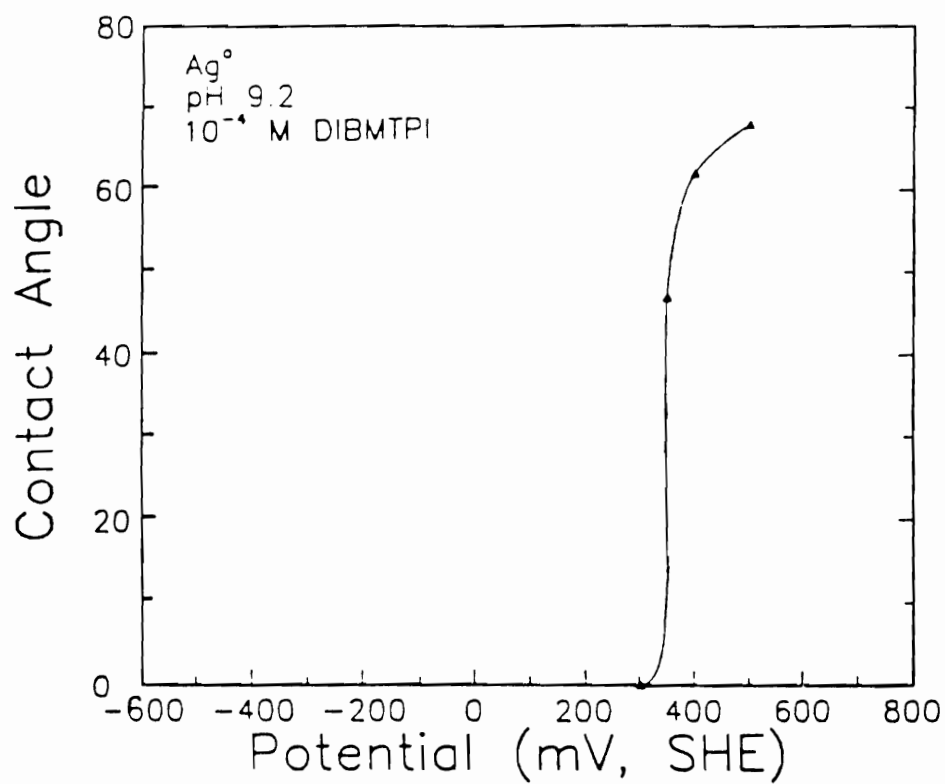


Figure 3.32. The effect of potential on the contact angle for Ag° in the presence of 1×10^{-4} M DIBMTPI at pH 9.2.

3.3.4. E_h -pH Diagram

The average solubility products of AgDIBDTPI and AgDIBMTPI obtained by titration method were 4.16×10^{-13} and 1.72×10^{-12} , respectively. The standard Gibbs free energy of formation (ΔG°) obtained from these data were -6.50 and -5.11 kJ/mol for AgDIBDTPI and AgDIBMTPI, respectively. Based on these data, the E_h -pH diagrams have been constructed for Ag/water/DTPI and Ag/water/MTPI systems are shown in Figures 3.33 and 3.34, respectively. For DTPI, only the E_h -pH diagram for the Ag° -DIBDTPI system has been constructed and compared with that for the Ag° -DIBMTPI system. The concentrations of DIBDTPI and DIBMTPI employed in these diagrams is 1×10^{-4} M and the pH of the system is 9.2.

As shown in these diagrams, silver reacts with DIBDTPI⁻ and DIBMTPI⁻ and starts to form AgDIBDTPI and AgDIBMTPI at approximately 0.30 and 0.35 V, respectively. These potentials are nearly the same as those observed in the voltammetry and FTIR measurements for Ag° at pH 9.2. Even for the Ag° -DIBDTPI system, although the concentration employed in voltammetry and FTIR experiments was 2×10^{-4} M, there is a good agreement between the results.

The E_h -pH diagrams for the Ag° -DIBDTPI and Ag° -DIBMTPI systems are similar to that for the Ag° -DCMTP system except at the lower potential region. After all the silver react with reagent and form silver-reagent compound, the other conditions do not influence the reactions any more. Therefore, the E_h -pH diagrams for these three systems are similar to each other at the higher potential region.

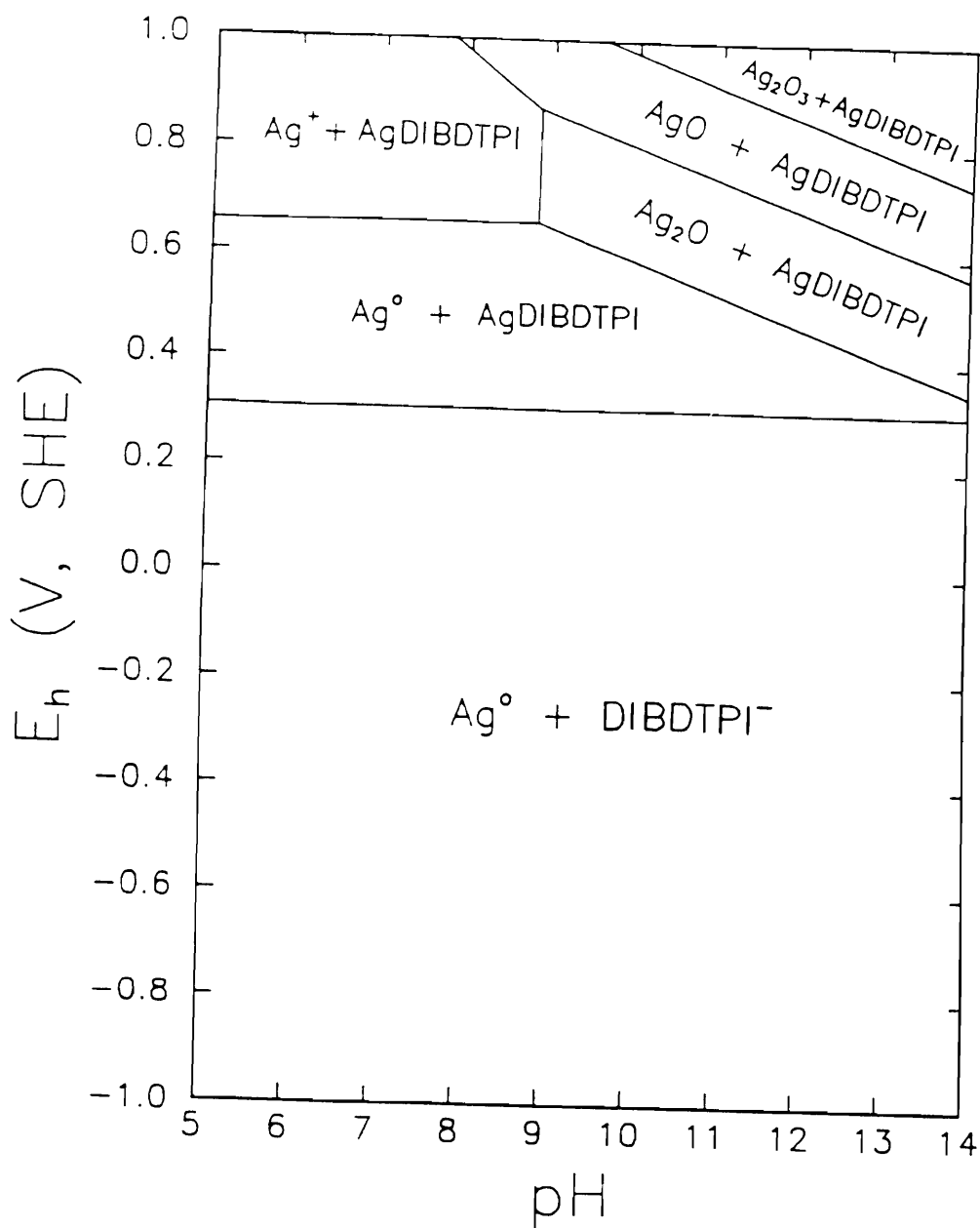


Figure 3.33. E_h -pH diagram for the silver/water/DTPI system for an initial collector concentration of 1×10^{-4} M.

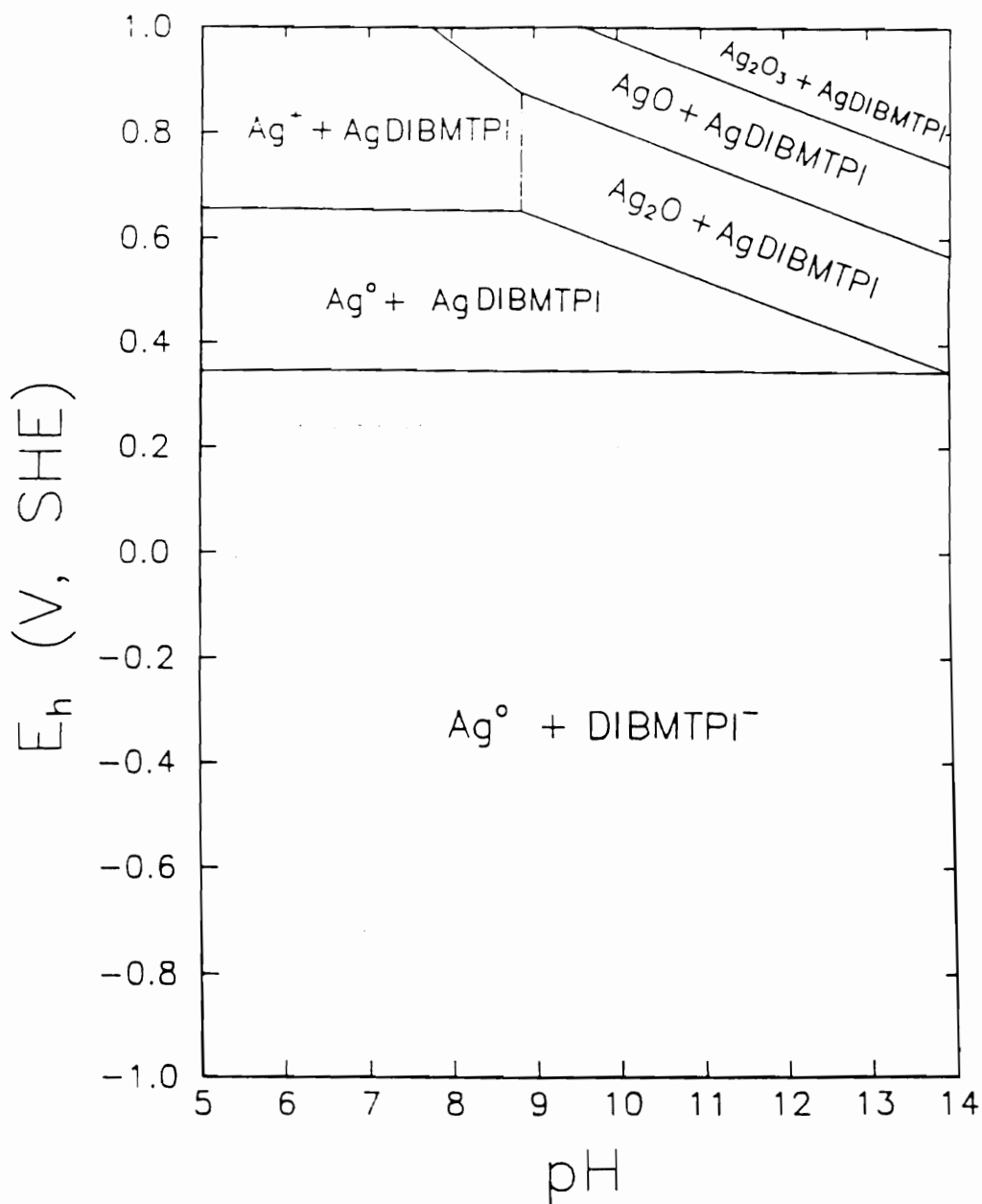


Figure 3.34. E_h -pH diagram for the silver/water/MTPI system for an initial collector concentration of 1×10^{-4} M.

3.4. Summary

The adsorption of dialkyl di- and mono-thiophosphinates on gold, silver, and gold-silver alloys (80:20, 50:50) have been studied. The results from voltammetry, IR spectroscopy, and contact angle measurements indicate that the di- and mono- thiophosphinates adsorb on Ag° and Au-Ag alloys through the formation of corresponding silver complex via an EC-mechanism. The adsorption process involves an initial electrochemical reaction (E), which is the oxidation of silver, followed by the chemical reaction (C) leading to the formation of the Ag-thiophosphinate compound.

The results also show that, in the case of dithiophosphinate, both a dimer, $(\text{DTPI})_2$, and silver complex, AgDTPI , are formed on Au-Ag alloys. On Au° electrode, the $(\text{DTPI})_2$ is the only hydrophobic species formed. For the case of DIBMTPI, however, there are no indications of dimer formation on Au° and Au-Ag alloys.

The potentials for the onset of thiophosphinate adsorption as determined by voltammetry, FTIR and contact angle measurements are in good agreement with each other. It is found that the onset potential decreases with increasing silver content of a Au-Ag alloy. These results are in good agreement with the E_a -pH diagrams constructed from thermodynamic data.

Chapter 4. Ethyl Xanthate System

Part I. Silver/Ethyl Xanthate System

4.1. Introduction

The interaction of thiol flotation collectors with sulfide-mineral and metal surfaces is characterized, for a number of systems, by a charge-transfer chemisorption process that precedes the formation of the metal collector compound. Such underpotential deposition of a chemisorbed layer has been demonstrated for ethyl xanthate on galena (Woods, 1971, Gardner et al., 1977, Pritzker et al., 1984), copper (Szegłowski et al., 1977, Woods et al., 1987, Woods, 1990), and chalcocite (Woods, Young et al., 1990, O'Dell, 1984, Richardson et al., 1984, O'Dell, Walker et al., 1986, Basilio et al., 1985, Leppinen, 1989), for propyl and butyl xanthates on galena (Gardner and Woods, 1977), and for diethyl dithiophosphate on chalcocite (Chander and Fuerstenau, 1974, Buckley and Woods, 1991).

The equilibrium coverage of chemisorbed ethyl xanthate on copper and chalcocite surfaces over a range of potentials has been determined (Woods et al., 1990) from measurements of the charge passed in desorbing the layer formed on electrodes of these materials. It was found that the data fitted a *Frumkin* isotherm (Schultze, 1980):

$$[\theta/(1-\theta)] \exp g\theta = K a_A \exp [\gamma FE/RT] \quad (1)$$

where θ is the fractional surface coverage, g and K are constants, a_A is the activity of the adsorbate in solution, γ the electrosorption valency, and the other terms have their usual meaning. The term $g\theta$ arises from

variation of the free energy of adsorption with coverage, through either heterogeneity of the surface or interactions between adsorbed molecules. When g is zero, equation (1) reduces to the corresponding *Langmuir* isotherm. The electrosorption valency, γ , reflects changes in the double layer associated with the adsorption process, in addition to the number of electrons involved in the charge transfer reaction. The latter is unity for the adsorption of ethyl xanthate because only one electron is involved in this reaction:



For each of the mineral/collector systems studied (Gardner et al., 1977, O'Dell et al., 1984), the chemisorbed layer has been found to be hydrophobic and the potential for the onset of flotation shown to lie within the chemisorption region. For ethyl xanthate chemisorption on chalcocite (Woods et al., 1990) and galena (Buckley and Woods, 1991), correlations have been made between flotation recovery and ethyl xanthate chemisorption coverage.

It is common practice to present thermodynamic data in the form of an E_h -pH diagram and to use such diagrams to predict the flotation response. For the systems in which chemisorption occurs, the E_h -pH diagram will not accurately represent flotation behavior if the normal practice is followed in which the only collector species considered are the collector itself, metal collector compounds, and the disulfide oxidation product. Such conventional diagrams will predict a potential of onset of flotation significantly higher than is observed in the experiments. Since the isotherm is also a thermodynamic expression, coverages derived from the isotherm can be included in E_h -pH diagrams. E_h -pH diagrams including chemisorbed species were constructed for the first time for the

copper/water/ethyl xanthate and chalcocite/water/ethyl xanthate systems (Woods et al., 1990). These diagrams accurately predict the potential of onset of flotation.

In a recent publication (Talonen et al., 1991), an *in situ* FTIR study was carried out for the investigation of ethyl xanthate adsorption on gold, silver, and copper electrodes under controlled potential. These authors observed a prewave on silver prior to silver ethyl xanthate formation similar to that found for copper and assigned the prewave to the deposition of a monolayer of xanthate.

In the first part of this chapter, detailed studies are presented for the silver/ethyl xanthate system in which the isotherm for the chemisorbed layer has been derived, an E_p -pH diagram that includes chemisorbed xanthate constructed, and the influence of surface species on the contact angle determined. Investigations to define the nature of the adsorbed layer are also presented.

4.2. Experiments

4.2.1. Voltammetry

A conventional three-electrode system was used for the voltammetric experiments. The cells were deoxygenated with high-purity nitrogen. The silver electrode employed depended on the techniques used for examining the surface layer. When only electrochemical parameters were determined, the electrode consisted of a 33 mm² disc of silver sealed into epoxy resin. A fresh surface was generated before each run by wet polishing with 800-grit silicon carbide paper and then rinsing with hot ethanol in an ultrasonic bath. When the products of interaction with xanthate were to be examined by FTIR spectroscopy, the electrode was a 10 x 40 mm silver plate. The surface of this electrode was polished with alumina and washed

three times with hot ethanol in an ultrasonic bath before each measurement. In experiments in which the solution composition was monitored by UV/Vis spectroscopy, the electrode consisted of 5.25 gm of silver wool obtained from Fisher Scientific. The silver wool was contacted with a platinum wire.

The electrode potential was controlled with a Pine Instrument Model RDE4 Potentiostat/Galvanostat and a PAR Model 175 programmer. The reference electrode was a silver/silver chloride electrode in 4 mol/l potassium chloride. All potentials are given on the standard hydrogen electrode (SHE) scale, taking the potential of the silver/silver chloride electrode to be 0.20 V against the SHE (Bates, 1964). Voltammograms were recorded on a Hewlett Packard 7015B X-Y recorder.

4.2.2. Adsorption Isotherm for Ag^+

The charge associated with the chemisorption of xanthate was determined from the charge passed in cathodically stripping the layer from the silver surface after holding the electrode in the potential region of the initial peak. The coverage of chemisorbed xanthate was determined from this charge. Figure 4.1 shows the way how the experiment was conducted for obtaining this. In the prewave region, the electrode was held at a selected potential. It took about 1 min for the current to reach zero and it means that the chemisorption reaction was completed at the potential held and equilibrium state had been established. After this, the electrode was scanned cathodically at 20 mV/sec and the cathodic charge passed between the starting potential and the lower limit was integrated. Voltammograms were recorded during this scan. Returned to the lower limit, the silver electrode was held for 1 min before next scan to reduce the chemisorbed xanthate completely.

It can be seen that as the holding potential increases the height of

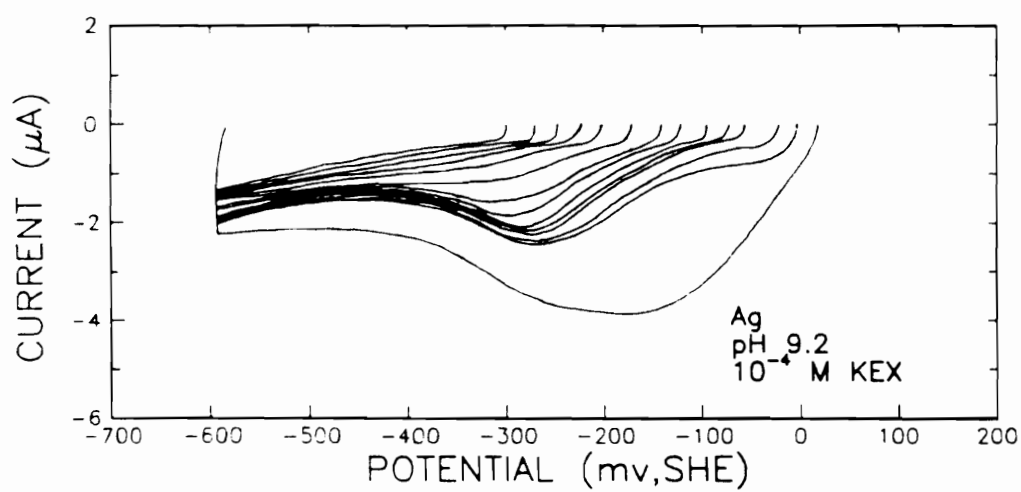


Figure 4.1. Cathodic scans for cyclic voltammograms for silver in solution of pH 9.2 containing 1×10^{-4} M ethyl xanthate. Scans at 20 mV/sec to different upper potential limits.

the cathodic peak also increases and it implies more xanthate has been chemisorbed on the surface as potential increases in the region of initial peak. The large cathodic peak shown for the negative going scan started from the potential higher than 0 mV represents the metal xanthate formed at above 0 mV is being reduced during the cathodic scan. Therefore, the occurrence of large cathodic peak during a consecutive cathodic scan means metal xanthate has been formed on the electrode surface already. The change due to xanthate desorption was taken as the difference between the charges passed on scans from the same potential run in the presence and absence of xanthate. Chemisorption was investigated at pH 6.8 (0.1 M KH_2PO_4 , 0.1 M NaOH) and pH 9.2 (0.05 M $\text{Na}_2\text{B}_4\text{O}_7$) containing 1×10^{-2} , 10^{-3} , 10^{-4} , and 10^{-5} M potassium ethyl xanthate.

In order to convert the charge associated with the chemisorption of xanthate to fractional surface coverage, it is necessary to know the charge corresponding to a monolayer. Since the real surface area of the electrode can not be measured accurately due to the surface roughness, it is difficult to derive the monolayer charge from theoretical considerations. Thus, same methodology applied previously to copper and chalcocite systems (Woods et al., 1990) was adopted in this work.

The assumption was made that, at equilibrium, the coverage of chemisorbed xanthate reaches a monolayer before silver ethyl xanthate develops. Since no silver xanthate can form at potentials below the reversible value of the silver/silver xanthate couple, the charge corresponding to stripping the layer formed at a potential just below the reversible value was taken to represent a monolayer. At all other potentials, surface coverage was taken as the ratio of the measured charge to that determined from the monolayer. The validity of this assumption is supported by the charge being independent of potential in the region just below the reversible silver/silver xanthate value.

4.2.3. FTIR Spectroscopy

To obtain FTIR reflectance spectra of ethyl xanthate adsorbed, the silver plate was polished with 0.3-, and 0.05- μm alumina (Buehler, Ltd.). The sample was washed first in an ultrasonic bath in ethyl alcohol, then with water. Next, the sample was immediately immersed into the electrochemical cell and held at constant potential for 1 min, withdrawn from the solution, rinsed with distilled water, dried, and transferred into the FTIR spectrometer to record the spectra.

When investigating the low potential region, the solution containing ethyl xanthate was drained from the cell until the bottom of the electrode was just immersed. The circuit was then opened and deoxygenated sodium borate solution flowed down the electrode surface to remove any xanthate-containing solution. The electrode was then removed from the cell, washed and dried in the normal manner. This procedure ensured that the state of the electrode surface corresponded to that at the set potential. Spurious results can be obtained by interaction of xanthate with the surface occurring when the electrode is on open circuit and in contact with air.

Spectra were recorded on a Perkin Elmer 1710 FTIR spectrometer equipped with a MCT detector using an external reflection attachment (Spectra Tech) with one reflection. The MCT detector was cooled with liquid nitrogen and the angle of incidence was 80° . The spectrometer was purged with nitrogen gas to minimize the amount of water vapor and carbon dioxide present. For each measurement, 100 spectra were scanned, co-added and signal averaged. The spectral resolution was 4 cm^{-1} . A wire grid polarizer (Harrick Scientific Corporation) was used to polarize the incident beam parallel to the plane of reflection (p-polarized). To obtain the reference spectra, the transmission spectra of silver ethyl xanthate in KBr pellets were prepared and measured in the standard way.

4.2.4. UV/Vis Spectroscopy

In experiments in which the solution composition was monitored spectroscopically in the UV/Vis wavelength region, an electrochemical cell was employed containing a working electrode of silver wool (Fisher Sci.) with high surface area. The cell solution was continuously circulated through a Perkin Elmer Lambda Array 3840 UV/Vis rapid-scan spectrophotometer.

Figure 4.2 shows the schematic representation of the experimental set-up for the UV/Vis adsorption kinetic studies. The solution was deoxygenated with highly pure nitrogen gas at least 1 hour before experiments. For the circulation of solution through the flow UV/Vis and electrochemical cell, a Masterflex tubing pump system was adopted.

Following deoxygenation of the pH 9.2 cell solution, the silver electrode was held at -0.43 V to reduce any surface oxide. A reference spectrum was recorded and ethyl xanthate was added to make the solution 2×10^{-5} M in this reagent. A full spectrum (190-900 nm) was then recorded and the potential either changed stepwise or on a 1 mV/sec scan. For potential steps, full spectra were recorded at each point while for sweeps, the 301 nm peak characteristic of xanthate was recorded continuously. When the latter procedure was adopted, a full spectrum was always recorded at the beginning and the end of the applied potential cycle.

4.2.5. Contact Angle Measurements

Contact angle measurements were made on silver electrodes under potential control using a modified electrochemical cell. The potential was first held at -0.5 V to remove any oxidized species from the electrode surface. It was then increased to the selected value and the contact

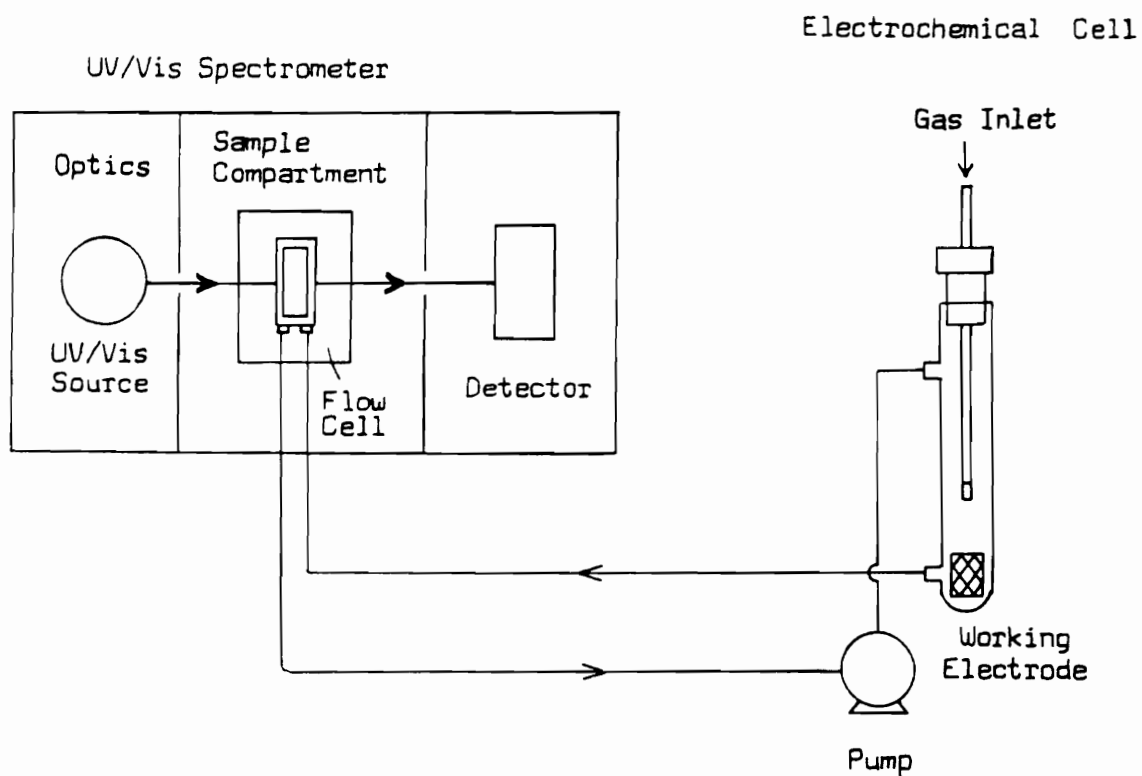


Figure 4.2. Schematic representation of the experimental set-up for the UV/Vis adsorption kinetic studies.

angle measured after 1 min using a Rame Hart Model 100 goniometer. The potential was returned to -0.5 V prior to next experiment.

4.2.6. E_h -pH Diagram

The rest potential of the silver electrode was measured in pH 6.8 and pH 9.2 solutions containing 1×10^{-2} , 10^{-3} , 10^{-4} , and 10^{-5} M potassium ethyl xanthate to calculate the thermodynamic data for the construction of E_h -pH diagram. The electrodes were first taken to potentials in the region in which silver ethyl xanthate is formed on the electrode surface in addition to chemisorbed xanthate. Following the deposition of silver xanthate on the electrode surface, the electrical circuit was opened and the rest potential measured when it had reached a constant value. This generally occurred within 1 hour but the values after 2 hour at open circuit were taken to ensure equilibrium conditions had been established. The SOLGASWATER program was adapted to allow consideration of chemisorbed species. The E_h -pH diagrams were restricted to the range pH 5-14 because the acid form of xanthate, xanthic acid, is unstable. The ratio of silver to water in the system was adopted as the same value as that for the copper and copper sulfide systems (Woods et al., 1990; 1987) to simulate the conditions in a flotation pulp. The system is assumed to contain 0.118 M of silver, and this is equivalent to a pulp containing 30 % by weight of an ore (S.G.=3.0) assaying 2 % silver.

4.3. Results and Discussion

4.3.1. Voltammetry

Voltammograms for a silver electrode in a quiescent solution of pH 9.2 containing 1×10^{-4} M ethyl xanthate are shown in Figure 4.3(a). The positive going scans show an anodic peak at -0.2 V and the return scans a cathodic peak at about -0.25 V. On the scans to the higher upper potential limits, a second anodic appears at about 0.1 V, with a corresponding cathodic peak at about -0.05 V. The influence of stirring the electrolyte during the recording of voltammogram is shown in Figure 4.3(b). It can be seen that the height of the initial anodic peak is not significantly affected by stirring but the peak at more positive potentials is much greater when the solution was stirred. This indicates that the process giving rise to the second peak is mass transport controlled. In the stirred solution, the extent of reaction in the region of the second peak is enhanced and hence the corresponding cathodic reduction peak is also increased.

The height of the first anodic peak was found to be essentially independent of xanthate concentration, whereas the peak at more positive potentials increased with increase in concentration (not shown here). The behavior observed on stirring the solution, and on changing the xanthate concentration, is similar to that observed for copper and chalcocite electrodes (Woods et al., 1990), and is symptomatic of the initial formation of a monolayer of chemisorbed xanthate according to equation (2), followed by the development of a multilayer phase of a metal xanthate:



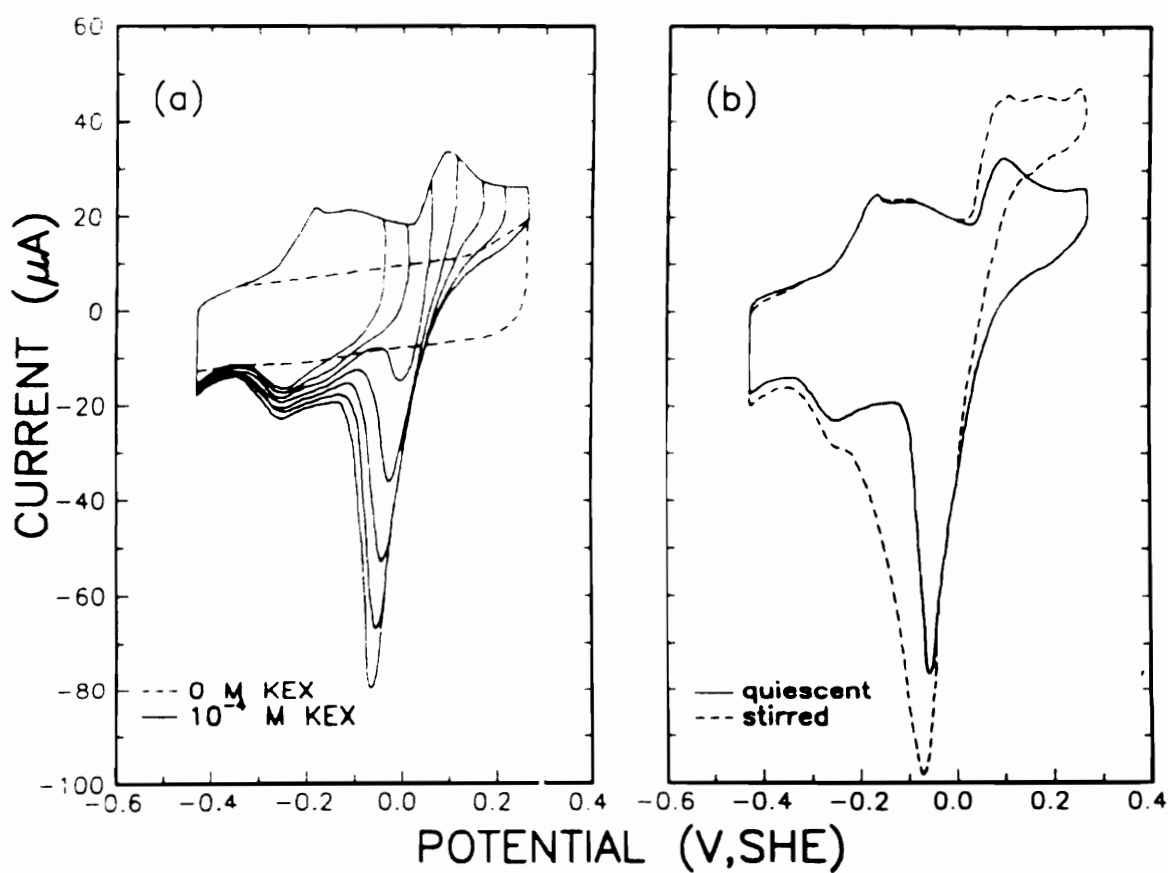


Figure 4.3. Voltammograms at 20 mV/sec for a silver electrode in pH 9.2 solution containing 1×10^{-4} M ethyl xanthate: (a) influence of upper potential limit in quiescent solution; (b) effect of stirring the solution.

This interpretation of the voltammetry is in agreement with that of other investigation (Talonen et al., 1991).

4.3.2. Adsorption Isotherm for Ag⁺

The experimental points in Figure 4.4 are the fractional surface coverages of xanthate on silver in solutions of pH 6.8 and 9.2 containing 1×10^{-2} , 10^{-3} , 10^{-4} , 10^{-5} M ethyl xanthate. The data were fitted with a *Frumkin* isotherm of the form of Equation (1). It can be seen that the surface coverage at each potential is the same at the different pH values, as expected for the adsorption reaction (2).

The shift in the potential for one-half coverage of ethyl xanthate on silver averages 52 mV for each ten-fold change in xanthate concentration. The value expected for a one-electron process with an electrosorption valency of unity is 59 mV. Thus, the value of γ for ethyl xanthate adsorption on silver, calculated from the concentration dependence of the potential for half-coverage, is 1.133.

The differential of the isotherm, Equation (1), at half-coverage is $(4+g)RT/\gamma F$ volt. The average slope at half-coverage in Figure 4.4 is 0.1875 V for silver. Thus, the g value for this system is approximately 4. The value for K in Equation (1) can be then obtained by substituting the values of γ and g and the average potential corresponding to $\theta = 0.5$ for the four concentrations investigated. This gives the isotherm for adsorption of ethyl xanthate on silver to be:

$$[\theta/(1-\theta)] \exp 4\theta = 4.25 \times 10^7 [X] \exp [E/0.023] \quad (4)$$

where $[X]$ is the concentration of ethyl xanthate in solution. These isotherms are presented on Figure 4.4 for the four xanthate concentrations

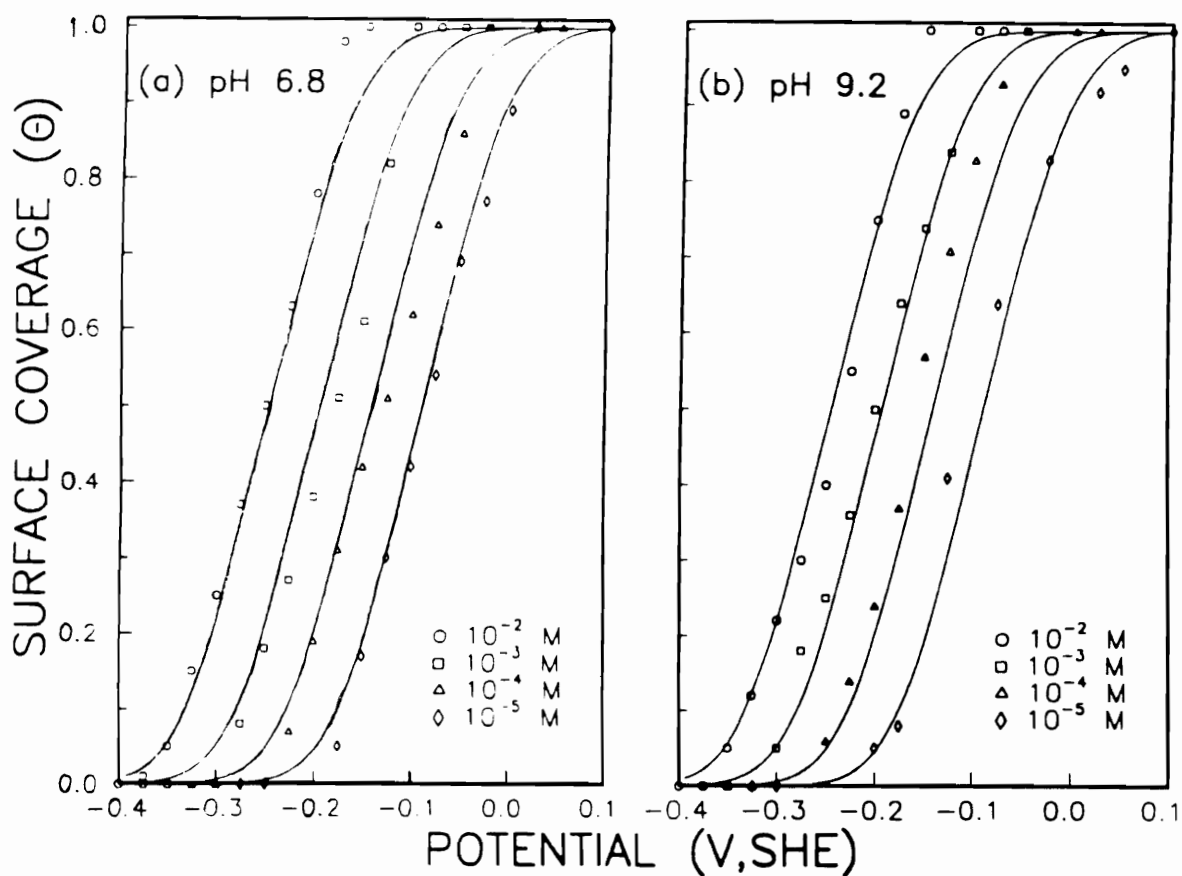


Figure 4.4. Potential dependence of coverage of chemisorbed xanthate on silver in solutions of pH (a) 6.8 and (b) 9.2 containing various concentrations of ethyl xanthate (M/dm^3). The solid lines are the derived isotherm.

and compared with the experimental data.

Recent study (Woods et al., 1990) showed that, for copper, the experimental coverages were greater than the derived isotherm at both low and high coverages. This could arise from a positive g at low potentials and a negative g value at high potentials. The absence of an $\exp g\theta$ term in the *Frumkin* isotherm for copper would then be due to the factors which result in these g -values compensating one another in the middle-coverage region. A negative g -term is indicative of attraction between adsorbate neighbors and this could be associated with hydrophobic interactions between adsorbed xanthate molecules. The fit between the experimental data and the derived isotherm is good for the case of chalcocite, suggesting that g is essentially independent of coverage on this surface. The positive g -value ($g = 4$) for chalcocite may be explained by heterogeneity of the mineral surface.

The voltammograms for chalcocite in a pH 9.2 solution containing 1×10^{-2} M xanthate showed two anodic peaks constituting chemisorption. Similar overlapping chemisorption peaks have been reported for xanthate adsorption on natural chalcocite electrodes (Kowal and Pomianowski, 1973, Richardson et al., 1984, O'Dell et al., 1984, Woods, 1990). The multiple peaks indicate sites of different adsorption energy on the electrode surface. These sites could be related to the two copper atoms in Cu_2S or reflect variations in stoichiometry of the surface.

The finite g -value is reflected in the voltammogram for silver (Figure 4.3), which shows a shoulder on the initial peak at the high potential side. Silver is, therefore, similar to chalcocite which shows two peaks in the chemisorption region and also gives a g -value of 4. It differs from copper which has a single prewave peak and a g -value of zero. The value of γ is similar to that of 1.2 found for copper (Woods, Young et al., 1990). The derived isotherms represented as solid lines in Figure

4.4 shows a good agreement with the surface coverages obtained experimentally.

4.3.3. FTIR Spectroscopy

The previous results of voltammetry showed that the interaction of ethyl xanthate with silver was characterized by a voltammetric prewave appearing at underpotentials to the formation of bulk silver ethyl xanthate. The process giving rise to the prewave corresponds to chemisorption and renders the surface hydrophobic. In order to investigate the nature of the chemisorbed layer, *ex situ* FTIR reflectance spectra were recorded with electrodes polarized at selected potentials.

Figure 4.5(a) shows the spectra obtained following polarization at potentials below (-0.4 V), within (-0.15 V and -0.05 V), and above (0.05 V) the prewave region. The reference spectrum of silver ethyl xanthate is given in Figure 4.5(b). It can be seen that at 0.05 V the spectrum shows peaks at 1200 , 1145 , 1117 , and 1030 cm^{-1} , which is characteristic of the spectra for bulk silver xanthate (Figure 4.5(b)). At potentials of -0.15 to -0.05 V, only the peak at 1210 cm^{-1} is evident, which may be attributed to chemisorbed xanthate. This peak is also present in the spectrum at 0.05 V and indicates that silver xanthate forms on the chemisorbed layer. For this reason, it was considered that after the chemisorbed layer has been formed on the electrode the silver atoms begins to diffuse out from the electrode surface as the potential increases. These silver atoms are thought to react with the xanthate molecules in the solution and form a bulk silver xanthate layer on the chemisorbed layer. Because the size of silver atom is very small compared with the size of xanthate molecule and the chemisorbed layer is not an ideally close-packed layer, there is enough space between chemisorbed xanthate molecules through which silver atoms can diffuse out.

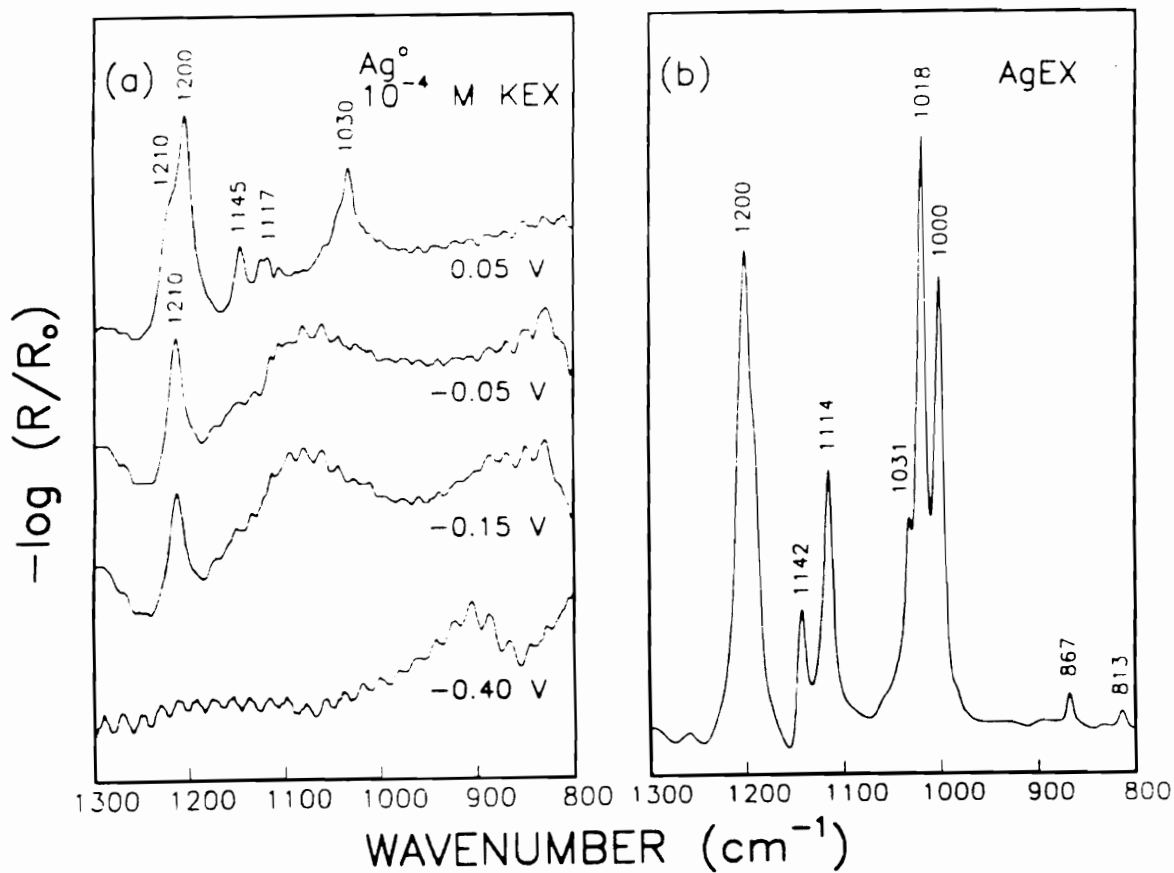


Figure 4.5. FTIR reflectance spectra of (a) a silver electrode held at different potentials in a pH 9.2 solution containing 1×10^{-4} M ethyl xanthate, and (b) silver ethyl xanthate.

The appearance of a dominant peak at about 1200 cm⁻¹ for the silver electrode polarized in the double layer region was also observed by other investigators (Talonen et al., 1991) using an *in situ* FTIR technique. These authors found the position of the peak to be strongly potential-dependent. They considered this to arise from a change in the electron distribution between silver atoms and the xanthate ions bound to silver influencing the bonds on the adsorbate itself.

The comparison of the results of FTIR spectroscopy with the voltammograms presented before shows that no adsorption peak of ethyl xanthate was found below the prewave region. It could be possible that ethyl xanthate may be physisorbed on silver even below the prewave region. However, because the silver plate was rinsed with distilled water before scanning FTIR spectrum, the physisorbed ethyl xanthate would be removed from the electrode surface and shows no absorption peak.

4.3.4. UV/Vis Spectroscopy

4.3.4.1. UV/Vis Spectra of the Chemisorbed Xanthate and Bulk Silver Xanthate

Recent *ex situ* FTIR studies of the copper/ and chalcocite/ethyl xanthate systems (Mielczarski et al., 1990) failed to detect the chemisorbed xanthate. In contrast to the previous *in situ* FTIR investigations (Leppinen et al., 1989), no spectra that could be associated with xanthate were observed after polarization in the prewave region. This raised questions concerning the identification of the prewave with the chemisorption of xanthate. However, the absence of xanthate spectra may have been due to the oxidation of chemisorbed xanthate on exposure to air during transfer to the FTIR spectrometer and the recording of the spectra.

With silver, gold and silver/gold alloys (Leppinen et al., in press), *ex situ* FTIR measurements showed an absorption band near 1200 cm^{-1} , that was attributed to unknown species rather than chemisorbed xanthate. The results presented in these investigations using *ex situ* FTIR spectroscopy are in conflict with those presented in the previous section which show the presence of chemisorbed xanthate.

In order to examine this, investigations were carried out in which the solution composition was monitored spectroscopically during electrochemical procedures. Figure 4.6 shows the intensity of the absorbance at 301 nm, the characteristic value for xanthate (Pomianowski and Leja, 1963), during a 1 mV/sec potential cycle applied following a 2 min period at -0.43 V and reversed at 0.14 V. It can be seen that xanthate begins to be abstracted from solution at about -0.35 V, which is the potential at which the prewave commences. When the potential was close to the upper limit of the cycle, the rate of abstraction increased since the formation of silver ethyl xanthate also took place. The potential at which the rate of abstraction changes corresponds with the potential of the onset of bulk silver ethyl xanthate formation in the voltammogram.

When the scan was reversed, the silver xanthate was reduced and then the chemisorbed layer desorbed. Figure 4.7 shows the full spectra recorded before and after the potential scan. It can be seen from the height of the 301 nm peak that 95 % of the xanthate re-appeared in solution following the electrochemical procedure. The small amount of xanthate that was lost appeared to have formed a species that absorbs UV strongly around 200 nm. Carbon disulfide, which is one of the decomposition products of xanthate, has a characteristic absorption at around 200 nm in the UV/Vis spectrum (Pomianowski and Leja, 1963). Therefore, the increased absorption peak around 200 nm in Figure 4.7 might

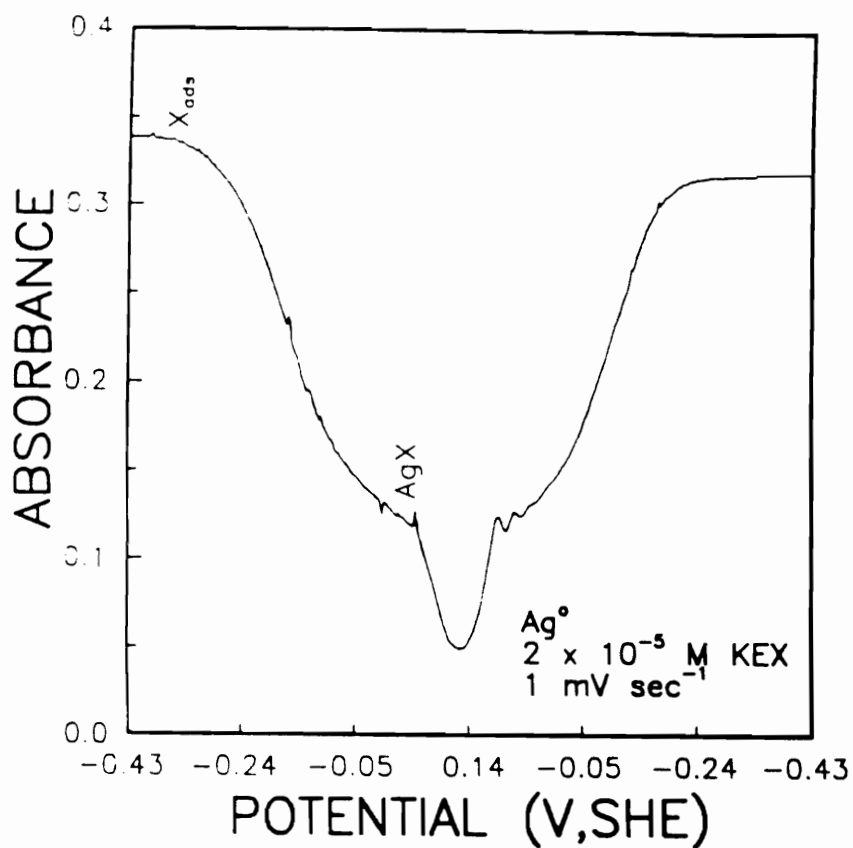


Figure 4.6. Absorbance at 301 nm of a pH 9.2 solution initially containing $2 \times 10^{-5} \text{ M}$ ethyl xanthate being circulated through a silver wool electrode. Potential held at -0.43 V for 2 min then a triangular potential cycle at 1 mV/sec applied between -0.43 and 0.14 V .

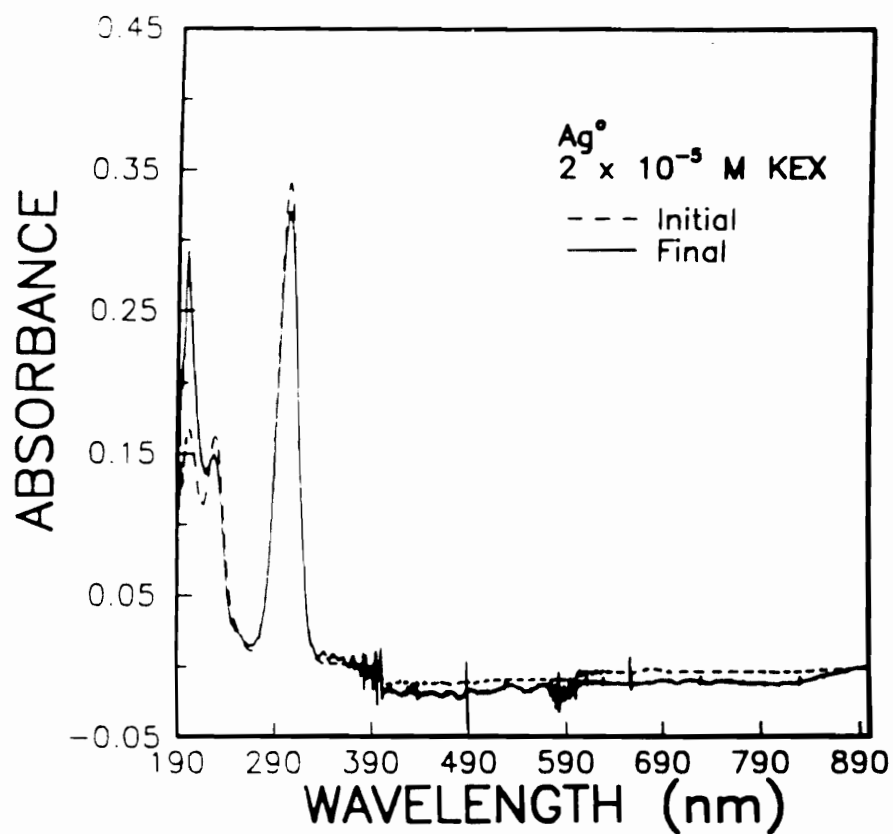


Figure 4.7. UV/Vis spectra recorded for a pH 9.2 solution initially containing $2 \times 10^{-5} \text{ M}$ ethyl xanthate being circulated through a silver wool electrode (1) prior to, and (2) following a triangular potential cycle at 1 mV/sec applied between -0.43 and 0.14 V.

be due to the decomposition of small amount of ethyl xanthate and the formation of carbon disulfide during the experiment.

The efficiency of recovery of xanthate on desorption was greater when the potential at which the xanthate was abstracted onto the electrode surface was restricted to the chemisorption region. Figure 4.8 shows spectra recorded when the potential was first held at potentials below the prewave, after holding at -0.11 V for 4 min in the prewave region, and after returning to the initial potential. In this case, close to 100 % of the xanthate was recovered. These results establish that the prewave is associated with the attachment of xanthate to the electrode surface without any change in its molecular composition.

The absorbance at 301 nm in this case did not show a change in the rate of abstraction of xanthate from the solution, whereas the abstraction rate changed during potential scanning when the upper limit of cycle was located in the potential region of bulk silver xanthate formation. The recovery of xanthate from the electrode to the solution was higher for the case that the potential cycle was limited within the prewave region. Therefore, it may be said that the decomposition amount of ethyl xanthate increases as the upper limit of potential cycle increases. Also, the chemisorption of xanthate can be regarded as a quite reversible reaction, whereas the formation of bulk silver xanthate is not so reversible.

In some experiments, a peak developed at around 350 nm in the spectrum of the solution. This could be explained by the formation of perxanthate ($C_2H_5OCS_2O^-$) (Jones and Woodcock, 1978). The development of the 350 nm peak appeared to be associated with the presence of residual oxygen in solution; hydrogen peroxide can be formed during the reduction of oxygen on the silver surface and it is known (Jones and Woodcock, 1978) that this species reacts with xanthate to form perxanthate.

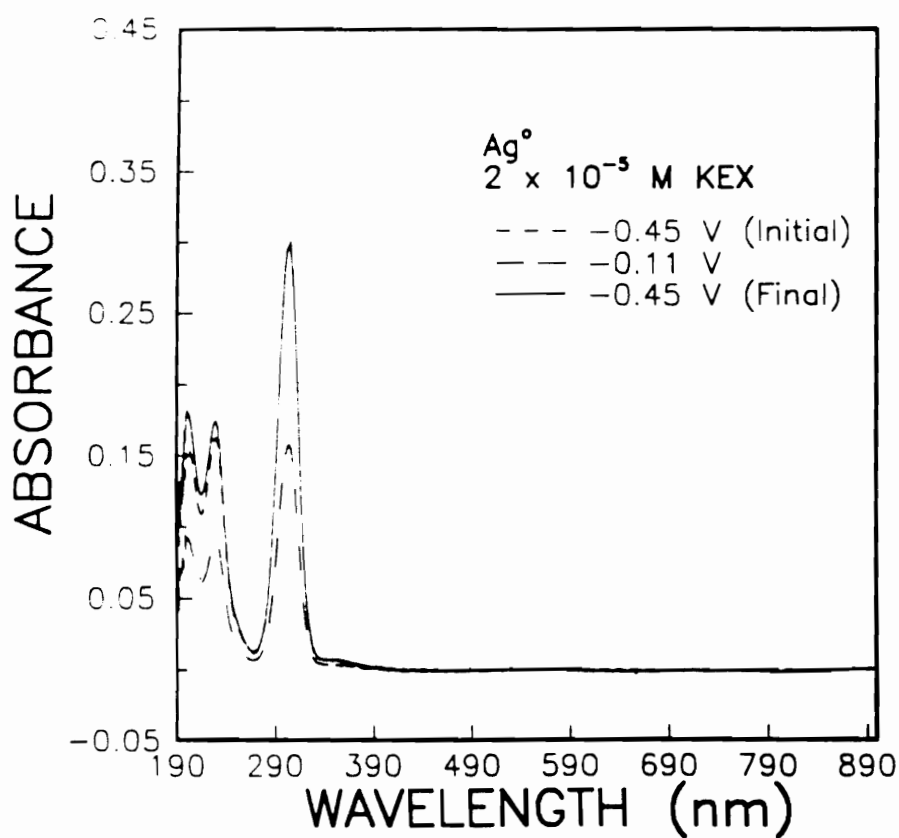


Figure 4.8. UV/Vis spectra recorded for a pH 9.2 solution initially containing $2 \times 10^{-5} \text{ M}$ ethyl xanthate being circulated through a silver wool electrode (1) at the initial potential of -0.45 V, (2) after stepping the potential to -0.11 V and holding for 4 min, and (3) after returning to -0.45 V.

4.3.4.2. Stability of the Chemisorbed Ethyl Xanthate

The stability of the chemisorbed layer when it is exposed to air and the surface water is removed from the electrode was determined using the UV/Vis spectroscopy system. The silver wool electrode was polarized in the prewave region for 4 min and removed from the cell. The electrode was washed and dried in a manner that simulated that used for the *ex situ* FTIR studies. After 20 minutes, the electrode was returned to the cell containing a xanthate-free pH 9.2 solution. The potential was then set at -0.42 V to desorb any xanthate from the electrode surface.

Figure 4.9 shows the initial xanthate spectrum, the spectrum after holding the potential at -0.13 V for 4 min, and the final spectrum at -0.42 V again. The xanthate abstracted from the solution is given by the difference between the first two spectra while that returned to solution is given by the final spectrum. The height of the 301 nm peaks shows that 88 % of the xanthate was recovered from the electrode. This indicates that the *ex situ* FTIR spectrum obtained after polarization in the prewave region does arise from the chemisorbed xanthate.

It can be also seen that the height of the peak at around 200 nm, which may be associated with carbon disulfide, decreased much more than the peak at 301 nm when the electrode was returned to the cell after exposure to air. It means that the decomposed amount of carbon disulfide is greater than the amount of decomposed xanthate when the electrode is exposed to air. The reason for this observation might be due to the reaction of carbon disulfide with oxygen in the air to form carbon dioxide and sulfur dioxide (Gilman, 1930). Therefore, when the electrode was returned to the xanthate-free solution, the UV/Vis spectra had a lower carbon disulfide absorption peak compared with the other peaks. However, the absorption peak of carbon disulfide after holding the electrode at -0.13 V shows relatively higher absorbance than others. This may be

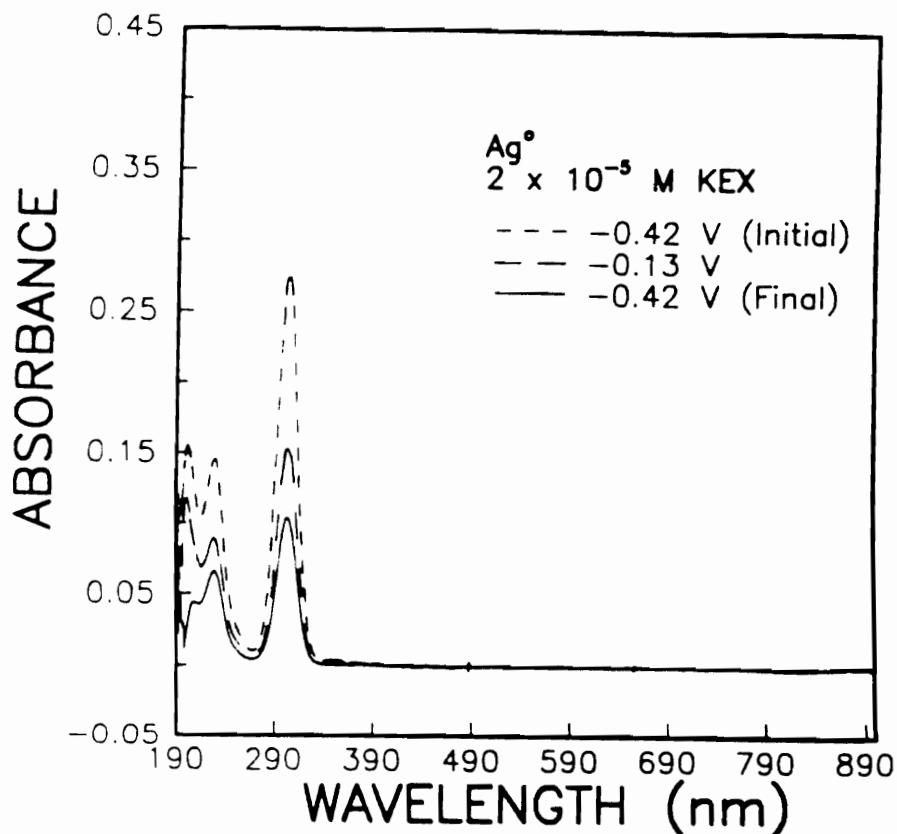


Figure 4.9. UV/Vis spectra recorded for a pH 9.2 solution initially containing $2 \times 10^{-5} \text{ M}$ ethyl xanthate being circulated through a silver wool electrode (1) at the initial potential of -0.42 V, (2) after holding at 0.13 V for 4 min and (3) after washing and drying the electrode, holding for 20 min under conditions simulating those used for FTIR spectroscopy, returning to the cell containing xanthate-free solution, and potentiostating at -0.42 V.

because the solution contains higher amount of carbon disulfide since the electrode was not exposed to the air.

The influence of applying potentials to a silver electrode in xanthate solution more negative than those used in the above experiments was explored. It was found that xanthate was removed from solution when the applied potential was lower than -0.53 V. Xanthate was not recovered when the potential was returned to -0.43 V. Hence, at high negative potentials, xanthate is believed to decompose. The spectrum of the solution after cathodic treatment contained peaks at around 230 and 200 nm, but there was no contribution at wavelengths higher than 280 nm. The observation that xanthate is reduced at potentials lower than -0.53 V indicates that care must be exercised in the pretreatment of electrodes when investigating the interaction of xanthate with electrode surfaces.

4.3.5. Contact Angle Measurements

Figure 4.10 represents the measurements of contact angle established for a silver electrode in pH 9.2 solution containing 1×10^{-4} M ethyl xanthate after polarization at different potentials. It can be seen that the contact angle increases with increase in potential above around -0.4 V and reaches a plateau at around -0.1 V. Comparison with Figures 4.4 and 4.10 shows that the increase in contact angle corresponds to the development of the chemisorbed layer. Above 0 V, silver ethyl xanthate is also produced on the electrode surface. It can be seen from Figure 4.10 that the presence of silver ethyl xanthate neither enhances nor diminishes the hydrophobicity of the surface. That is, the surface hydrophobicity of silver is entirely dependent on the chemisorption of xanthate.

Therefore, in an actual flotation system, the potential and other conditions at which chemisorption can occur should be considered carefully since the flotation efficiency is governed by the surface hydrophobicity

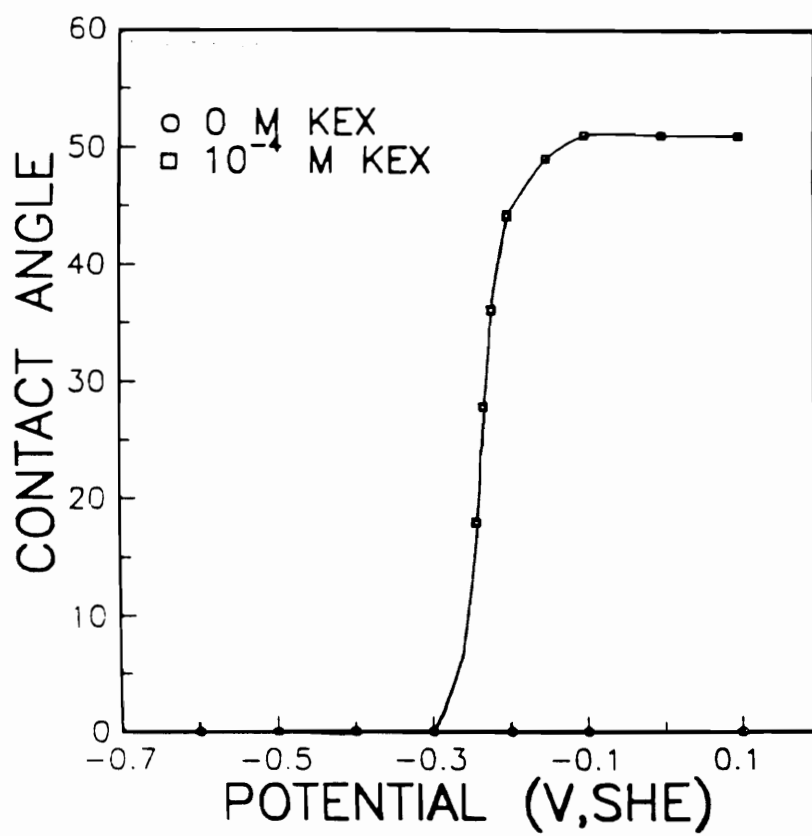


Figure 4.10. Dependence of contact angle on potential for a silver electrode in pH 9.2 solution containing 1×10^{-4} M ethyl xanthate.

and the surface hydrophobicity is closely related to chemisorbed xanthate on the silver surface.

4.3.6. E_h -pH Diagram

4.3.6.1. Rest Potential Measurements

The rest potentials determined for pre-anodized silver electrode in xanthate solution at different pH's are presented in Figure 4.11. It can be seen that the rest potentials are independent of pH and are linearly dependent on the log of xanthate concentration. The rest potential of a silver that has been polarized in a xanthate solution at potentials in the chemisorption region will vary with xanthate coverage according to the isotherm derived previously. However, a silver electrode that has been pretreated to deposit a silver ethyl xanthate phase on the surface in addition to a monolayer of chemisorbed xanthate should act as an electrode of the third kind. Thus, under these circumstances, the rest potential is a measure of the reversible potential of the silver/silver xanthate couple.

The rest potentials of a silver electrode in 1×10^{-2} , 10^{-3} , 10^{-4} , and 10^{-5} M ethyl xanthate at pH 6.8 were -0.145, -0.070, 0.0, and 0.063 V, respectively, and the corresponding values at pH 9.2 were -0.150, -0.070, 0.0, and 0.065 V. Linear regression analysis of the data gave the Nernst relationship;

$$E = -0.280 - 0.0591 \times \log[X] \quad (5)$$

where $[X]$ represents ethyl xanthate concentration. The relevant reaction for above Nernst relationship is;

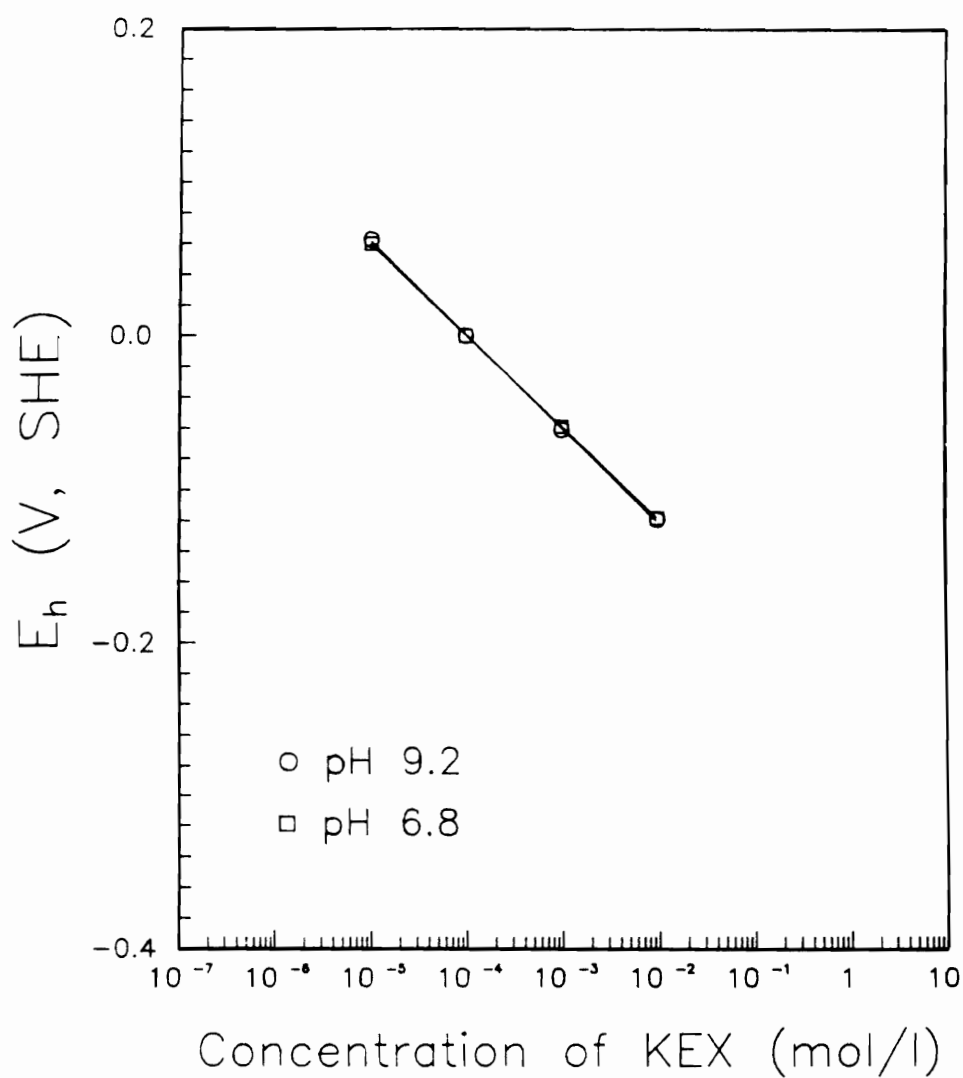


Figure 4.11. Rest potential measurements for silver electrode in ethyl xanthate solutions at pH 9.2 and pH 6.8.



The difference in standard *Gibbs* free energy of formation (ΔG°) between solid silver ethyl xanthate and aqueous ethyl xanthate ions, calculated from the formal potential of -0.28 (Equation (5)), is -27.0 kJ/mol. This value is comparable with that of -27.2 kJ/mol derived from the solubility product of silver ethyl xanthate (Kakovsky, 1957).

4.3.6.2. E_h -pH Diagram

The chemisorption isotherm and the *Gibbs* free energy of formation of silver ethyl xanthate obtained previously were used for the construction of E_h -pH diagram. Figure 4.12 shows an E_h -pH diagram for the silver/water/ethyl xanthate system at xanthate concentration of 10^{-4} M, in which chemisorbed xanthate is considered in addition to silver xanthate. In constructing this diagram, a free energy for chemisorbed xanthate was used so that it corresponded to the onset of adsorption, which was defined as the potential at which the fractional coverage, given by the appropriate isotherm, was 0.01. This allowed the stability domains of the various species to be determined. In defining the stability zone of chemisorbed xanthate, it was assumed that this species would only exist in regions in which elemental silver is stable. Dashed lines have been included in the E_h -pH diagram corresponding to fractional coverages of chemisorbed xanthate of 0.1, 0.5, and 0.8. These coverages were calculated from the isotherms, with mass balance considerations taken into account.

It can be seen from Figure 4.12 that a region of stability of chemisorbed xanthate exists below that at which the metal xanthate develops. At higher potentials, silver xanthate is stable in addition to the chemisorbed layer. Chemisorbed xanthate does not exist when the

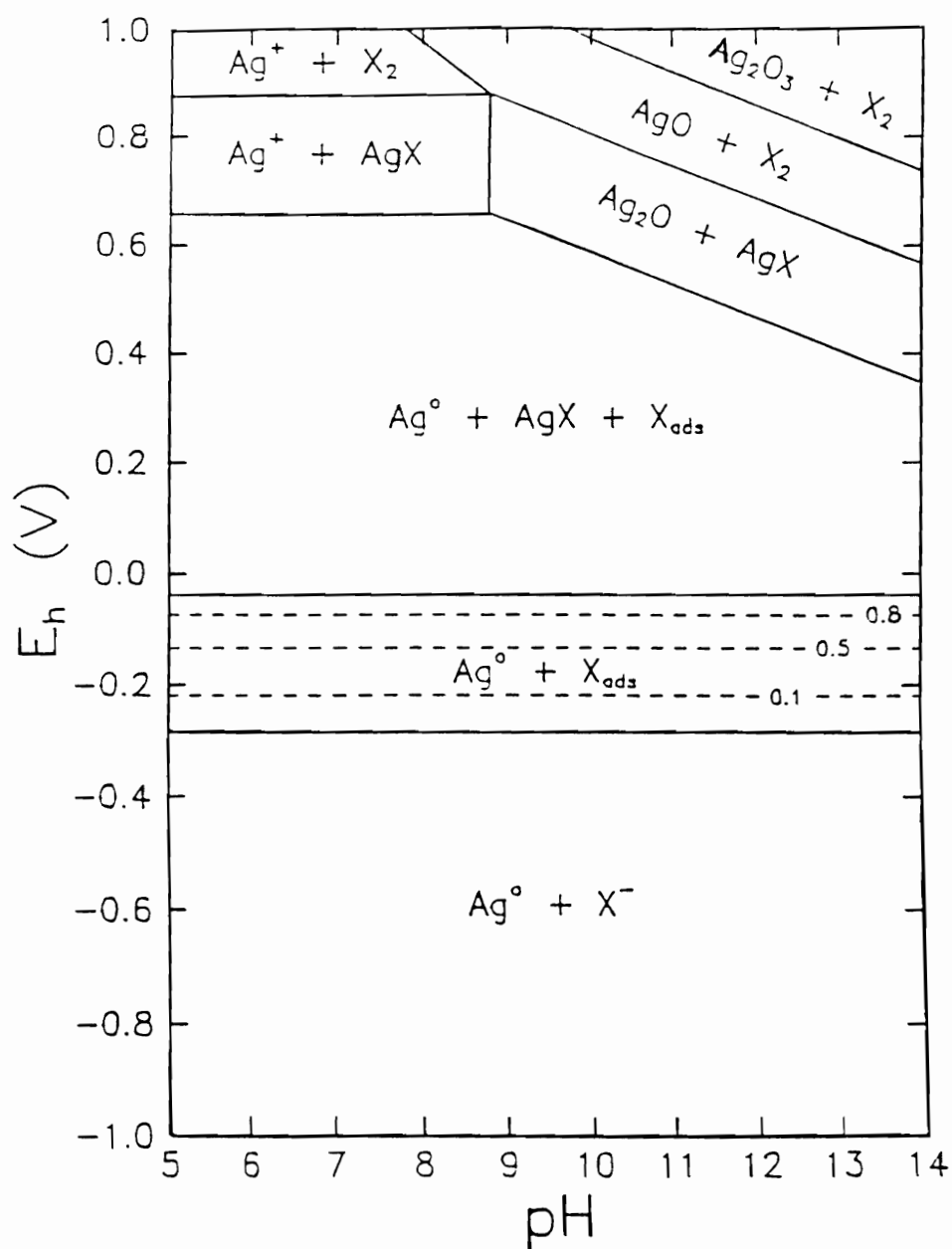


Figure 4.12. E_h -pH diagram for the silver/water/ethyl xanthate system for an initial xanthate concentration of 1×10^{-4} M. Dashed lines are fractional surface coverages as indicated.

silver is oxidized to Ag_2O because it requires an elemental silver surface. Silver xanthate co-exists with Ag_2O but is oxidized to dixanthogen (X_2) at about the same potential that Ag_2O is oxidized to AgO under the conditions selected for the diagram. Since the potential for the oxidation of silver ethyl xanthate is above the stability range of water, silver xanthate is not likely to be oxidized under the conditions pertaining in flotation pulp. At the highest potentials considered, AgO is oxidized further to Ag_2O_3 .

4.4. Summary

Voltammograms for ethyl xanthate at a silver electrode are characterized by a prewave occurring at potentials lower than that for the formation of silver ethyl xanthate. The prewave is assigned to the charge-transfer chemisorption of a monolayer of ethyl xanthate. The equilibrium coverage of chemisorbed xanthate can be fitted by the *Frumkin* isotherm with a g -value of 4 and a γ -value of 1.1.

Identification of the prewave with chemisorption was substantiated by monitoring solution composition with UV/Vis spectroscopy. Xanthate was abstracted from the solution when the potential was taken into the chemisorption region, and released again when the potential was returned to lower values.

Ex situ FTIR spectra of surfaces polarized in the chemisorption region showed a dominant peak at 1210 cm^{-1} . Xanthate could be recovered into the solution phase by reduction of the surface layer following treatment that simulated that used for FTIR spectroscopy. Thus, the spectrum arises from the chemisorbed layer. FTIR spectra of surfaces obtained at potentials above the silver/silver ethyl xanthate reversible value displayed the peaks characteristic of the metal xanthate.

The rest potential of a silver electrode in xanthate solutions obey

the *Nernst* equation. From the formal potential of the silver/silver ethyl xanthate couple, the difference in standard Gibbs free energy of formation between silver ethyl xanthate and ethyl xanthate ions was calculated to be -27.0 kJ/mol.

Contact angle measurements show that the chemisorbed xanthate layer imparts hydrophobicity to the silver surface. The additional formation of silver ethyl xanthate does not alter the degree of hydrophobicity.

An E_h -pH diagram for the silver/water/ethyl xanthate system, under conditions corresponding to those in flotation pulps, has been constructed from the chemisorption isotherm and the Gibbs free energy determined for silver ethyl xanthate. It shows a region of stability of chemisorbed xanthate below that for the development of silver ethyl xanthate. The upper limit of stability of silver xanthate is determined by the oxidation of this compound to AgO and dixanthogen. Since this only occurs at potentials above the stability region of water, silver ethyl xanthate is not likely to be oxidized under conditions existing in flotation pulps.

Part II. Gold/Silver/Ethyl Xanthate Systems

4.5. Introduction

The reaction mechanisms of ethyl xanthate with precious metals have been studied by means of FTIR spectroscopy, cyclic voltammetry, and X-ray photoelectron spectroscopy. Leppinen et al. (1991) showed that diethyl dioxanthogen ((EX)₂) and silver ethyl xanthate (AgEX) were the products of anodic oxidation on gold and silver, respectively. On gold-silver alloys, both (EX)₂ and AgEX are formed, with the latter being formed at potentials below that for (EX)₂. On the 50:50 and 80:20 gold-silver alloys, AgEX is formed about 50 mV and 100 mV above that for pure silver.

Based on an *ex situ* FTIR spectroscopy technique, Leppinen et al. (1991) observed the formation of unknown species at potentials below the reversible potential for the AgEX formation. However, an *in situ* FTIR technique employed by Talonen et al. (1991) showed that ethyl xanthate is chemisorbed in the potential region preceding silver ethyl xanthate formation. This finding is in agreement with the results shown in Part I of this chapter.

Since gold commonly occurs in the form of electrum, it is important to characterize the adsorption behavior of collectors on the alloys, rather than on pure gold, to establish the optimum flotation conditions. Because chemisorbed xanthate species, in addition to metal xanthates, are known to render minerals hydrophobic, it is essential to define the conditions under which xanthate chemisorbs on gold-silver alloys in addition to those under which AgEX and (EX)₂ are formed.

In Part II of this chapter, the reactivity of ethyl xanthate with gold-silver alloys has been investigated by voltammetry and contact angle measurements. Also, E_h-pH diagrams for gold-silver alloys/water/ethyl xanthate systems have been constructed using the chemisorption isotherms

obtained for gold-silver alloys.

4.6. Experimental Materials

Silver, gold, and gold-silver alloy electrodes were prepared by encapsulation into epoxy resin. They were 50:50 and 80:20 by weight gold-silver alloys, and were prepared by a double-melting homogenization procedure from 99.99 % pure metal. The composition was verified by the Technical Research Center of Finland using SEM/EDS and fire assay methods. The gold and silver samples (99.9985%, Puratronic) were provided by Aesar Company. The exposed surface areas of the Ag⁰, Au⁰, 50-50 Au-Ag, and 80:20 Au-Ag electrodes were 33, 36, 30, and 25 mm², respectively. A fresh electrode surface was generated before each run by polishing with alumina and washing three times with hot ethanol in an ultrasonic bath.

4.7. Results and Discussion

4.7.1. Voltammetry

Figure 4.13 presents voltammograms for silver and 50:50 and 80:20 gold-silver alloy electrodes in pH 9.2 solution containing 1×10^{-3} M ethyl xanthate. The main feature on each positive-going scan is large anodic waves which appear at positive potentials. It has been demonstrated by FTIR spectroscopy (Leppinen et al., 1991) that these anodic waves are due to the formation of AgEX according to reaction (3).

Voltammograms for gold obtained in 1×10^{-3} M KEX solutions show no anodic waves arising from xanthate oxidation below about 0.2 V; above this potential, an anodic current flows as a result of (EX)₂ formation (Woods, 1971). As found in the study of Woods (1971), the formation of AgEX commences at about 0.05 and 0.1 V more positive for the 50:50 and 80:20 gold-silver alloys, respectively, than for pure silver. This reflects a

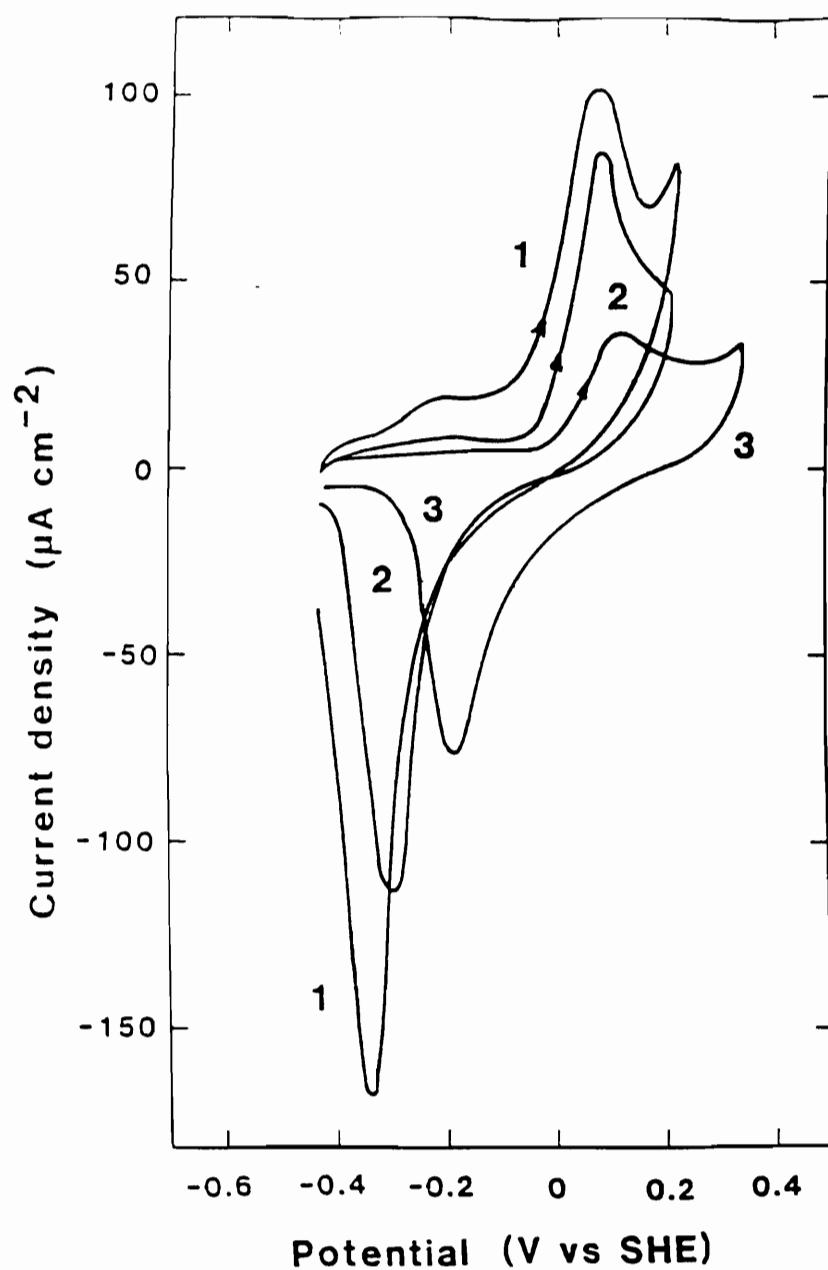


Figure 4.13. Voltammograms at 50 mV/sec in pH 9.2 solution containing 1×10^{-3} M ethyl xanthate for (1) silver, (2) 50:50 and (3) 80:20 (weight %) gold-silver alloys.

decrease in the activity of silver when alloyed with gold. The difference in the *Gibbs* free energy formation (ΔG°) between silver in the pure metal and in the 50:50 and 80:20 gold-silver alloys, calculated from the thermodynamic data (White et al., 1957), is -3.54 and -11.2 kJ/(gm atom), respectively. Thus, the shift in potential of the Ag/AgEX couple is expected to be 0.037 and 0.116 V for the respective gold-silver alloys. The shifts in the main anodic waves observed in the voltammograms (Fig. 4.13) are in agreement with the results of these thermodynamic calculations.

The voltammograms in Figure 4.13 are also characterized by prewaves appearing at approximately -0.2 V. In the case of pure silver, the prewave has been defined (Woods et al., in press) as a chemisorption process (reaction (2)). The prewaves observed for the gold-silver alloy electrodes may also be assigned to the same underpotential deposition phenomenon. The charges associated with the prewaves for the three electrodes are approximately proportional to the silver content of the surface. This may suggest that the chemisorption occurs only on silver sites of the alloy surfaces.

4.7.2. Adsorption Isotherm for Au-Ag alloy

4.7.2.1. Calculation of Adsorption Isotherm

The charge associated with the chemisorption of ethyl xanthate on the gold-silver alloy electrodes was determined as a function of potential. In order to convert this charge to fractional surface coverage (θ), it is necessary to know the charge corresponding to a monolayer. With the same assumption employed for silver, monolayer coverage on the gold-silver alloys is defined as the occupation of each available silver site in the surface. The coverages for the 80:20 and 50:50 gold-silver alloys are

presented as a function of potential in Figure 4.14.

4.7.2.2. Adsorption Isotherm

Coverage data for a silver electrode in pH 6.8 and 9.2 solutions containing 1×10^{-2} , 10^{-3} , 10^{-4} , and 10^{-5} M ethyl xanthate were found to fit a *Frumkin* isotherm (Fig. 4.4). The isotherm for ethyl xanthate chemisorption on a silver electrode at 25°C was;

$$[\theta/(1-\theta)] \exp 4\theta = 4.25 \times 10^7 [X] \exp [E/0.023]. \quad (7)$$

The isotherm derived for 1×10^{-3} M ethyl xanthate is presented in Figure 4.14, curve (1).

Analysis of the chemisorption of xanthate on silver sites in the gold-silver alloy surfaces must take into account the diminished activity of silver. Therefore, the isotherm is expected to be of the form;

$$[\theta/(1-\theta)] \exp q\theta = K a_{X^-} a_{Ag} \exp [\gamma FE/RT], \quad (8)$$

where a_{X^-} and a_{Ag} are the activities of xanthate in solution and silver in the alloy surface, respectively. For the gold-silver alloys, the isotherm should be;

$$[\theta/(1-\theta)] \exp 4\theta = 4.25 \times 10^7 a_{Ag} [X] \exp [E/0.023]. \quad (9)$$

Values of silver activity for the gold-silver alloys can be derived from the thermodynamic data (White et al., 1957). For the 50:50 and 80:20 gold-silver alloys, a_{Ag} is calculated to be 0.24 and 9.3×10^{-3} , respectively. Curves (2) and (3) in Figure 4.14 are the isotherms for the respective alloys obtained by inserting these values in equation (9). The

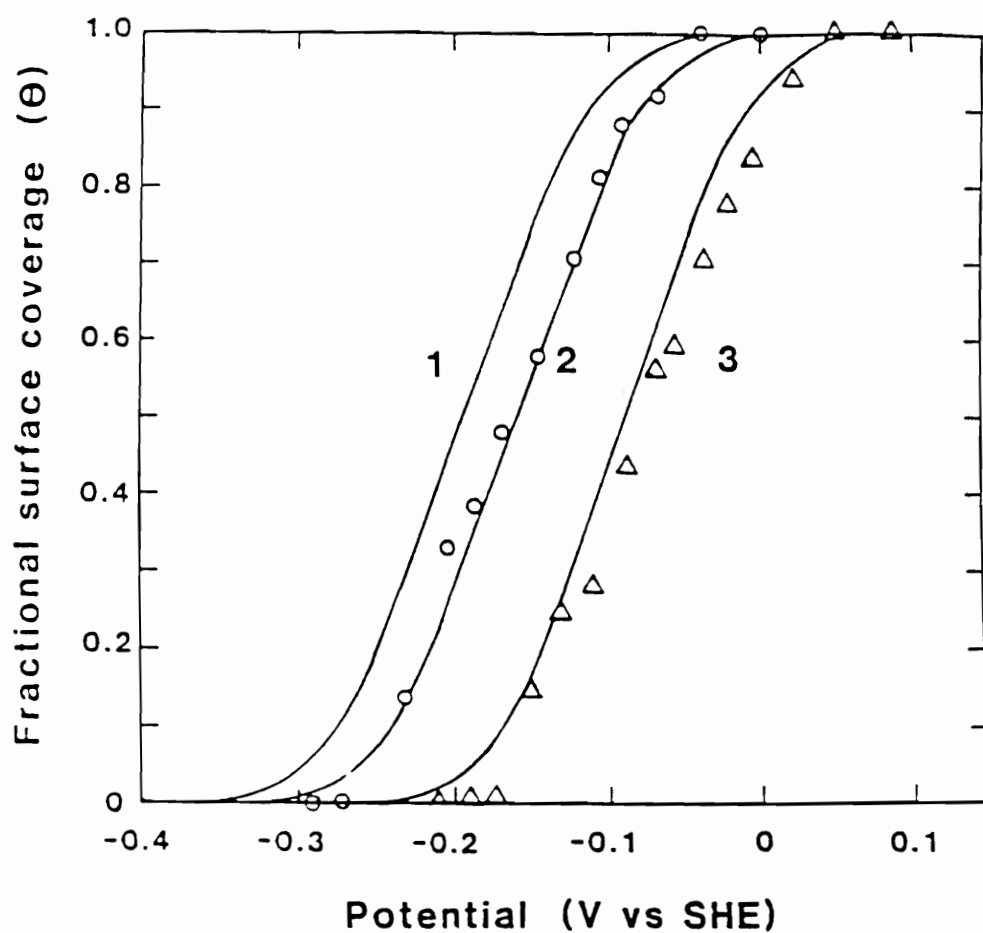


Figure 4.14. Potential dependence of fractional coverage of chemisorbed xanthate in solutions at pH 9.2 containing 1×10^{-3} M ethyl xanthate. Solid lines are isotherms for (1) silver, (2) calculated for 50:50 and (3) 80:20 gold-silver alloys. Points are experimental fractional coverages for 50:50 (O) and 80:20 alloys (Δ).

coverage data (θ) are shown to fit the derived isotherms within experimental error.

4.7.3. Contact Angle Measurements

Figure 4.15 shows the measurements of the contact angle established for silver, gold, 50:50 and 80:20 gold-silver alloy electrodes in pH 9.2 solution containing 1×10^{-3} M ethyl xanthate after polarization at different potentials. It can be seen that, for each electrode, the electrode surface is hydrophilic at the more negative potentials and that a finite contact angle develops at a critical potential. Comparison of Figures 4.14 and 4.15 shows that this critical value corresponds to the commencement of ethyl xanthate chemisorption and that the contact angle increases with increase in potential in a similar manner to chemisorption coverage. Thus, it is clear that the chemisorption of ethyl xanthate results in a hydrophobic surface and should render silver and gold-silver alloy particles floatable. The development of a silver ethyl xanthate phase is not necessary for flotation to occur.

For the silver and the 50:50 gold-silver alloy, the maximum contact angle is close to the value considered by Sutherland and Wark (1955) to be characteristic of ethyl xanthate for any surface that has responded fully to the collector. The maximum angle developed by the 80:20 gold-silver alloy in the prewave potential region is significantly less, being about 50° . This can be explained by a lower coverage of ethyl xanthate on the alloy surface. Although monolayer coverage is reached with respect to silver atoms, only small part of metal sites on the surface are bonded to ethyl xanthate. The other part of surface sites constitute gold atoms which are not hydrophobic in xanthate solutions at potentials below the region where dixanthogen is formed (Gardner et al., 1974).

The development of a finite contact angle for gold occurs at the

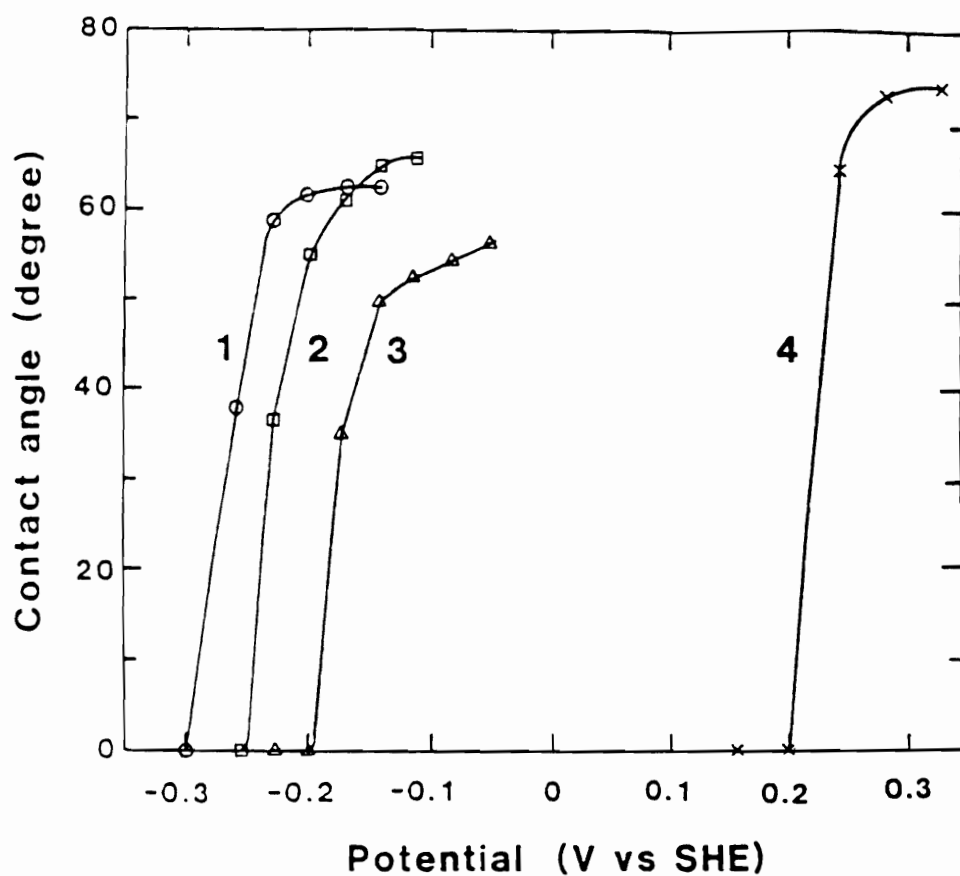


Figure 4.15. Dependence of contact angle on potential in pH 9.2 solution containing 1×10^{-3} M ethyl xanthate for (1) silver, (2) 50:50, (3) 80:20 gold-silver alloys, and (4) gold.

potential at which ethyl xanthate is known to oxidize to dixanthogen (Leppinen et al., 1991, Woods et al., 1987). It can be seen from Figure 4.15 that gold-silver alloys become hydrophobic at potentials substantially more negative than that of gold, the difference being approximately 0.45 and 0.4 V for the 50:50 and 80:20 gold-silver alloys, respectively.

4.7.4. E_h -pH Diagram

For the construction of E_h -pH diagrams, the chemisorption isotherms determined for gold-silver alloys were employed. The *Gibbs* free energies of formation of AgEX were taken from as described in section 4.3.6.1 of Part I of this chapter and those of silver in gold-silver alloys from White et al. (1957).

Figures 4.16, 4.17, and 4.18 show E_h -pH diagrams for the silver/water/ethyl xanthate system for silver, 50:50, and 80:20 gold-silver alloys in which chemisorbed xanthate is considered in addition to AgEX and (EX)₂. In other studies (Winter et al., 1973, Kakovsky, 1957), the reversible potential for the oxidation of ethyl xanthate to (EX)₂ was shown to be lower than that for the formation of gold(I) ethyl xanthate. Thus, on the gold electrode, the formation of (EX)₂ is thermodynamically more favorable than that of the metal xanthate. The experimental observations are consistent with this conclusion. There is no definite evidence for xanthate chemisorption at potentials below (EX)₂ and gold xanthate formation, although the kinetics of xanthate oxidation on gold may be indicative of chemisorbed xanthate being an intermediate in (EX)₂ formation.

Since the xanthate/dixanthogen redox reaction only involves the surface as a source or sink of electrons, its potential is independent of

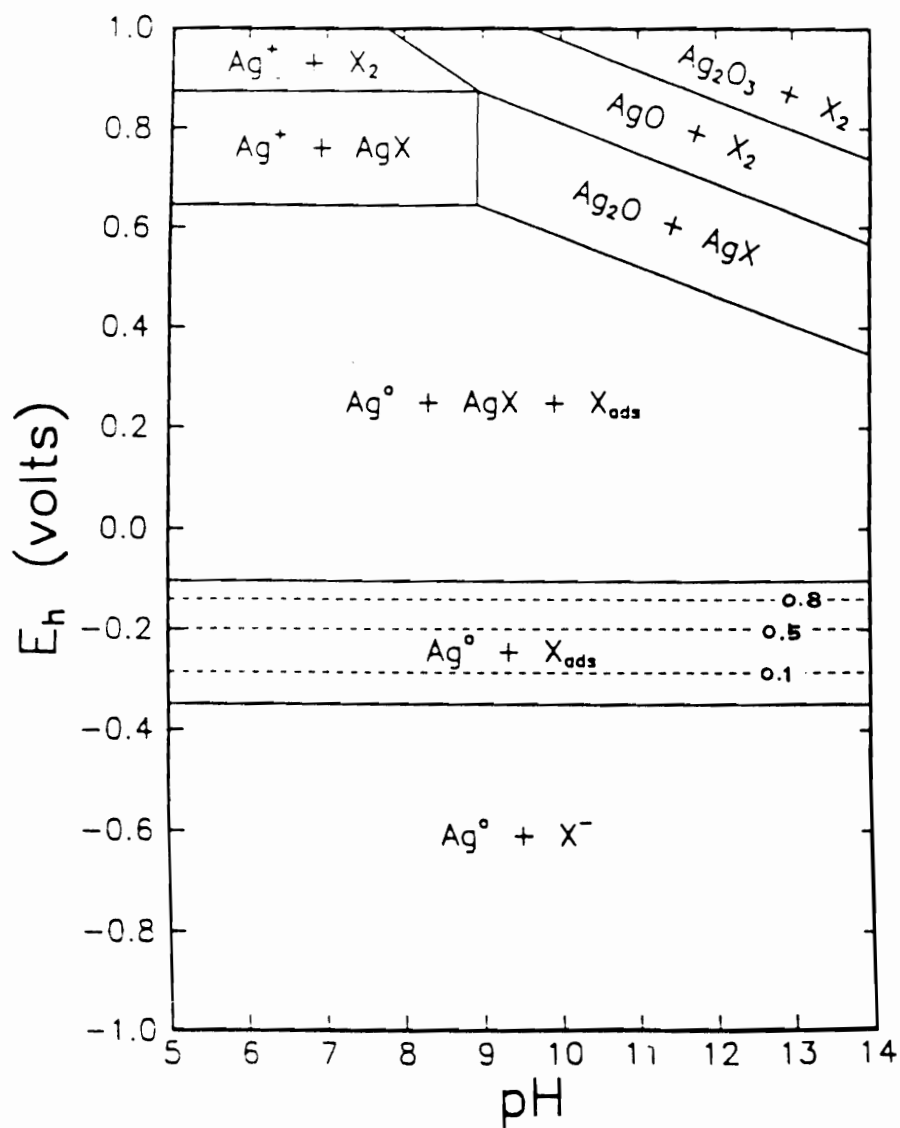


Figure 4.16. E_h -pH diagram for silver/water/ethyl xanthate system for an initial xanthate concentration of 1×10^{-3} M. Dashed lines are same fractional surface coverages as indicated in figure 4.12.

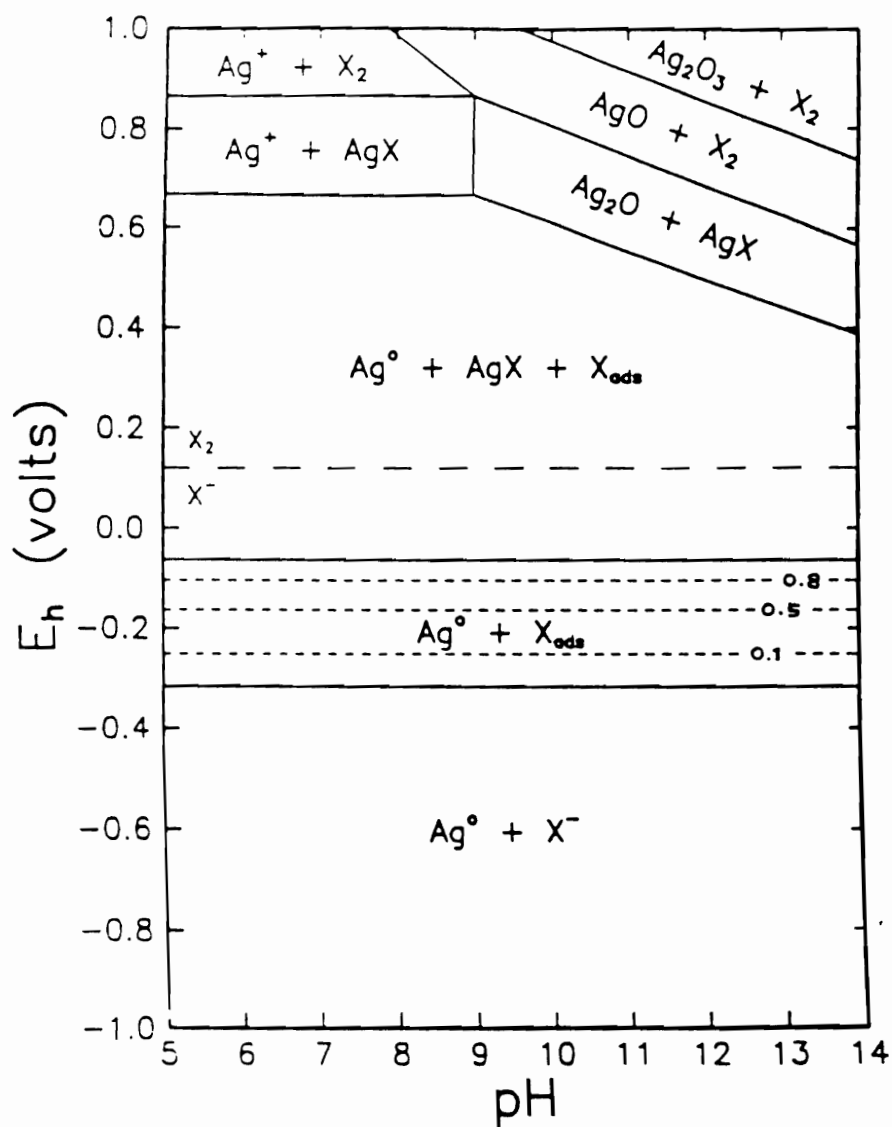


Figure 4.17. E_h -pH diagram for 50:50 gold-silver alloy/water/xanthate system for an initial xanthate concentration of 1×10^{-3} M. Dashed lines are same fractional coverages as indicated in figure 4.12.

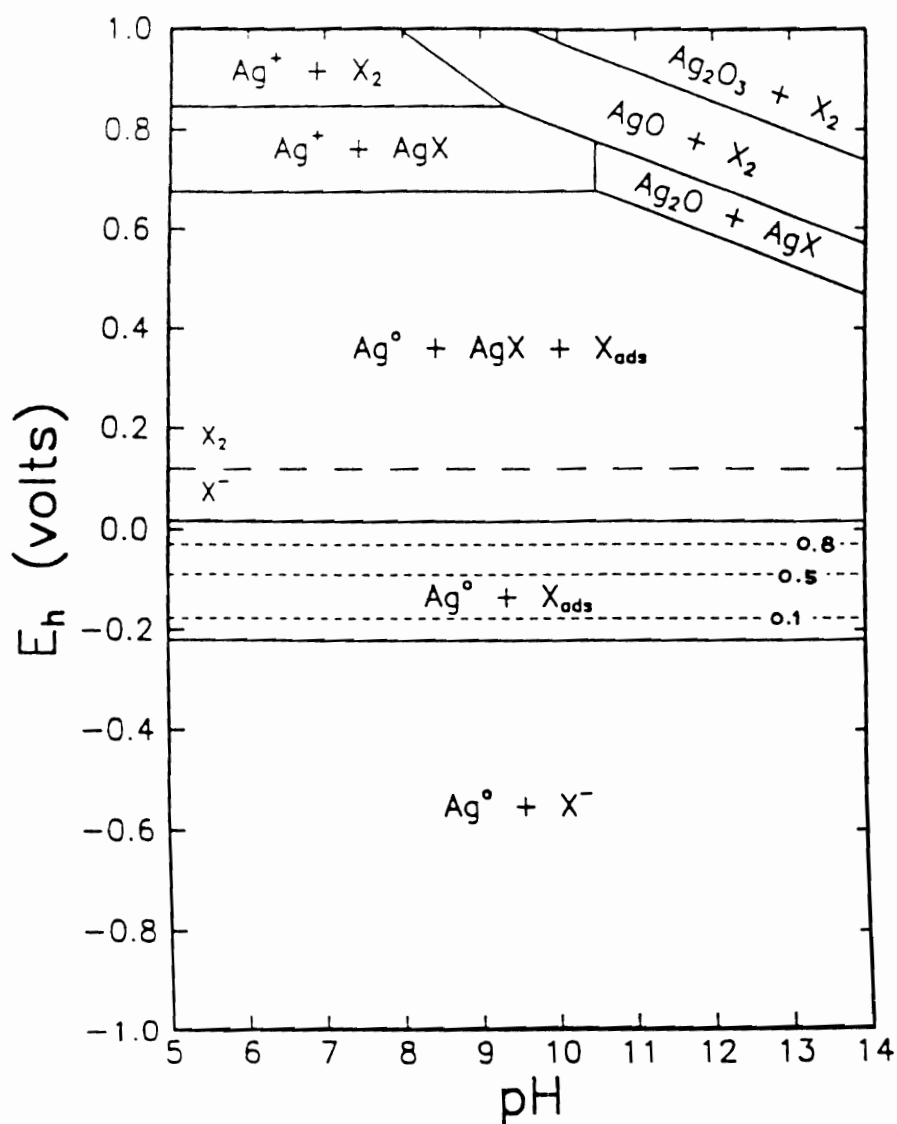


Figure 4.18. E_h -pH diagram for 80:20 gold-silver alloy/water/ethyl xanthate system for an initial xanthate concentration of 1×10^{-3} M. Dashed lines are same fractional surface coverages as indicated in figure 4.12.

the activity of gold in the alloy surface. On the other hand, the formation of gold xanthate will shift to higher potentials as the gold content of the surface is decreased. Thus, the formation of $(EX)_2$ will be the favored product on the alloys as well as on pure gold.

Under the conditions employed in the construction of these diagrams, no $(EX)_2$ will be formed on gold sites in the alloys since, at equilibrium, all the xanthate present will have reacted to form AgEX at potentials below the xanthate/dixanthogen value. In order to show where $(EX)_2$ would be formed if there are kinetic restrictions to complete conversion of xanthate to AgEX, the xanthate/dixanthogen reversible potential is included for the two gold-silver alloys as a dashed line (Figures 4.17 and 4.18).

It can be seen that the E_h -pH diagrams for the gold-silver alloys are similar to that for silver (Fig. 4.12). The only significant effect of alloying is to shift the stability regions of chemisorbed xanthate and silver xanthate to higher potentials. The higher potential regions of the three E_h -pH diagrams are the same since, once all the silver is converted to AgEX, the reactions are no longer influenced by the presence of gold.

4.8. Summary

Voltammograms for 80:20 and 50:50 gold-silver alloys in a pH 9.2 solution containing ethyl xanthate are similar to those of silver, being characterized by a chemisorption prewave occurring at potentials lower than that for the formation of AgEX. The charge associated with the prewave decreases with decreasing silver content in the alloy, indicating that ethyl xanthate chemisorbs only on silver sites on the alloy surface. The potential at which AgEX develops for the gold-silver alloy electrodes are shifted to higher potentials compared with that for the pure silver due to the decreasing activity of silver.

The potential dependence of the coverage of chemisorbed xanthate on the 80:20 and 50:50 gold-silver alloys can be explained using the *Frumkin* isotherm derived for silver when it is modified to account for the changes in the free energy of formation of silver in alloys.

The contact angle data obtained with silver and gold-silver alloys correlate well with chemisorption of xanthate; in the presence of KEX, Ag and Au-Ag alloys acquire hydrophobicity at the onset potential for the xanthate chemisorption. Gold, on the other hand, becomes hydrophobic at much higher potentials where dixanthogen is formed. These results are in agreement with the E_h -pH diagrams constructed for the 80:20 and 50:50 gold-silver alloys/water/ethyl xanthate systems. The correlation between the contact angle data and the E_h -pH diagram has been made possible because the free energy of chemisorbed xanthate is made available from the *Frumkin* isotherm established in the present work.

Chapter 5. Summary and Conclusions

5.1. Monothiophosphate

Monothiophosphate (MTP) is derived from the corresponding dithiophosphate (DTP) by replacing one of the sulfur atoms with oxygen. This substitution changes the electron distribution on the donor atoms and, hence, the pK_a and metal complexation properties. In the present work, the adsorption mechanisms of dicresyl monothiophosphate (DCMTP) has been studied in light of the EC-mechanism. This reagent is known as a true acid-circuit collector for sulfide minerals and precious metals.

The voltammograms of Ag^0 in the presence of DCMTP at pH 4.6 and 9.2 show an anodic current rise above 100 mV and 250 mV, respectively. The adsorption mechanisms may be represented by the following reaction;



which may be considered as a coupled chemical reactions of the EC-type. That is, the electrochemical step (E) involves the oxidation of Ag^0 ,



and the chemical reaction (C);



The electrochemical step should be controlled by the E_h of the system,

while the chemical step should be controlled by the pK value of the AgDCMTP compound. As such, both E_h and pK affect the adsorption of the DCMTP on Ag^0 .

At pH 9.2, DCMTP reacts with Ag^0 at pH 9.2 at potential higher than that observed at pH 4.6. This potential shift may be attributed to the possible tautomerism;



The thione form is more stable in alkaline conditions due to the high electronegativity of O as compared with S. However, as the pH is decreased, the availability of excess protons favors the thiol form. That reaction (1) occurs at a higher potential at pH 9.2 than at pH 4.6 may be given an explanation that the Ag-thione complex has a lower pK_a value than the Ag-thiol complex.

For Au^0 , the addition of DCMTP results in the passivation of the electrode surface over the entire scan range; however, there are no indications of an electrochemical interaction between DCMTP and Au^0 . This finding is also supported by the IR spectroscopic and contact angle measurements as a function of potential. The passivation of the Au^0 electrode may be attributed to the weak physisorption of DCMTP. It may be concluded, therefore, that the improved flotation recovery of gold by DCMTP, may not involve an Au^0 -DCMTP interaction.

The voltammograms of an Au-Ag alloy (80:20) show that the DCMTP begins to adsorb on the alloy at 250 and 400 mV at pH 4.6 and 9.2, respectively. These potentials are significantly higher than those observed for DCMTP interaction with pure Ag^0 . The anodic current rise may

be attributed to DCMTTP interacting with silver rather than with Au⁰.

The FTIR spectra of the Ag⁰ electrode contacted with a DCMTTP solution at pH 4.6 show signs of adsorption at potentials below 100 mV. The signals are very weak but the spectra are similar to that of pure DCMTTP. The spectra above 200 mV are similar to that of the AgDCMTTP compound, indicating the formation of AgDCMTTP on the electrode. The FTIR spectra obtained with alloys indicate that DCMTTP adsorption on the 50:50 Au-Ag alloy occurs at a potential higher than that for Ag⁰ but lower than that for 80:20 Au-Ag alloy. This finding suggests that the potential, at which DCMTTP begins to adsorb, is dependent on the silver content of the alloy. The same is also observed in the voltammetry and the contact angle measurements.

The standard free energy of formation (ΔG_f°) of AgDCMTTP has been determined to be -13.8 kJ/mol in the present work. Based on this value and other thermodynamic data available in literature, an E_h -pH diagram has been constructed to show that the results of voltammetry, IR spectroscopy, and contact angle measurements are in good agreement with thermodynamic predictions.

5.2. Di- and Monothiophosphinates

Dithiophosphinate (DTPI) is structurally similar to dithiophosphate (DTP); however, the metal complex of DTPI is several orders of magnitude more stable than those of DTP. Monothiophosphinate (MTPI) is derived from corresponding dithiophosphinate by replacing one of the sulfur atoms with oxygen. This change results in a more stable and stronger collector under certain pH conditions. MTPI, being a weaker acid than MTP, is more effective in the neutral and mildly alkaline pH conditions. The use of DTPI and MTPI has been shown to increase precious metal recoveries from ores.

The voltammograms of Au^0 in the presence of DEDTPI at pH 9.2 show an anodic current rise above 500 mV, which may be attributed to the oxidation of DEDTPI according to the reaction;



For Ag^0 , the addition of DEDTPI results in a new anodic peak starting above 0 mV, which is probably due to the formation of AgDEDTPI . This adsorption reaction may be the result of coupled reactions of the EC-type. The voltammograms for an 80:20 Au-Ag alloy indicate the anodic current rise above 250 mV. This potential is higher than that observed for the onset of DEDTPI adsorption on pure Ag^0 , which can be explained by the lower activity of silver in the alloy. For 50:50 Au-Ag alloy, the anodic current rises above 150 mV, which is lower than that for the 80:20 Au-Ag alloy, but higher than that for Ag^0 . Therefore, the onset of DEDTPI adsorption is dependent on the silver content of the alloy; the higher the silver content, the closer the adsorption potential moves toward that observed for pure Ag^0 .

The voltammograms obtained with Au^0 in the presence of DIBDTPI show that anodic current starts to rise at potentials around 550 mV. This may be attributed to the oxidation of DIBDTPI to $(\text{DIBDTPI})_2$, similar to the case of DEDTPI. For Ag^0 , the adsorption of DIBDTPI, which starts at about 250 mV, may be attributed to an EC-mechanism involving Ag^0 and DIBDTPI to form AgDIBDTPI . The results of voltammetry for the two Au-Ag alloys are similar to those obtained for DEDTPI, and indicate the formation of AgDIBDTPI , followed by $(\text{DIBDTPI})_2$. As is the case with DEDTPI, the potential for the onset of adsorption is directly related to the silver content of the alloy.

There are no indications of the oxidation of DIBMTPI on Au^0 , which is

contrary to that observed for the corresponding dithio analogue. The FTIR results also do not indicate the adsorption of DIBMTPI on gold. The voltammetric studies conducted with Ag° show that DIBMTPI begins to adsorb at around 250 mV. The interaction may be explained by the EC-mechanism which is similar to that for DTPI. The results obtained for the two Au-Ag alloys (80:20, 50:50) are similar to those for DTPI except that there is no indication of the formation of $(\text{DIBMTPI})_2$. The FTIR spectroscopic and contact angle measurements show results supporting the observations made in voltammetry experiments.

In the present work, the ΔG_f° for AgDIBDTPI and AgDIBMTPI have been determined to be -6.50 and -5.11 kJ/mol, respectively. The E_h -pH diagrams constructed using these values are in good agreement with the voltammetry, FTIR and contact angle results. The ΔG_f° values for AgDIBDTPI and AgDIBMTPI are approximately the same, which is reflected in the voltammetry experiments. That is, the onset potential for the adsorption of DIBDTPI and DIBMTPI on Ag° are almost the same; therefore, no significant difference in the reactivity with silver has been observed. However, DIBDTPI has a distinct advantage over DIBMTPI in gold flotation, because the former can be oxidized to form a dimer while the latter cannot.

It has been shown that ΔG_f° of AgDCMTP is more negative than those of AgDIBDTPI and AgDIBMTPI , suggesting that former is a stronger collector for silver. This difference is manifested by the fact that DCMTP adsorbs on silver at a lower potential than DIBDTPI and DIBMTPI .

5.3. Ethyl Xanthate

Voltammograms of Ag° in the presence of ethyl xanthate (EX) show a prewave occurring at potentials lower than that for the formation of AgEX . The prewave represents an underpotential deposition of EX on silver via

the following charge-transfer reaction;



which is referred to as chemisorption. This is followed by the formation of AgEX via the following reaction;



which occurs at a potential close to the thermodynamic (or reversible) potential. The height of the prewave is found to be independent of [EX⁻]; however, the peak at more positive potentials indicative of reaction (7) increases with increasing EX⁻ concentration, suggesting that reaction (7) is mass transport-controlled. The equilibrium coverage of chemisorbed xanthate can be fitted by the *Frumkin* isotherm.

The *ex situ* FTIR spectra taken in the prewave region show absorption bands which can be attributed to chemisorbed xanthate, while the spectra obtained above the reversible potential of reaction (7) show the characteristic bands of the AgEX. The UV/Vis spectroscopic analysis of the solution shows that EX⁻ is abstracted from solution and released again when the potential is taken into the prewave region and returned to the initial values. This means that the chemisorption reaction of EX with silver is reversible.

Contact angle measurements conducted under controlled potential conditions show that the contact angle increases with increasing coverage of chemisorbed xanthate. This finding suggests that the formation of AgEX above the reversible potential does not further increase the hydrophobicity of the surface. Hydrophobicity acquired by chemisorption of xanthate is sufficient to achieve a maximum flotation.

The ΔG_f° of AgEX, calculated from the formal potential, is -27.0 kJ/mol, which is more negative than those for AgDCMTP, AgDIBDTPI and AgDIBMTPI. It may be said, therefore, that EX has a stronger reactivity with silver than the other collectors. The strong reactivity of xanthate is manifested by the observation that the reversible potential for reaction (7) is about 0 mV, which is lower than those for DCMTP, DIBDTPI and DIBMTPI. Considering that EX also chemisorbs below this potential, EX is a stronger collector for Ag than the others.

Based on the *Frumkin* isotherm established in the prewave region, the ΔG_f° values of chemisorbed xanthates have been calculated. An E_h -pH diagram constructed using these values shows the regions of stability of chemisorbed xanthate (EX_{ads}) as well as those of the metal xanthate (AgEX). The E_h -pH diagram constructed as such support the results obtained from voltammetry, FTIR and contact angle experiments.

Voltammetry results show that AgEX begins to form at potentials about 50 mV and 100 mV more positive on the 50:50 and 80:20 Au-Ag alloys, than for pure Ag°. This reflects a decrease in the activity of silver when alloyed with gold. The shifts observed in the voltammogram are consistent with the thermodynamic calculations based on the free energies of Au-Ag alloys. The underpotential deposition of chemisorbed EX has also been observed with the Au-Ag alloys used in the present work. The charge associated with the chemisorption is approximately proportional to the silver content of the surface. This finding may suggest that the chemisorption of EX occurs only on silver sites on the alloy surfaces.

Contact angle measurements show that Au-Ag alloys become hydrophobic above the potentials at which EX begins to chemisorb. Contact angle increases with increasing potential in the prewave region and, hence, the coverage of chemisorbed species. Finite contact angles develop on gold electrode when the potential is sufficiently high enough to oxidize EX to

(EX)₂.

Based on the *Frumkin* isotherm obtained in the prewave region and the free energies of Au-Ag alloys, E_h -pH diagrams have been constructed. They are similar to that of Ag°. The only significant difference is that the stability regions of chemisorbed xanthate and AgEX shift to higher potentials. The E_h -pH diagrams constructed as such are consistent with voltammetry, FTIR and contact angle results.

Chapter 6. Recommendations for Future Study

Further electrochemical experiments should be conducted, particularly on silver and gold-silver alloy electrodes, using rotating disk electrodes (RDE) to complement cyclic voltammetry studies. In cyclic voltammetry, current peaks often arise from the back reduction or oxidation of the soluble species or the films formed on the electrode surface in the preceding sweeps. With the RDE, the soluble species can be spun away from the electrode surface so that the film formation can be distinguished and studied separately. Also, the anodic peaks attributed to collector interactions with silver need to be investigated more extensively to verify the proposed coupled chemical reaction.

Galvanic effects between different minerals have been known to affect floatability. Flotation tests conducted with artificial mixtures of gold and silver using the various reagents studied in this work will show whether galvanic interactions affect flotation. The concentrates can be analyzed by chemical analysis or using image analysis to determine the amount of each material recovered.

Flotation tests should be carried out to determine the relative strength of thiophosphate, thiophosphinates and xanthate. Besides measuring the recovery, the flotation rate should also be determined. Flotation rate is important in evaluating different collectors (Ackerman et al., 1984). The rate criterion, together with the ultimate recovery, helps in discriminating reagents. Knowledge of the flotation rate will give a clearer view of how these collectors compare against the standard flotation reagents. The flotation tests should also be carried out at different collector concentrations to determine the minimum amount of

collector required for desired recovery.

The role of oxygen in the flotation of precious metals with thiol collectors has always been a controversy. In the present work, experiments have been conducted in the absence of oxygen so as not to complicate the analysis of the results. Future work should include the addition of oxygen in the system so as to better approximate the conditions in actual flotation.

Kinetic studies are important in understanding the flotation chemistry of different reagents. The kinetics of adsorption of collectors on gold should also be determined. Together with the flotation rate constants, the effectiveness of different collectors can be clearly measured. Also, by conducting the experiments at several different temperatures, the activation energy for the adsorption process can be determined.

For the chemisorbed xanthate layer, further FTIR studies are necessary to elucidate its structure. Also, using the IRAS technique, the preferential adsorption studies should be carried out for precious metals. The competition between different collector for the absorption on gold, silver, and alloys should be studied. The results will represent the relative strength of the different collectors. The IRAS measurements may be complemented by other surface analysis techniques such as X-ray photoelectron spectroscopy, Auger spectroscopy, and mass spectroscopy.

The application of Pearson's HSAB (hard and soft acids and bases) principle to flotation systems is becoming more significant, especially in the design of new collector reagents. This theory has been shown to be useful in explaining the selectivity of thionocarbamates (Basilio, 1989). This type of study can be applied to precious metal flotation. Information on the relative softness or hardness of different precious metals and collectors will be valuable in understanding the collector

adsorption mechanisms. These data will provide explanations on why some collectors are applicable only to particular minerals and will help in synthesizing new reagents for specific applications.

Appendix

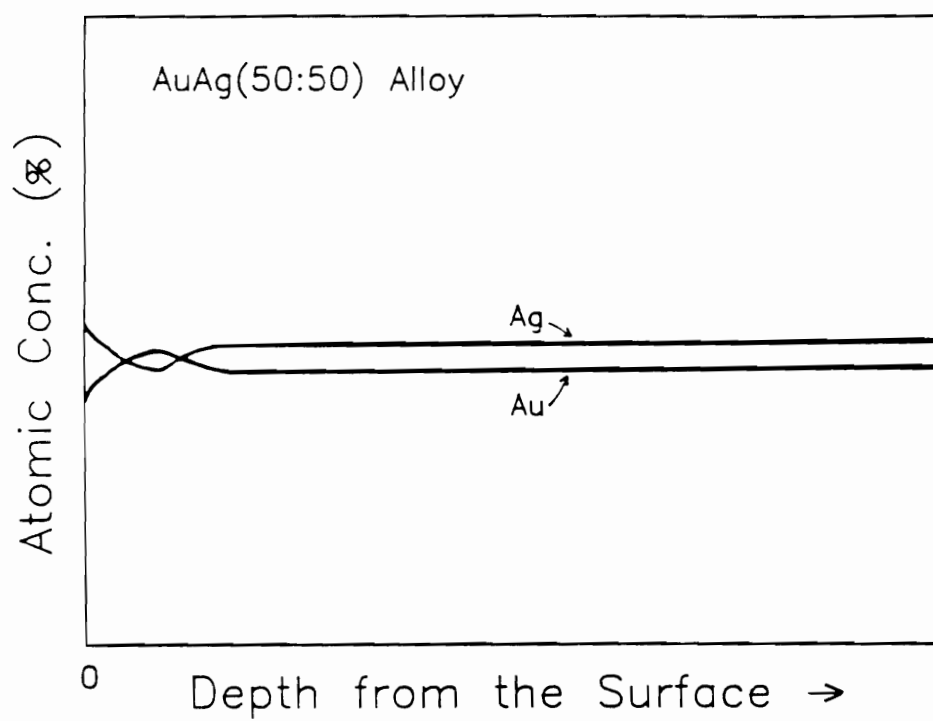


Figure A.1. Schematic AES depth profile of Au-Ag (50:50) alloy at room temperature.

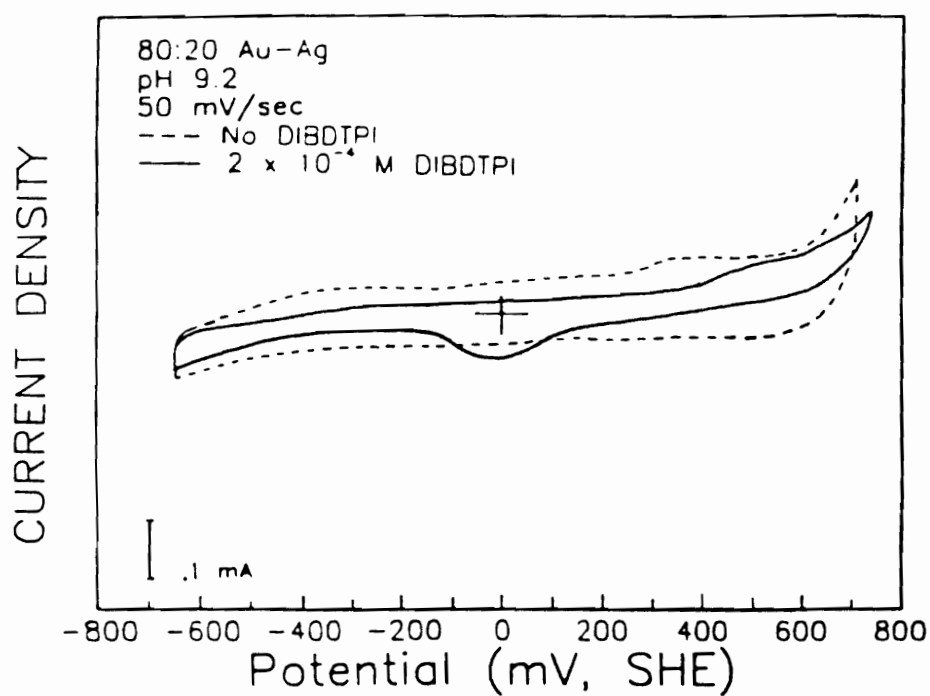


Figure A.2. Voltammograms for 80:20 Au-Ag alloy in the absence and presence of 2×10^{-4} M DIBDTPI at pH 9.2.

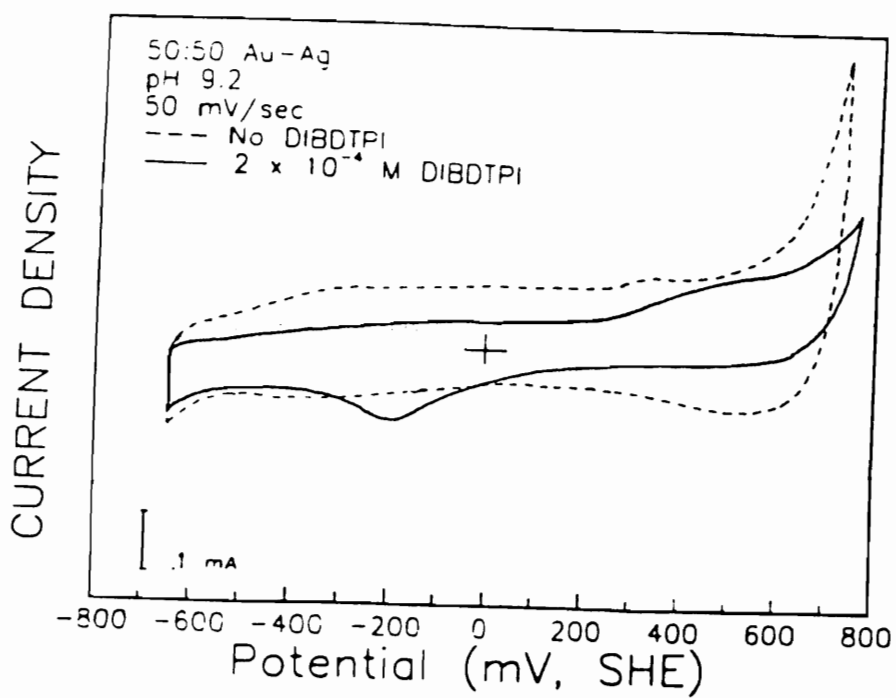


Figure A.3. Voltammograms for 50:50 Au-Ag alloy in the absence and presence of 2×10^{-4} M DIBDTPI at pH 9.2.

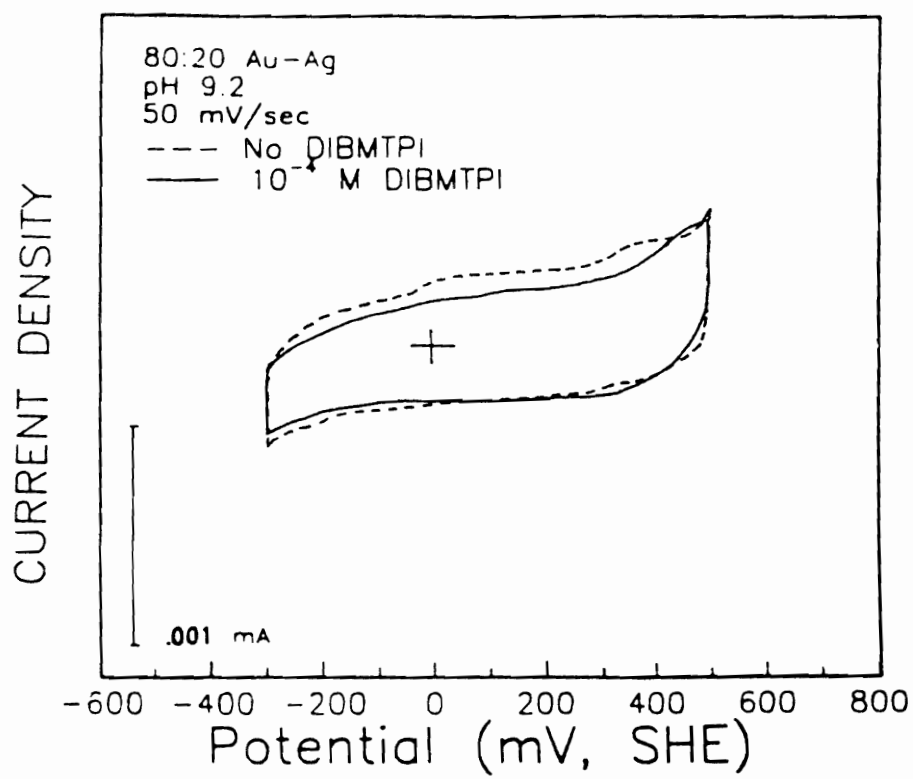


Figure A.4. Voltammograms for 80:20 Au-Ag alloy in the absence and presence of 1×10^{-4} M DIBMTPI at pH 9.2.

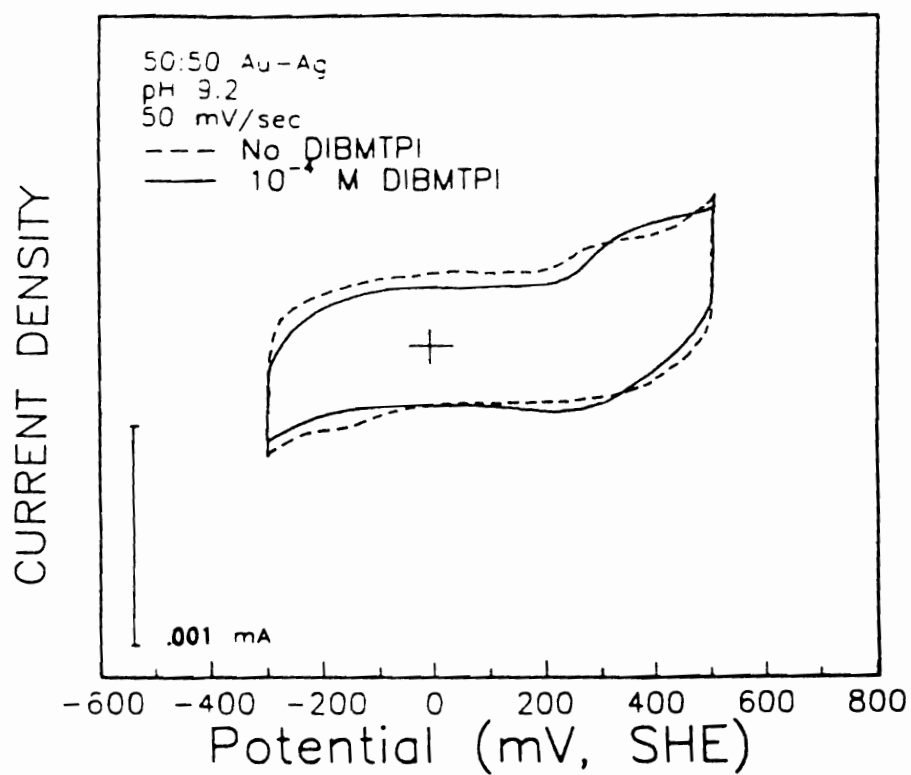


Figure A.5. Voltammograms for 50:50 Au-Ag alloy in the absence and presence of 1×10^{-4} M DIBMTPI at pH 9.2.

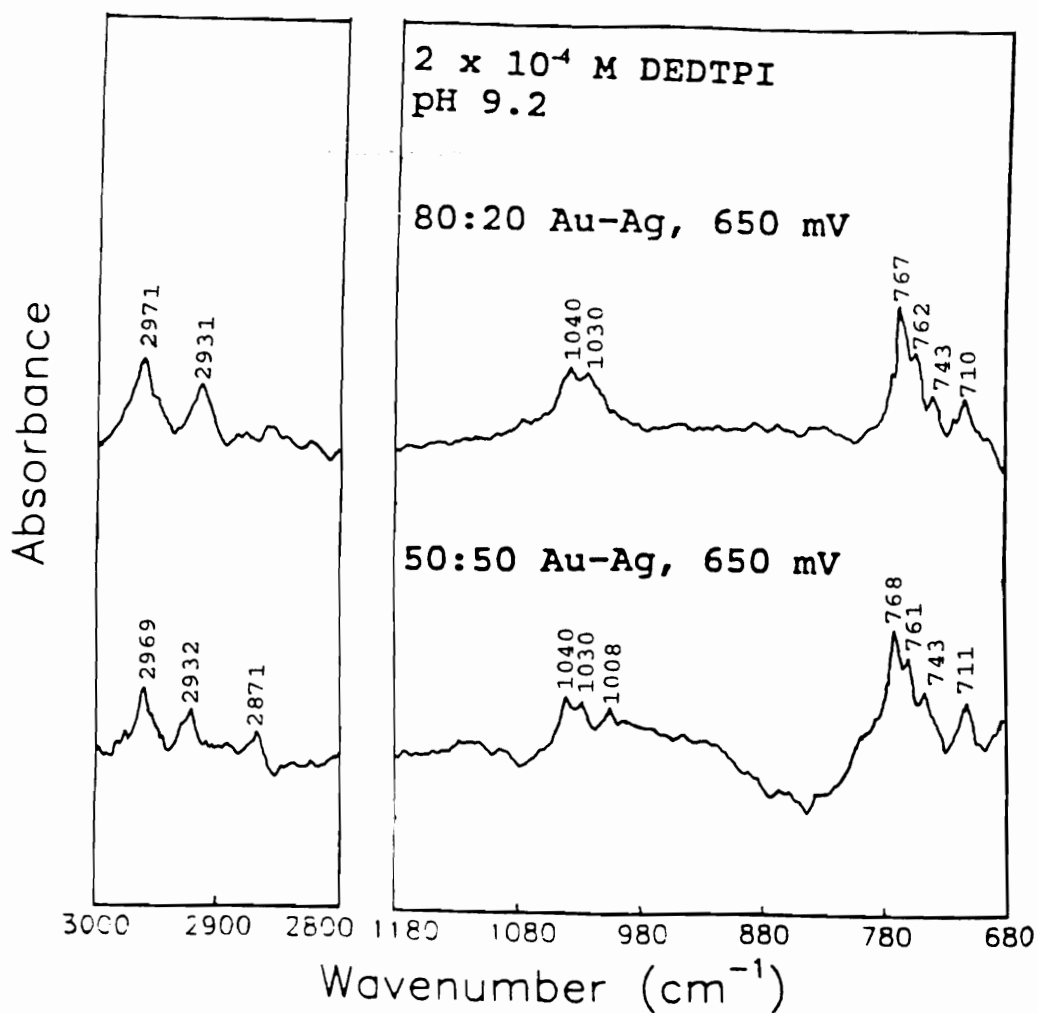


Figure A.6. FTIR reflection spectra of (a) 80:20 Au-Ag alloy at 650 mV and (b) 50:50 Au-Ag alloy at 650 mV in 2×10^{-4} M DEDTPI.

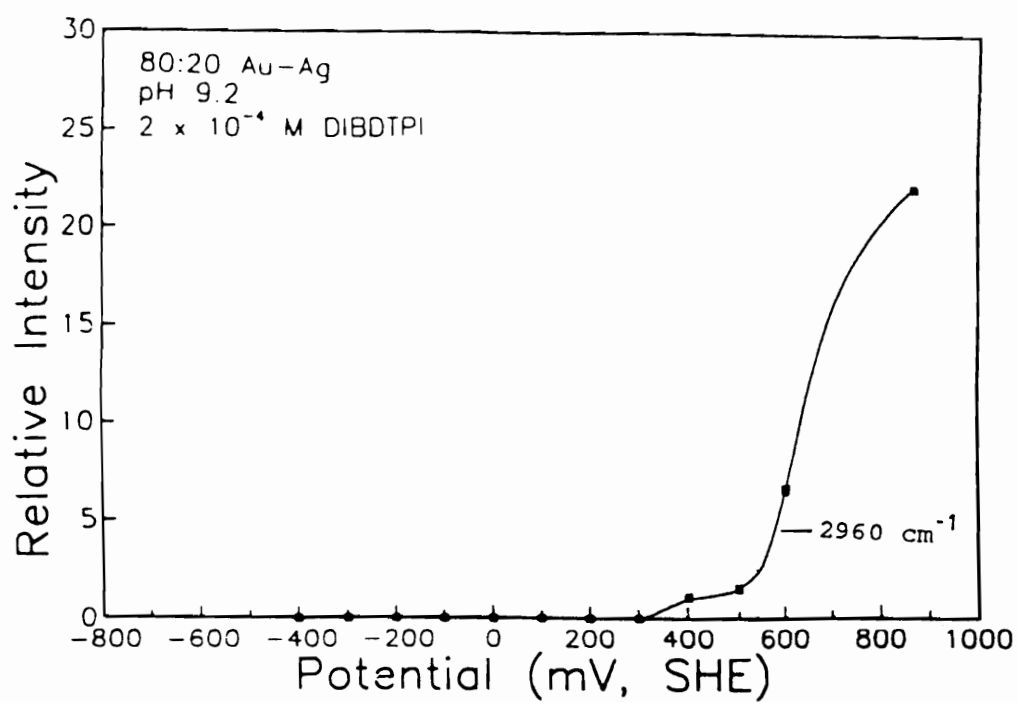


Figure A.7. The effect of potential on the IR signal intensity (2960 cm^{-1}) of adsorbed DIBDTPI for 80:20 Au-Ag alloy in the presence of 2×10^{-4} M DIBDTPI at pH 9.2.

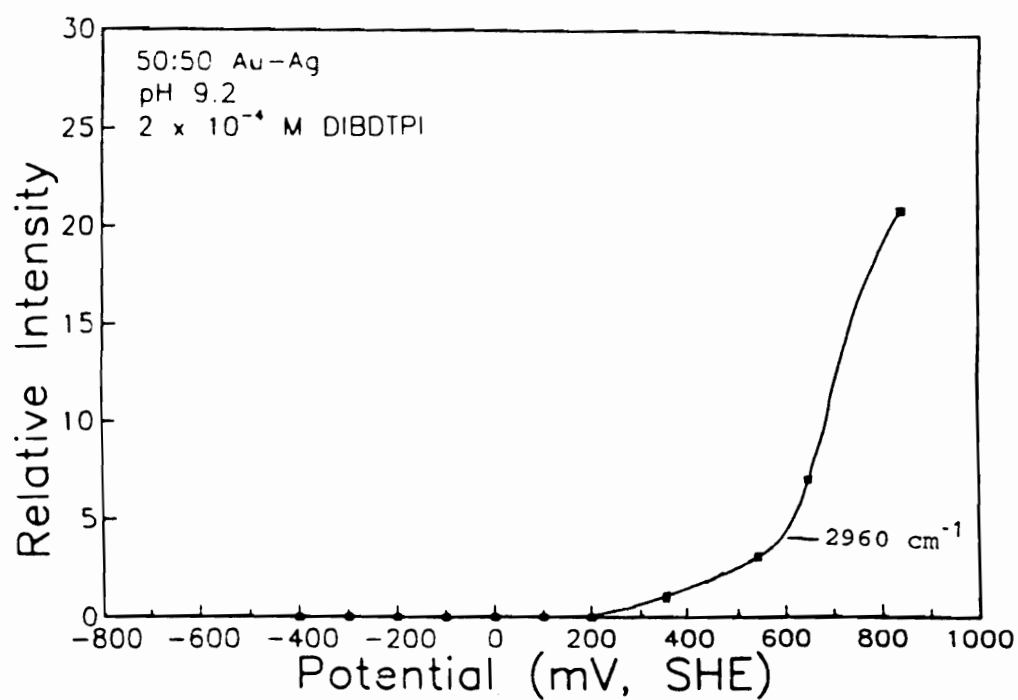


Figure A.8. The effect of potential on the IR signal intensity (2960 cm^{-1}) of adsorbed DIBDTPI for 50:50 Au-Ag alloy in the presence of 2×10^{-4} M DIBDTPI at pH 9.2.

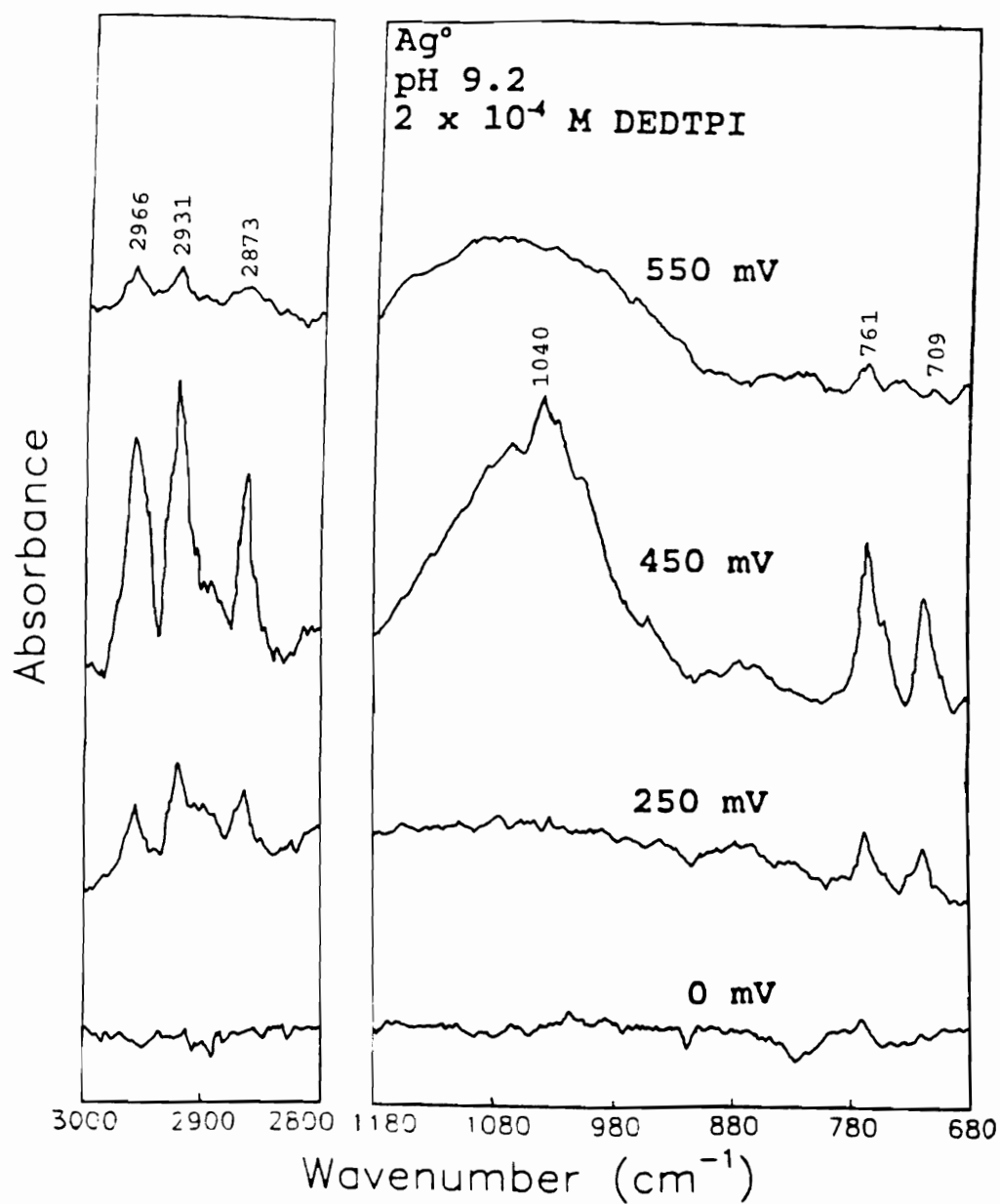


Figure A.9. FTIR reflection spectra of Ag^0 at different potentials in 2×10^{-4} M DEDTPI.

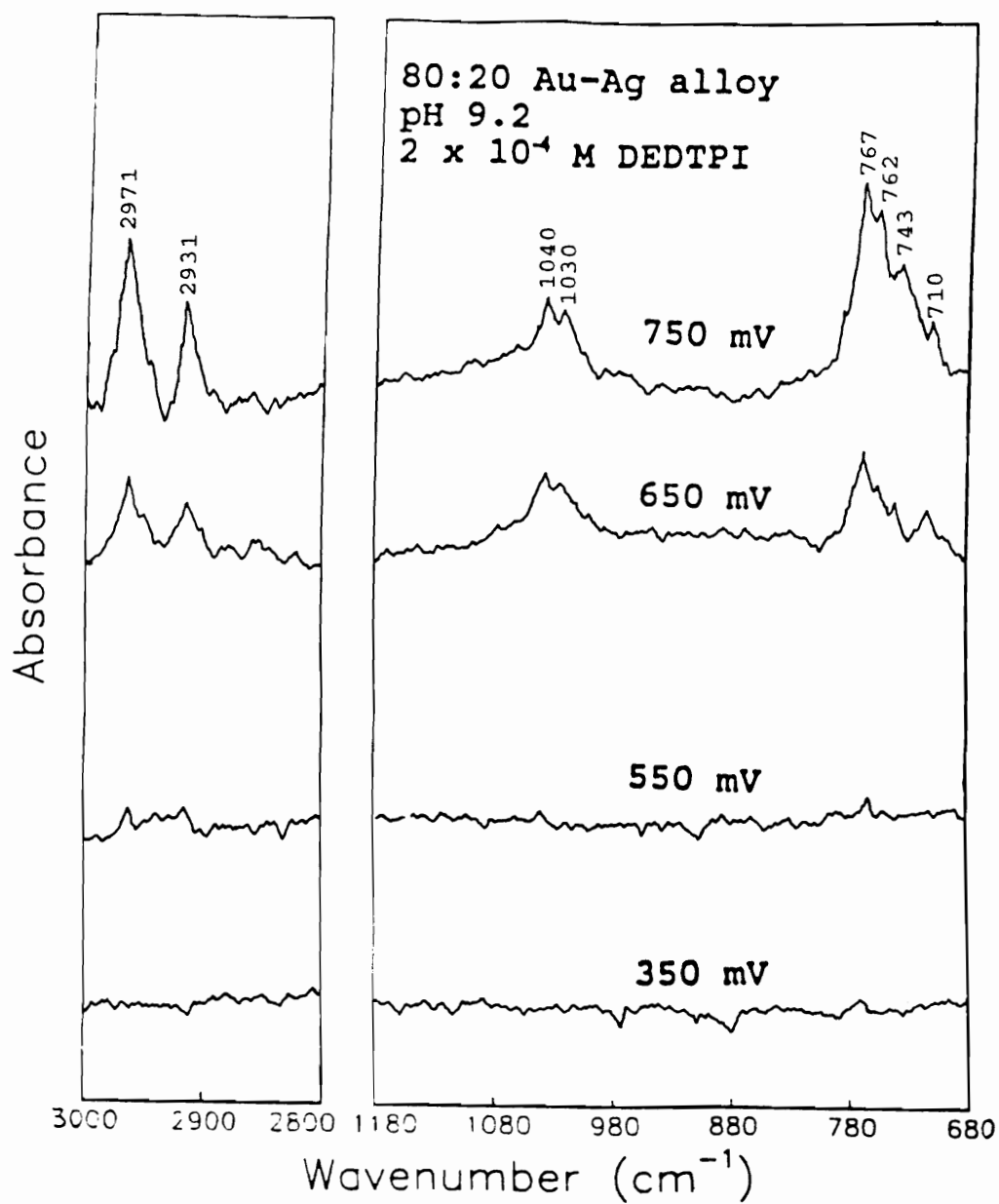


Figure A.10. FTIR reflection spectra of 80:20 Au-Ag alloy at different potentials in 2×10^{-4} M DEDTPI.

Bibliography

- Ackerman, P. K., Harris, G. H., Klimpel, R. R., and Aplan, F. F., Effect of alkyl substituents on performance of thionocarbamates as copper sulfide and pyrite collectors, In; M. P. Jones and R. Oblatt (Editors), Reagents in the Minerals Industry, Inst. Min. Metall., London, 251-264, 1984.
- Anisimov, S. M. and Svistunov, N. V., Izv. Vysshikh Ucheb. Zaved., Tsvetnaya Metallurgia, 3, 31-43, 1968.
- Arbusov, Batuev, and Vinogradova, Compt. Rend. Acad. Sci. U.S.S.R., 54, 599, 1946.
- Barnes, Gore, Liddel, and Van Zandt Williams, Infrared Spectroscopy, Reinhold, 1944.
- Basilio, C. I., Fundamental studies of thionocarbamate interactions with sulfide minerals, Ph. D. Thesis, VPI & SU, 1989.
- Basilio, C. I., Kim, D. S., Yoon, R. H., and Naragaj, D. R., 1991b, Studies on the use of monothiophosphates for precious metals flotation, Minerals Engineering, to be published.
- Basilio, C., Pritzker, M. D. and Yoon, R. H., SME-AIME Annual Meeting, New York, preprint N. 85-86, 10, 1985.
- Basilio, C. I., Yoon, R. H., Nagaraj, D. R., and Lee, J., 1991a, The adsorption mechanisms of modified thiol-type collectors, SME-AIME Annual Meeting, Denver, Colorado, Preprint 91-171.
- Bates, R. G., Determination of pH, Theory and Practice, John Wiley, New York, NY, 1964.
- Bellamy, L. J., The Infrared Spectra of Complex Molecules, Vol. 1, 3rd ed., Chapman and Hall, New York, Ch. 18, 1975.
- Bellamy, L. J., Advances in Infrared Group Frequencies, Methuen, London, 1968.
- Bergmann, Littauer, and Pinchas, J. Chem. Soc., 847, 1952.
- Blaskett, K. J. and Woodcock, J. T., Treatment of gold ores, In; Ore dressing methods in Australia and adjacent territories, Ed. by H. H. Dunkin, 5th Empire mining and metallurgical congress, Vol. 3, 1-94, 1953.
- Bogdanov, D., AIME Annual Meeting, 1977
- Bomstein, Analyt. Chem., 25, 512, 1953.
- Born, M. and Wolf, E., Principles of Optics, Pergamon, Oxford, 1959.

- Buckley, A. N. and Woods, R., *Colloids and Surfaces*, 53, 33, 1991.
- Butts, A. and Coxe, C. D., *Silver; Economics, Metallurgy, and Use*, D. Van Nostrand, 1967.
- Chander, S., and Fuerstenau, D. W., *J. Electroanal. Chem.*, 56, 217, 1974.
- Chittenden, D. and Thomas, E., *Spectrochim. Acta*, 20, 1679, 1964.
- Cotton, F. A. and Wilkinson, G., *Advanced Inorganic Chemistry*, Wiley-Interscience Publications, New York, 1980.
- Daasch and Smith, *Analyt. Chem.*, 23, 853, 1951.
- Demidov, V. I., *Simultaneous recovery of gold and silver from polymetallic ore*, *Tsvetnye Metally*, 4, 77-80, 1975.
- Dollish, Fateley, and Bentley, *Characteristic Raman Frequencies of Organic Compounds*, Wiley, New York, 1974.
- Elvey, G., *J. Chem. Soc. Farad. Trans. 1*, 134, 1977
- Emeleus, Haszeldine, and Paul, *J. Chem. Soc.*, 563, 1955.
- Erchikovskii, G. O., *Formation of Flotation Froth*, Gonti, 1939.
- Eriksson, G. A., *Anal. Chim. Acta*, 112, 375, 1979.
- Francis, S. A. and Ellison, A. H., *J. Opt. Soc. Am.*, 49, 131, 1959.
- Fraser, K. S., Walton, R. H., and Wells, J. A., *Processing of refractory of gold ores*, *Mineral Eng.*, 4, 7, 1029-1041, 1991.
- Friedel, Peirce, and McGovern, *Analyt. Chem.*, 22, 418, 1950.
- Gardner, J. R. and Woods, R., *Aust. J. Chem.*, 30, 981, 1977.
- Gardner, J. R. and Woods, R., *Aust. J. Chem.*, 27, 2139, 1974.
- Gaudin, A. M., *Principles of Mineral Dressing*, McGraw-Hill, New York, 223, 1939.
- Gilman Jr., A. F., *Inorganic Reactions*, The Eclectic Publishers, Chicago, 1930.
- Glynn, C., Michalopoulos, C., and Green, T., *Gold, Consolidated Gold Fields, Ltd.*, London, 1979
- Gore, *Discuss. Faraday Soc.*, No. 9, 138, 1950.
- Greenler, R. G., *J. Chem. Phys.*, 44, 310, 1966.
- Harvey, A. E., *Anal. Chim. Acta*, 8, 246, 1973
- Harvey and Mayhood, *Can. J. Chem.*, 33, 1552, 1955.
- Henley, K. J., *Gold-ore mineralogy and its relation to metallurgical treatment*, *Minerals Sci. Engng*, 7, 4, 289, 1975.

- Hensen, C. and Killey, J., SME-AIME Annual Meeting, Salt Lake City, Utah, Preprint 90, 1990.
- Hogfeldt, E., Stability Constants of Metal-Ion Complexes, Pergamon Press, Oxford, 1982.
- Holmstedt and Larsson, Acta Chem. Scand., 5, 1179, 1951.
- Hudson, Structure and Mechanisms in Organo-Phosphorus Compounds, Ch. 3, Academic Press, New York, 1965.
- Jha, M. C. and Kramer, M. J., Recovery of gold from arsenic ore, Precious Metals, Ed. by V. Kudryk et al., AIME, 337, 1984.
- Jones, J. and Katritzky, K., J. Chem. Soc., 4376, 1960.
- Jones, M. H. and Woodcock, J. T., Int. J. Miner. Process., 5, 285, 1978.
- Kabachnik, M. I., Ioffe, S. T., and Mastryukova, T. A., Zh. Obshch. Khim., 25, 684, 1955.
- Kabachnik, M. I., Mastryukova, T. A., Matrosov, E. I., and Fisher, B., Infrared spectra and structure of salts of phosphorus monothioacids, Zhurnal Strukturnof Khimii, 6, 5, 691-698, 1965.
- Kakovsky, I. A., in J. H. Schulman (Ed.) Proceedings 2nd International Congress on Surface Activity, Butterworths, London, Vol. 4, 225-237, 1957.
- Kakovsky, I. A., Flotation of Native Metals, Trudy Nauchno-Tekhnicheskoi Sessii Instituta Mekhanobr, 1955.
- Katritzky, K., Quart. Reviews, 13, 353, 1959.
- Kowal, A. and Pomianowski, A., J. Electroanal. Chem., 46, 411, 1973.
- Kozachenko, D., Gold Bull. 12, 21, 1976
- Kudryk, V., Corrigan D. A., and Liang, W. W., Precious Metals; Mining, Extraction, and Processing, Metallurgical Society of AIME, New York, 1984.
- Leja, J., Surface Chemistry of Froth Flotation, Plenum Press, New York and London, 1982.
- Leppinen, J. O., Basilio, C. I., and Yoon, R. H., In-Situ FTIR study of ethyl xanthate adsorption on sulfide minerals under conditions of controlled potential, Int. J. Miner. Process., 26, 259-274, 1989.
- Leppinen, J. O., Mielczarski, J. A., and Yoon, R. H., FTIR studies of ethyl xanthate adsorption on gold, silver, and gold-silver alloys, Colloids and Surfaces, in press.
- Li, A. F., Mineral. Essled. Rud Tsvet. Redk. Metal., 117-132, 1967.
- Meyrick and Thompson, J. Chem. Soc., 225, 1950.

- Mielczarski, J. A. and Yoon, R. H., FTIR reflection study of molecular orientation in spontaneously adsorbed layers on low-absorption substrates, *J. Phys. Chem.*, 93, 2034, 1989.
- Mielczarski, J. A., Zachweija, J. B., and Yoon, R. H., The Dual Role of Xanthate in the Induction of Hydrophobicity of Hydrophobicity of Chalcocite, Preprint, SME Annual Meeting, Salt Lake City, Utah, 1990.
- Miller, L. and Wilkins, H., *Anal. Chem.*, 24, 1253, 1952.
- Mingione, P. A., Use of AEROPHINE 3418A promoter for sulfide minerals flotation, SME-AIME Annual Meeting, Denver, Colorado, Preprint 91, 1991.
- Myasnikova, G. A., Plaksin, I. N., and Okolovich, A. M., Flotation-Concentration of Arsenic-Pyrite Ores, 1955.
- Nagaraj, D. R., In: P. Somasundaran and B. Moudgil (Eds.), *Reagents in Mineral Technology*, Marcel Dekker, New York, Ch. 9, 1987.
- Nagaraj, D. R. and Avotins, P. V., In: Y. A. Aytekin (eds), *Proceedings of the II International Mineral Processing Symposium*, Izmir, Turkey, 1988.
- Nagaraj, D. R., Basilio, C. I., and Yoon, R. H., The Chemistry and structure-activity relationships for new sulfide collectors, SME-AIME Annual Meeting, Las Vegas, Nevada, Preprint 89-175, 1989.
- Nagaraj, D. R., Brinen, J., Farinato, R., and Lee, J., SME-AIME Annual Meeting, Denver, Colorado, Preprint 91, 1991.
- Nagaraj, D. R., Lewellym, M. E., Wang, S. S., Mingione, P. A., and Scanlon, M. J., New Sulfide and Precious Metals Collectors: For acid, neutral and mildly alkaline circuits, In: E. Forssberg (ed), *Proceedings of the XVI International Minerals Processing Congress*, Stockholm, Sweden, Elsevier Press, 121-132, 1988.
- Nicholson, R. S. and Shain, I., Theory of stationary electrode polarography, *Anal. Chem.*, 36, 40, 706-723, 1964.
- Norwood, G. L., *J. Chem. Ed.*, 30, 576, 1969
- Nyquist, *Applied Spectroscopy Part II*, 161, 1957.
- OB TI Glavzoloti, Vol. 46, 1956.
- O'Dell, C. S., Walker, G. W., and Richardson, P. E., *J. Appl. Electrochem.*, 16, 544, 1986.
- O'Dell, C. S., Walker, R. K., and Richardson, P. E., in P. E. Richardson, S. Srinivasan, and R. Woods (Eds), *Proc. Int. Symp. Electrochemistry in Mineral and Metal Processing*, Electrochem. Soc., Pennington, NJ, 81-95, 1984.
- Parker, E. A., *Plating*, 45, 631, 1957
- Plaksin, I. N., *The Metallurgy of Precious Metals*, 1958.
- Pomianowski, A. and Leja, J., *Can. J. Chem.*, 41, 2219, 1963.

- Pritzker, M. D. and Yoon, R. H., in P. E. Richardson, S. Srinivasan, and R. Woods (Eds) Proc. Int. Symp. Electrochemistry in Mineral and Metal Processing, Electrochem. Soc., Pennington, NJ, 26-53, 1984.
- Putnam, G. L., J. Chem. Ed., 30, 576, 1953
- Ramdohr, L. H., Acta Chem. Scand. Ser. A28, 740, 1979
- Randle and Whiffen, Molecular Spectroscopy, Inst. of Petroleum, 111, 1955.
- Rao, S. R., Xanthates and Related Compounds, Marcel Dekker, New York, 1971.
- Richards, R. H. and Locke, C. E., Textbook of Ore dressing, McGraw-Hill, New York and London, 1940.
- Richardson, P. E., Stout III, J. V., Proctor, C. L., and Walker, G. W., Int. J. Miner. Process., 12, 73, 1984.
- Salamy, S. G. and Nixon, J. C., The application of electrochemical methods to flotation research, In; Recent Development in Mineral Dressing, IMM, 503, 1953.
- Schultze, J. W., The role of elementary steps in the kinetics of adsorption processes, in S. Bruckenstein, J. D. E. McIntyre, B. Miller, and E. Yeager (Eds), Proceedings of the 3rd Symposium on Electrode Processes, The Electrochemical Society, Princeton, N. J., 1979.
- Seeton, V. B., AIME Annual Meeting, New Orleans, 1979
- Smith, I. C. and Carson, B. L., Silver, Trace Metals in the Environment, Vol. 2, Ann Arbor Sci., Ann Arbor, 12, 1977.
- Somasundaran, G., Australian IMM Regional Conference, 1986
- Southampton Electrochemistry Group, Instrumental Methods in Electrochemistry, Halsted Press, New York, 1985.
- Subrahmanyam, T. V. and Forssberg, K. S., Developments in gold processing technology, Ed. by Brawner, Gold Mining 88, 265, 1988.
- Sutherland, K. L. and Wark, I. W., Principles of Flotation, Aust. IMM, Melbourne, Australia, 97, 1955.
- Swalen, J. D., Rabolt, J. F., Fourier Transform Infrared Spectroscopy, Academic Press, New York, Vol. 4, Ch.7, 283, 1985.
- Szeglowski, Z., Czarnecki, J., Kowal, A., and Pomianowski, A., Tans IMM, 86, C115, 1977.
- Taggart, A. F., Handbook of Mineral Dressing, John Wiley and Sons, New York, 1976.
- Taggart, A. F., del Guidice, G. R. M., and Ziehl, O. A., The case for the chemical theory of flotation, Trans. AIME, 112, 348-381, 1934.
- Talonen, P., Rastas, J., and Leppinen, J., Surf. Interface Anal., 17, 669, 1991.

- Thomas, E., Chem. and Ind., 198, 1957.
- Thomas and Chittenden, Spectrochim. Acta, 26A, 781, 1970.
- Varsanyi, Vibrational Spectra of Benzene Derivatives, Academic Press, New York, 1969.
- Vartanyan, K. T. and Shukakidze, N. D., The flotation of antimony and antimony-arsenic ores, Byulleten Kavkazskogo Inst. Miner. Syrya (Tblis), No. 1, 1958.
- Waldron, E. and Hornig, J., J. Amer. Chem. Soc., 75, 6079, 1953.
- Wang, S. S. and Avotins, P. V., The use of dialkyl dithiophosphinates in sulfide flotation, SME-AIME Annual Meeting, Dallas, Texas, Preprint 81-155, 1982.
- West, J. M., Bur. Mines. Prepr. Bull., 667, 1978
- White, J. L., Orr, R. L., and Hultgren, R., Acta Met., 5, 747, 1957.
- Wilson, J., Phys. Review, 45, 706, 1934.
- Winter, G. and Woods, R., Sep. Sci., 8, 261, 1973.
- Woods, R., J. Phys. Chem., 75, 354, 1971.
- Woods, R., in E. A. Mular, G. Gonzales, and C. Barama (Eds), Copper 87, Vol. 2, Mineral Processing and Control, University of Chile, Santiago, 121-135.
- Woods, R., Basilio, C. I., Kim, D. S., and Yoon, R. H., J. Electroanal. Chem., in press.
- Woods, R., Yoon, R. H., and Young, C. A., Int. J. Miner. Process., 20, 109, 1987.
- Woods, R., Young, C. A., and Yoon, R. H., Int. J. Miner. Process., 30, 17, 1990.
- Zaitseve, S. P. and Plaksin, I. N., An examination of the influence of reagent collector combination on their adsorption by copper, silver, and by alloys of gold, silver, and copper, Izv. AN SSSR OTN, 7, 1956.

Vita

The author was born in Pusan, South Korea on February 16 (March 21 of the solar calendar), 1962 to KyoungSeung Kim and YoungJa Kim. He entered the Seoul National University in Seoul in 1981 to pursue a Bachelor of Science degree in Metallurgical Engineering. Upon graduation in February, 1985, he entered the graduate school of the same university to pursue a Master of Science degree in Metallurgical Engineering and received his M. S. degree in February, 1987. After discharged from military service, he continued his study to pursue a Ph. D. degree in Mining and Minerals Engineering at Virginia Polytechnic Institute & State University from 1988. He is a member of the Korean Metallurgical Association.

DongSu Kim

A handwritten signature in cursive script that reads "DongSu Kim". The letters are fluidly connected, with a prominent loop for the 'D' and a trailing flourish at the end of the name.